DEFORMATIONAL HISTORY, STRATIGRAPHIC CORRELATIONS AND GEOCHEMISTRY OF EASTERN QUESNEL TERRANE ROCKS IN THE CROOKED LAKE AREA, EAST CENTRAL BRITISH COLUMBIA, CANADA

by

MARY ANNE BLOODGOOD

B.S., STATE UNIVERSITY OF NEW YORK AT ALBANY, 1983

A THESIS SUBMITTED IN PARTIAL FULFILMENT OF

THE REQUIREMENTS FOR THE DEGREE OF

MASTER OF SCIENCE

in

THE FACULTY OF GRADUATE STUDIES

GEOLOGICAL SCIENCES

We accept this thesis as conforming

to the required standard

THE UNIVERSITY OF BRITISH COLUMBIA

MARCH 1987

In presenting this thesis in partial fulfilment of the requirements for an advanced degree at The University of British Columbia, I agree that the Library shall make it freely available for reference and study. I further agree that permission for extensive copying of this thesis for scholarly purposes may be granted by the Head of my Department or by his or her representatives. It is understood that copying or publication of this thesis for financial gain shall not be allowed without my written permission.

GEOLOGICAL SCIENCES

The University of British Columbia
2075 Wesbrook Place
Vancouver, Canada
V6T 1W5

Date: MARCH 1987

ABSTRACT

The Eureka Peak are lies within the Quesnel terrane of the Intermontane Belt, adjacent to the Omineca Belt - Intermontane Belt tectonic boundary. It represents a convergent zone between the arc related Quesnel terrane and parautochthonous Barkerville terrane. The terrane boundary is defined by the Eureka thrust.

Underlying the area are middle Triassic to early Jurassic sedimentary and volcanic rocks, represented by the Quesnel River Group and Takla Group, respectively. Petrologic and geochemical studies of the Takla Group volcanics suggest protoliths of island arc and marginal basin affinities. The Quesnel terrane structurally overlies Hadrynian to early Paleozoic metasediments of the Snowshoe Group (Barkerville terrane). The base of the Quesnel terrane is marked by mylonitized mafic and ultramafic rocks of the Crooked Amphibolite.

Correlation of features across the plate boundary has established the structural continuity in the region, and recognition of structural phases common to both terranes which developed in response to plate convergence. The deformational history involves two phases of coaxial folding of a mechanically heterogeneous lithologic sequence, accompanied by extensive pressure solution, and later overprinting by NW trending extensional fractures. Synchronous to F_1, detachment surfaces developed along major stratigraphic contacts due to contrasting rheologies of adjacent lithologies. Second phase deformation established the regional map pattern, folding the detachment surfaces and the tectonic boundary.

Synchronous to deformation, regional metamorphism is evidenced by the growth of minerals characteristic of amphibolite facies in the Barkerville terrane, and greenschist facies in the Quesnel terrane. Dissipation of heat from the underlying sequences is suggested by the rapid transition in metamorphic grade observed across

the boundary. Cleavage surfaces have acted as a locus along which pressure solution has occurred, providing a pathway for the escape of fluids generated during metamorphism. Deposition of material within extensional fractures occurred throughout the deformational history. Fracturing is prominent adjacent to the Quesnel River Group and Takla Group contact, where the viscosity contrast between the two lithologies provided an effective barrier to extensive fluid flow. Concentration of fluids along the contact may have had a buoying effect on the volcanics, allowing furter eastward translation during deformation.

ACKNOWLEDGEMENTS

I would like to acknowledge Dr. John V. Ross for initially suggesting the Eureka Peak area as a Masters' thesis projest. His reliable advice and continued support throughout the duration were essential to the success of the project. Field and laboratory expenses were provided by NSERC Grant 67-2134 to Dr. J.V. Ross.

Laboratory and technical assistance were provided by Dr. Stanya Horsky, whose patience and wisdom is gratefully acknowledged. I am also indebted to Dr. Cathie Hickson for her programming finesse and untold patient hours at the computer terminal.

I would also like to thank everyone at the Geological Survey Branch of the B.C. Ministry of Energy, Mines and Petroleum Resources for the opportunity to continue my studies in the Quesnel area. Special thanks are due to Dr. Andre Panteleyev for his vote of confidence, and complete support throughout the final stages of the completion of the thesis.

Discussions with Dave McMullin, Steve Garwin, and Richard Friedman helped to clarify my thoughts and ideas as the project evolved. The unwavering enthusiasm of Jeffrey A. Fillipone is gratefully recognized; whose able assistance in the field and continued advice and encouragement contributed significantly to the development of the project.

TABLE OF CONTENTS

ABSTRACT ii

ACKNOWLEDGEMENTS iv

1. INTRODUCTION 1
   1.1. Location 1
   1.2. Previous Work 3

2. STRATIGRAPHY 7
   2.1. UPPER PALEOZOIC CROOKED AMPHIBOLITE 8
      2.1.1. Crooked Amphibolite 8
   2.2. QUESNEL RIVER GROUP 10
      2.2.1. Phyllites 10
      2.2.2. Phyllites and tuffs 21
      2.2.3. Volcaniclastic Breccia 27
   2.3. TAKLA GROUP 30
      2.3.1. Crystal tuffs 30
      2.3.2. Basaltic pillow lavas 31
      2.3.3. Flows and flow breccias 34
      2.3.4. Volcanic flows and breccia 36
   2.4. REGIONAL CORRELATIONS 38

3. IGNEOUS PETROGRAPHY AND GEOCHEMISTRY 41
   3.1. IGNEOUS PETROGRAPHY 41
      3.1.1. Volcanic rocks east of Eureka Peak 42
      3.1.2. Volcanic rocks west of Eureka Peak 51
   3.2. MAJOR AND TRACE ELEMENT GEOCHEMISTRY 54
      3.2.1. Major element diagrams 54
      3.2.2. Trace element diagrams 60
   3.3. DISCUSSION AND SUMMARY 66
      3.3.1. Chemical distinction based on major elements 66
      3.3.2. Chemical distinctions based on trace elements 68
      3.3.3. Summary 70

4. STRUCTURE 71
   4.1. STRUCTURAL ELEMENTS 72
      4.1.1. Bedding 72
      4.1.2. Cleavage 74
      4.1.3. Lineations 79
   4.2. MESOSCOPIC STRUCTURES 81
      4.2.1. Folds 81
      4.2.2. Fractures 83
      4.2.3. Faulting 91
   4.3. MICROSCOPIC STRUCTURES 96
      4.3.1. Cleavage 96
      4.3.2. Fractures 98
   4.4. FOLD SETS 102
      4.4.1. Phase 1 structures 102

4.4.2. Phase 2 structures 106
4.5. SUMMARY AND DISCUSSION 111

5. METAMORPHISM 117
5.1. METAMORPHIC MINERALOGY AND MICROTEXTURAL STUDIES .. 119
5.1.1. Crooked Amphibolite 119
5.1.2. Phyllites 125
5.1.3. Takla Group Metavolcanics 129
5.2. CONDITIONS OF METAMORPHISM 134

6. DISCUSSION - TECTONIC INTERPRETATION 140

7. REFERENCES 146

8. APPENDIX 1 155
8.1. METAMORPHIC MINERAL ASSEMBLAGES 156
8.2. IGNEOUS PETROGRAPHY 158

9. APPENDIX 2 160
9.1. MAJOR AND TRACE ELEMENT ANALYSES BY XRF 160
9.1.1. Major Element Analysis 160
9.1.2. Trace Element Analyses 160
9.2. REDUCED GEOCHEMICAL DATA 161

48. Stereographic projection of S_2 orientation data. 107
49. Stereographic projection of F_2 orientation data. 108
50. F_2 deforming F_1 structure. 110
51. Development of hydraulic fractuers. 114
52. Distribution of metamorphic isograds. 118
53. Post F_1 biotite. 121
54. Photomicrograph of poikiloblastic epidote. 122
55. Inclusion trails of opaques. 124
56. Photomicrograph of albite porphyroblasts. 127
57. Photomicrograph of chloritoid porphyroblasts. 128
58. Photomicrograph of metamorphic actinolite. 130
59. Photomicrograph of kinked chlorite in pressure shadow. 132
60. Tectonic model. 144
61. Sample location map. ..... BP
62. Geologic map of the Eureka Peak area. ..... BP
63. Geologic cross section. ..... BP

List of Figures

1. Generalized tectonic map of the Canadian Cordillera. 2
2. Location map of the study area. 4
3. Photograph of the amphibole schist-Crooked Amphibolite. 9
4. Stratigraphic correlations. 11
5. Photograph of micaceous quartzite. 13
6. Photograph of porphyroblastic phyllite. 17
7. Photograph of bedding within unit 6. 20
8. Fault relations at contact between units 6 and 7. 22
9. Photograph of granular quartzites, unit 7b. 24
10. Colour laminations in unit 7b. 26
11. Photograph of volcaniclastic breccia. 28
12. Contact of the Quesnel River Group and the overlying Takla Group. 32
13. Basaltic pillow lavas. 33
14. Textural features of porphyritic flows. 35
15. Photograph of volcanic breccia. 37
16. Photomicrograph of clinopyroxene completely enveloped by a rim of actinolite and biotite. 43
17. Photomicrograph of alteration of pyroxene and hornblende. 44
18. Photomicrograph of euhedral apatite crystals. 46
19. Photomicrograph of clastic textures in a tuffaceous horizon. 47
20. Photomicrograph of chloritic fragments within calcareous tuff. 48
21. Photomicrograph of twinned and zoned hornblende within a porphyritic flow. 50
22. Photomicrograph of pumice fragment within volcaniclastic unit. 52
23. Plot of $K_2O + Na_2O$ versus SiO_2. 56
24. Plot of FeO/MgO versus SiO_2. 58
25. AFM plot distinguishing the tholeiitic and calcalkaline fields. 59
26. Ti - Y - Zr discriminant diagram. 61
27. Plot of V versus Ti. 62
28. Discriminant plot of Ti/Cr versus Ni. 64
29. Discriminant plot of Cr versus Y. 65
30. Primary sedimentary structures. 73
31. Photograph of the two cleavage morphologies. 75
32. Cleavage stripes. 76
33. Mineral lineation. 80
34. Fold style at lower structural levels. 82
35. Fold style at higher structural levels. 84
36. Fold classification - t' vs. α. 85
37. Schematic structural profile. 86
38. Geometry of filled fractures. 88
39. Spaced fractures. 89
40. Geometry and orientation of fractures. 90
41. Geometry of minor faults. 93
42. Cleavage development adjacent to fault zone. 95
43. Cleavage selvages in photomicrograph 97
44. Photomicrograph of filled fracture. 99
45. Photomicrograph of antitaxial vein. 101
46. Stereographic projection of S_1 orientation data. 104
47. Stereographic projection of L_1 orientation data. 105

1. INTRODUCTION

The Canadian Cordillera may be separated into five distinctive belts (Fig. 1). The Eureka Peak area lies within the Quesnel terrane of the Intermontane Belt, and is adjacent to the Omineca Belt - Intermontane Belt tectonic boundary. It is interpreted as a convergent zone between the arc-related Quesnel terrane and parautochthonous Barkerville terrane. As illustrated in figure 2, the terrane boundary is defined by the Eureka thrust (Struik, 1986). The area is underlain by middle Triassic to early Jurassic sedimentary and volcanic rocks of the Quesnel River Group and Takla Group, respectively.

1.1. LOCATION

The Eureka Peak area lies approximately 100 kilometres east of Williams Lake, in central British Columbia, and is located within NTS sheet 93A/7. Two major routes provide easy access to the area via good all season roads from both 100 Mile House and 150 Mile House along the Cariboo Highway. A well-maintained gravel road exists from 100 Mile House passing through Canim Lake and Hendrix Lake, approaching Eureka Peak from the southwest. To the west, a paved road exists between 150 Mile House and the town of Horsefly. From Horsefly an all season gravel road proceeds south and east via Black Creek to the Eureka Peak area. At Crooked Lake, a forestry recreation site provides a suitable base camp from which day trips can be organized.

The limits of the mapped area are shown in figure 2. The area is bounded to the north by Horsefly Lake, and to the south by Crooked Lake. McKusky Creek and the MacKay River define the western and eastern boundaries of the area, respectively. Fieldwork in the area was initially undertaken during the summer of 1984, and involved detailed geologic mapping of the Eureka Peak syncline. This work was

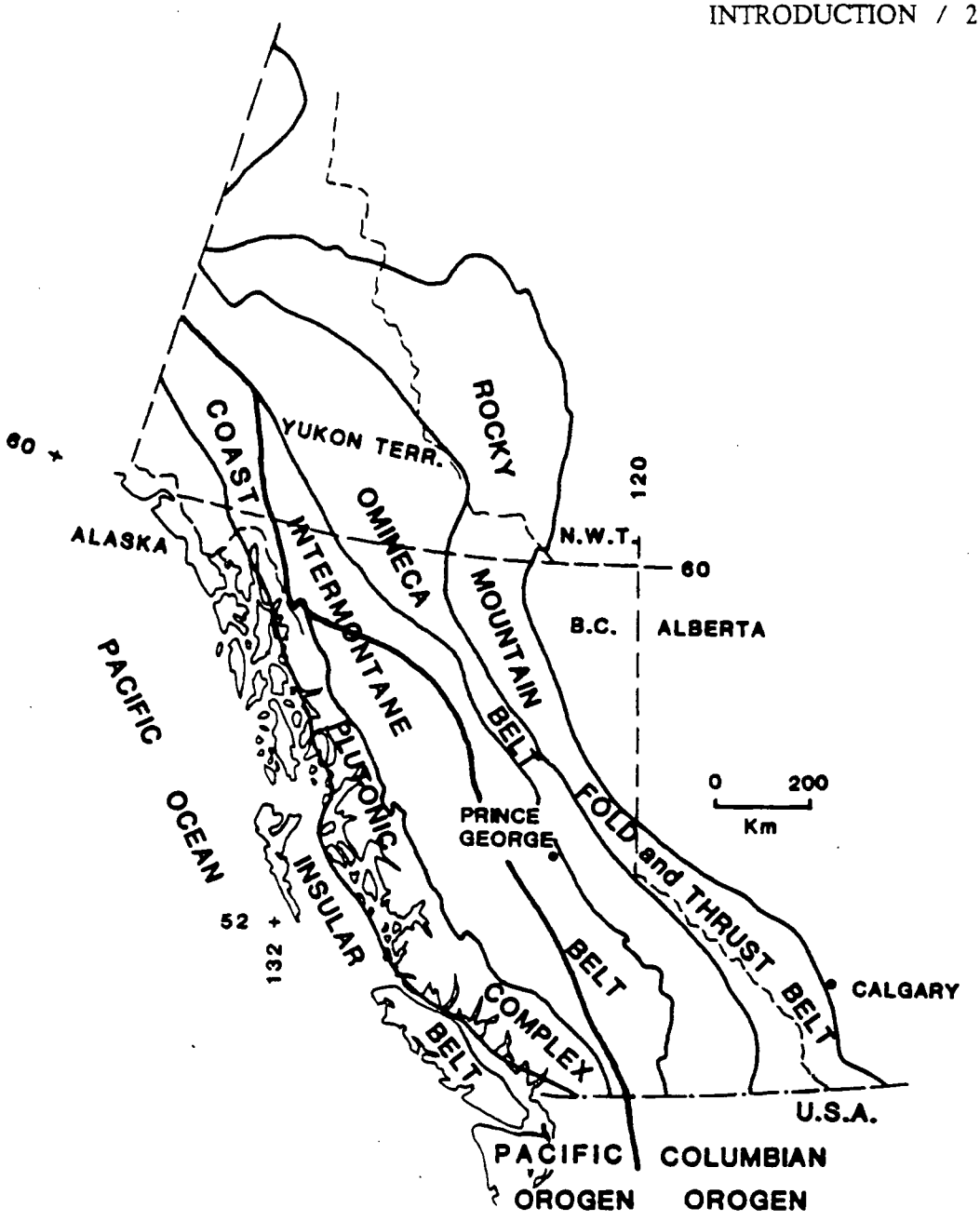

Figure 1: Generalized tectonic map of the Canadian Cordillera showing the major structural divisions (after Wheeler and Gabrielse, 1972).

supplemented with two additional weeks during the 1985 field season. The area has since been expanded to its present limits by work conducted during the 1986 field season as part of a regional project sponsored by the B.C. Ministry of Energy, Mines and Petroleum Resources, and funded through the Mineral Development Agreement.

1.2. PREVIOUS WORK

The original mapping in the region was conducted by the Geological Survey of Canada. Initial work attempted to correlate stratigraphy from the Quesnel Highlands and Cariboo Mountains to the Rocky Mountains (Sutherland-Brown, 1963; Campbell, et al. 1973; Campbell, 1973; Campbell, 1978), which were interpreted as a laterally continuous stratigraphic sequence. Campbell, et al. (1973) considered the sequences to the east of the Intermontane Belt - Omineca Belt boundary to represent the western, finer grained facies-equivalents of the Kaza Group sediments to the east. These are currently separated into two distinct terranes, the Cariboo terrane, and the Barkerville terrane (Struik, 1986), which represent continental shelf sediments, and continental shelf sediments and intercalated volcanics, respectively. Within the areas adjacent to the Eureka Peak area, metasediments of the Snowshoe Group comprise the Barkerville terrane (Fillipone, 1985; Elsby, 1985; Carye, 1985). Recent work has confirmed that metavolcanics overlying the Barkerville terrane from Dunford Lakes to north of Quesnel Lake are allochthonous, and much of the Paleozoic is absent at the contact with the underlying Snowshoe Group of the Barkerville terrane. This unit has previously been correlated with the Antler Formation of the Slide Mountain Group (Campbell, 1978; Ross et al. 1985; Fillipone, 1985; Elsby, 1985; Carye, 1985) based upon lithologic similarities. Further to the north, the Slide Mountain Group occupies the same structural position with respect to the Barkerville terrane, and is recognized as a

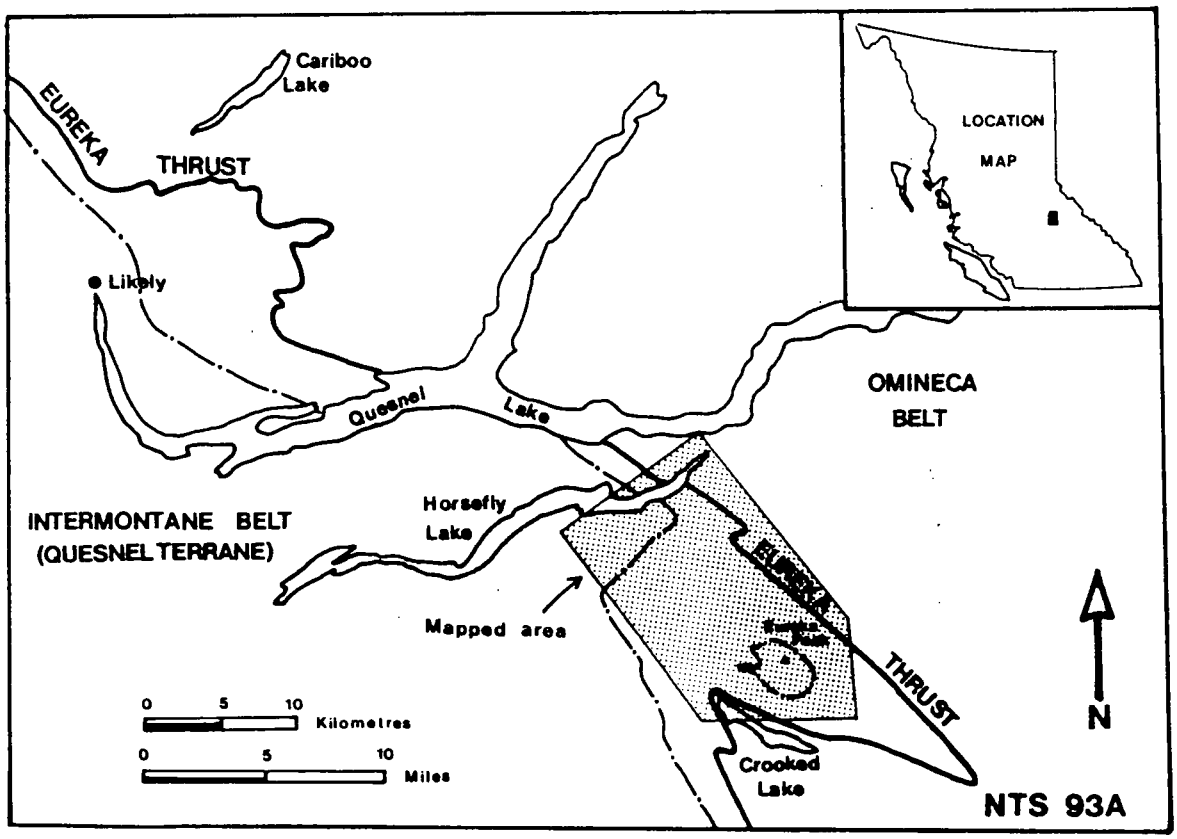

Figure 2: Location of the map area with and the configuration of the Omineca - Intermontane Belt boundary define by the Eureka thrust.

separate terrane, the Slide Mountain terrane. However, no physical link has been established to prove that the two units are laterally equivalent, and the metavolcanic unit is now designated as the Crooked Amphibolite (Struik, 1986), which may be the sheared metamorphic equivalent of the Antler Fm; or could represent Mesozoic basement to the Quesnel area.

Structurally overlying the Crooked Amphibolite are Triassic to Jurassic metasediments and volcanics comprising the Quesnel terrane. These units extend as a continuous belt from north and east of Kamloops, to north of Prince George (Tipper et al. 1981). Regional mapping in the Quesnel Lake map sheet (NTS 93A) during the 1960's as part of a GSC reconnaissance project assigned both the metasediments and the volcanics to the Quesnel River Group (Campbell, 1978). Subsequent mapping to the north (Tipper, 1978), and in the vicinity of Quesnel Lake (Rees, 1981) has correlated the volcanic units to the Takla Group. The abundance of augite porphyry breccias in the volcanic sequence has suggested that the Takla Group rocks described in the Quesnel Lake region are correlative to the Nicola Group rocks of southern British Columbia. Both the Takla and Nicola Group rocks are considered to be time equivalent units.

Current interpretation of the Quesnel Lake area involves a Jurassic convergent event during which the Quesnel terrane was thrust eastwards over the Barkerville terrane. Sedimentary and volcanic assemblages of Upper Paleozoic and Mesozoic age comprising the Quesnel terrane were emplaced upon Proterozoic to early Paleozoic rocks of North American affinity, the Barkerville terrane. The obduction of the Quesnel terrane resulted in intense crustal deformation, involving folding and the development of extensive mylonitized zones within the crustal rocks, and regional metamorphism ranging from greenschist to amphibolite facies (Fillipone, 1985; Montgomery, 1985; Elsby, 1985

and Carye, 1985). Detachment surfaces developed during eastward transport of the allochthonous assemblages, resulting in imbrication at the higher structural levels. Regional deformation following final emplacement of the Quesnel terrane resulted in folding of the tectonic boundary, as illustrated in figure 2.

2. STRATIGRAPHY

Rocks within the Eureka Peak area may be separated into three distinct stratigraphic assemblages. Each assemblage is bounded by a fault contact and contains a unique internal stratigraphy. From oldest to youngest the assemblages are:

1. Metavolcanics belonging to the Crooked Amphibolite (Struik, 1986).
2. Triassic metasediments of the Quesnel River Group (Tipper, 1972).
3. Takla Group massive volcanics of Upper Triassic to Jurassic age (Tipper et al. 1979; Rees, 1981).

Emphasis of the study is placed on the mappable stratigraphic and structural relations of the lithologic units underlying the area. Determination of units of stratigraphic significance internal to each assemblage is based on distinguishing individual lithologies that are mappable at a scale of 1:15,840. The Quesnel River Group metasediments are represented by eight distinctive lithologic units in the Eureka Peak area (Fig. 62). Subsequent work to the northwest, along the southern shore of Horsefly Lake, and to the south, near Elbow Lake, suggest that the stratigraphy established at Eureka Peak can be recognized on a regional scale. The Takla Group volcanics have been separated into two mappable lithologies. Rapid facies changes across and along strike within the volcanics have limited further subdivision of the volcanic sequence at the scale of mapping. However, lithologies of similar composition, texture and structural position have been correlated throughout the area where possible.

The stratigraphic succession underlying the Eureka Peak area may be correlated regionally to rocks of the Quesnel terrane (Struik, 1986), occurring in a belt approximately 300 km long. Conodants obtained from limestones north of Quesnel Lake have yielded ages on the lithologic successions and provide some constraints on the interpretation of the evolution of the Quesnel terrane.

2.1. UPPER PALEOZOIC CROOKED AMPHIBOLITE

2.1.1. Crooked Amphibolite

Map unit = **Pca**

The Crooked Amphibolite crops out along the southern flank of Peak 6935', and is composed of mafic metavolcanics. The contact between the metavolcanic rocks and the overlying Quesnel River Group sediments is well exposed and defines the southernmost limit of mapping north of Crooked Lake.

A section of the Crooked Amphibolite approximately 40 m thick was observed on the southern flank of Peak 6935' but was not traced to its lowermost contact with the Snowshoe Group rocks. The lowermost part of the Crooked Amphibolite is dark green, chlorite–feldspar–amphibole schist, which weathers pale to chalky green. Alignment of chlorite and fine amphiboles defines a schistose foliation. Minor pyrite cubes, 2–3 mm in size, also occur along the major foliation surfaces. Alternation of mafic and felsic layers define a very fine lamination on the scale of millimetres. Stringers and lenses of quartz and feldspar varying from several millimetres to tens of centimetres in size are commonly surrounded by chlorite and amphibole. Localized, but pervasive epidotization has resulted in a distinctive yellow–green alteration halo or mantle surrounding the stringers and lenses. An identical succession has been described on the western flank of Boss Mountain (Fillipone, 1985) and on the southern flank of the Mt. Perseus area (Elsby, 1985), where the same contact is observed.

Immediately overlying the chlorite–feldspar–amphibole schist and in sharp contact with them, is a coarse grained hornblende schist, or garbenschiefer (Fig. 3). Total

Figure 3: Coarse grained amphibole schist. Alternation of quartz and feldspar-rich interbeds with amphibolitic horizons defines compositional layering.

thickness of the garbenschiefer observed in outcrop is approximately 10 m. Due to lack of continuous exposure, a maximum true thickness could be as much as 30–45 m.

A well developed colour banding is associated with the garbenschiefer. Dark coloured bands are defined by coarse grained, acicular, dark green hornblende, up to 1–1.5 cm in length. Light coloured bands of quartz and feldspar rich interbeds weather chalky and vary from 3–4 mm to 4–5 cm thick. Biotite flakes define a well developed schistose foliation. Acicular, radiating amphiboles are contained within the foliation plane but, show no preferred directional orientation within that plane. In profile, coarse hornblende crystals are observed growing across the foliation planes.

2.2. QUESNEL RIVER GROUP

2.2.1. Phyllites

The previously unnamed black phyllites are here assigned to the Quesnel River Group (Tipper, 1978; Campbell, 1978). Conodants from limestone bearing lithologies exposed further to the north have yielded an age range of Middle to Late Triassic. The Quesnel River Group is separated into eight mappable units. Subsequent work during the 1986 field season in conjunction with the Ministry of Energy, Mines and Petroleum Resources has enabled correlation of the Quesnel River Group metasediments in the Eureka Peak area with surrounding areas. A stratigraphic section through the metasedimentary sequence was measured along the Archie Creek road along the southern shore of Horsefly Lake. The Archie Creek section is included with stratigraphic sections from the Eureka Peak area to illustrate stratigraphic variations and correlations through the area (Fig. 4). The Triassic rocks in the map area consist of a

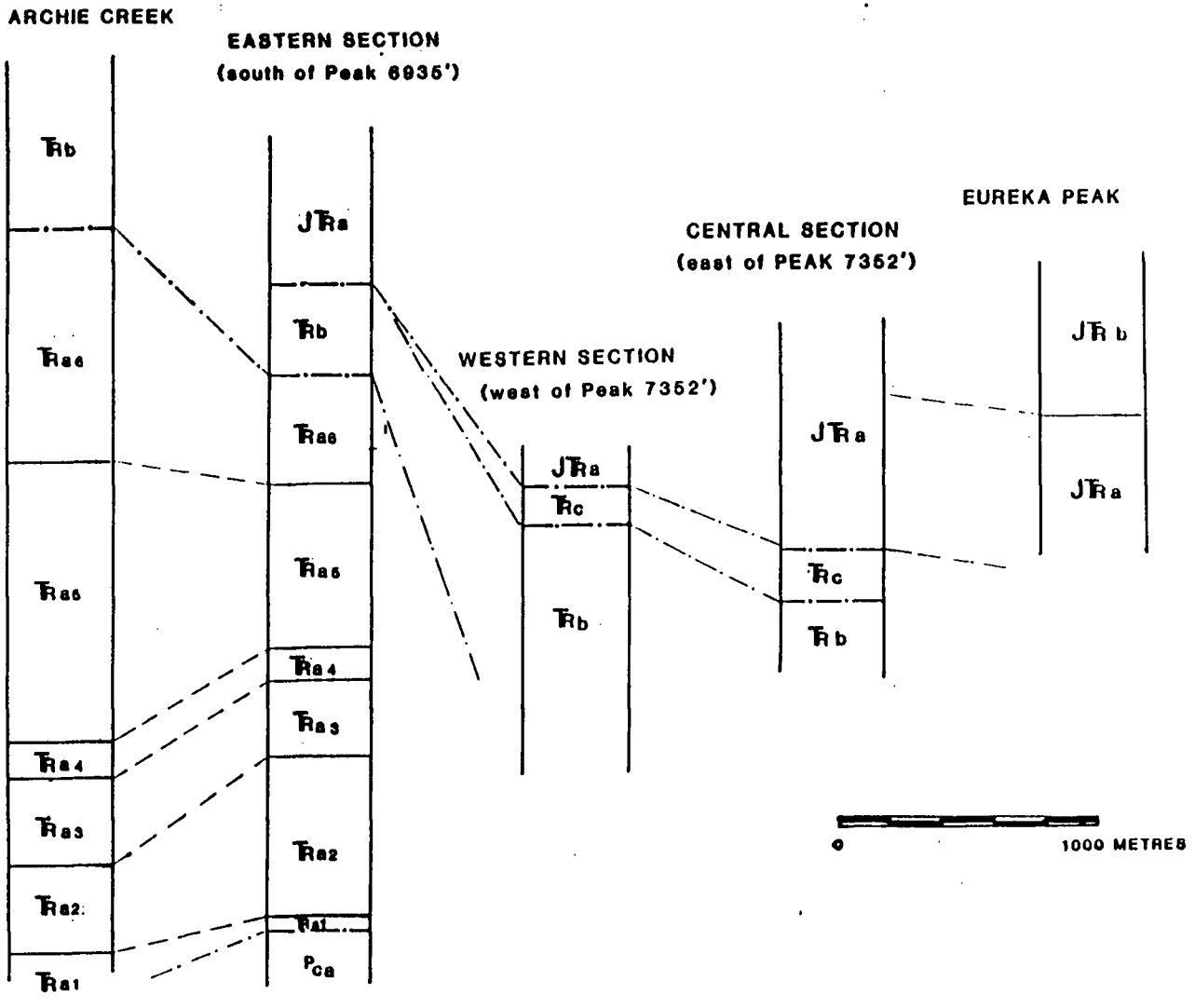

Figure 4: Stratigraphic correlations throughout the Eureka Peak area.

sequence of siliceous phyllites overlain by phyllitic siltstones, which in turn are overlain by graphitic phyllites.

Unit 1 - Micaceous quartzite

Approximate thickness 5-100 m

Map unit = Ra1

The basal member of the Upper Triassic sedimentary sequence is a rusty weathering, micaceous quartzite. Bedding within the micaceous quartzite is well defined by thin, pale grey to white, parallel laminated quartzite beds (Fig. 5). Bed thickness varies from 0.5 to 6 cm. Planar alignment of rusty weathering muscovite defines the strongly developed bedding parallel schistosity.

Where observed, the contact of the micaceous quartzite with the underlying garbenschiefer of the Crooked Amphibolite is sharp and conformable, although concordant and discordant relations have been documented along the strike length of the contact. Imbrication of the contact has been documented at the southeastern end of Crooked Lake (Campbell, 1971; Carye, 1985), and in the Mt. Perseus area (Elsby, 1985). The micaceous quartzite crops out along both the southern and northern limbs of the Eureka Peak syncline, but varies in thickness throughout the area. On the southern limb, within the limits of mapping, a maximum thickness of approximately 20 m is observed. On the northern limb, thickness varies from 20 to 150 m (Elsby, 1985). Further to the northwest at Archie Creek, a minimum thickness of 100 m is observed, which may be the result of imbrication of a much thinner unit.

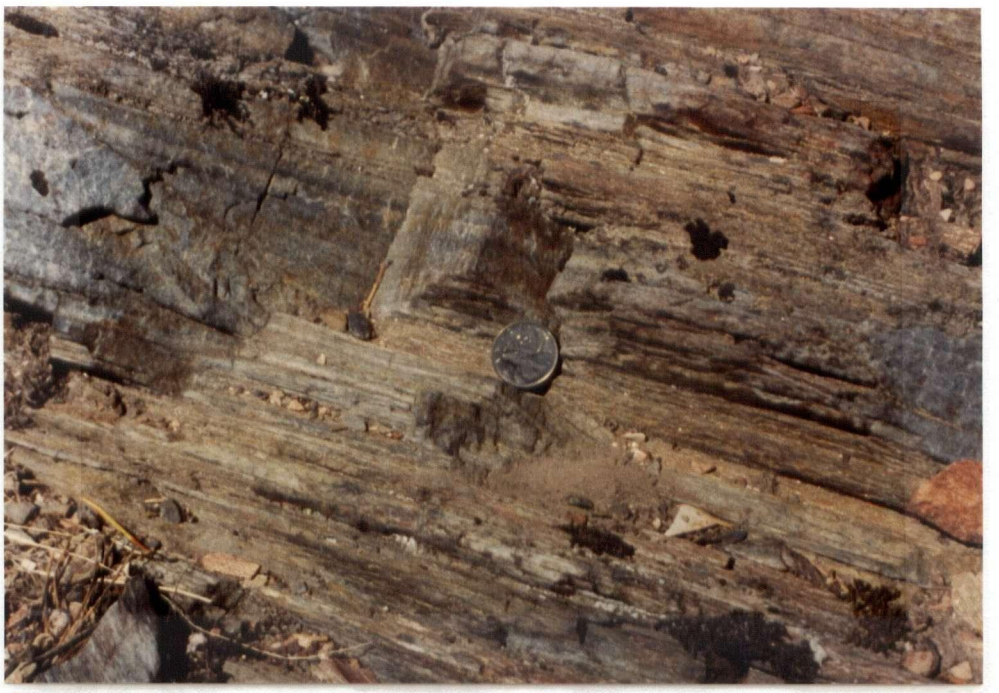

Figure 5: Bedding within the micaceous quartzite is defined by dark and light grey quartz sandstone beds. A small isoclinal fold of bedding occurs immediately below the quarter.

Unit 2 - Micaceous phyllite

Approximate thickness 650 m

Map unit = $\mathbb{R}a2$

The basal contact of the phyllites with the micaceous quartzite is not exposed in outcrop. A noticeable break in slope probably indicates the approximate location of the contact, which may be faulted. The upper contact between the micaceous phyllites and the phyllitic siltstone is gradational over a distance of 4 to 5 m.

The basal member of this unit is a very siliceous, dark rusty, grey to black weathering phyllite. The strongly developed phyllitic foliation is marked by a distinctive silvery fresh surface. Bedding is rare, although thin, pale grey weathering quartz sandstone beds averaging less than 1 cm in thickness do occur. Discontinuous bands and lenses of pale tuffaceous material locally occur within the sediments. Within the lowermost 10 m of the unit, garnet porphyroblasts are abundant and range in size up to 0.5 cm. Small, chalky weathering plagioclase porphyroblasts averaging 2 to 3 mm in size are also developed, and occur throughout the unit. Thin quartz veins, 1 to 4 cm thick and parallel to bedding are common near the base of the unit.

Unit 3 - Phyllitic siltstone

Approximate thickness 350 m

Map unit = $\mathbb{R}a3$

Overlying the siliceous phyllites and in gradational contact with them, is a phyllitic siltstone unit. In outcrop, the siltstone weathers very dark grey to black, medium grey on the fresh surface. Particle size varies from sand to silt-sized. Bedding is defined by a locally well developed millimetre scale banding. No definitive

stratigraphic way-up indicators were observed. Due to the dark weathering colour of the unit, the banding is often difficult to distinguish in outcrop. Cleavage is well developed and defined by a very planar, slaty parting. Small quartz filled veins occur throughout this unit and are most commonly oriented parallel to bedding.

Unit 4 - Laminated phyllite

Approximate thickness 120 m

Map unit = Ra4

Overlying the phyllitic siltstone, and in gradational contact with it, is a medium, pale grey weathering, finely laminated phyllite. Bedding is defined by pale grey to rusty weathering quartz sandstone beds, up to 1 cm thick, and averaging 1 to 3 mm in thickness. A very strongly developed phyllitic foliation is marked by a very rusty weathering cleavage surface. Porphyroblasts of plagioclase are locally abundant, up to 1 cm in diameter and averaging 2 to 3 mm in size (Fig. 6). On the southern flank of Peak 6935' the unit bears abundant porphyroblasts of plagioclase up to 1 cm in diameter, averaging 2-3 mm in size. In thin section, porphyroblasts of garnet and chlorotoid have been identified. On the northern limb of the syncline, south of the MacKay River, two porphyroblast phases are visible in hand specimen, and have been identified as chloritoid and probable plagioclase. Bedding parallel quartz lenses up to 1 m thick and 3 m long have also been noted at several locations within the unit, and are common on the northern limb of the syncline.

Unit 5 - Silty slates

Approximate thickness 650 m

Map unit = Ra5

The porphyroblastic phyllite grades stratigraphically upwards into coarser grained dark grey to black weathering silty slates with interbedded dark grey quartz sandstones. Bedding is defined by dark, dull grey quartz sandstone beds ranging in thickness from 10 to 12 cm. The interbedded sandstones, vary from silt to coarser sand-size particles

Figure 6: Close up of plagioclase porphyroblasts in unit 4. Dime for scale.

and weather reddish brown to dark brown. The silty slates have a well developed planar parting and are locally very speckled and rusty weathering. Thinner, pale grey to white, parallel laminated quartz sandstone layers are interbedded throughout the unit and range from 1 mm to 1 cm thick. Pale weathering quartzites, and pale grey to green weathering tuffs occur as discontinuous lenses parallel to bedding, 1 to 4 cm thick, and a general strike length of 20 to 25 cm. Within the Archie Creek succession, and along the south side of the MacKay River, this unit is dominated by graphitic phyllites, but still bears the reddish brown sandstones characteristic of this unit.

Unit 6a - Graphitic phyllites

Approximate thickness 120 m

Map unit = Ra6

Immediately overlying the silty slates, and in gradational contact with them, is a sequence of graphitic phyllites and interbedded quartzites. Within the lowermost part of the unit, the phyllites are very fissile and graphitic, weathering dark, dull grey to black, and are slightly calcareous. Bedding is very subtle within this portion of the unit and is defined by thin, parallel laminated, dark grey to black quartz siltstone beds. The beds weather dark, dull, rusty grey, and range in thickness from 1 to 2 cm thick.

Unit 6b - Dull grey phyllites

Approximate thickness 200 m

Map unit = Ra6

The phyllites grade upward into dull grey phyllites interbedded with rust weathering pale quartzite beds. The quartzite beds are parallel laminated and average 2 mm to 1 cm in thickness, rarely exceeding 2 cm in thickness. Locally, this unit becomes graphitic and fissile but is generally more silty and competent, though still well cleaved throughout the section. Well defined bedding of this unit is a prominent feature which enables it to be readily differentiated from the underlying phyllitic sequences (Fig. 7).

Unit 6c - Graphitic phyllites/limestones

Approximate thickness 100 m

Map unit = Ra6

In the uppermost portion of the section, the phyllites gradually become more fissile and graphitic, weathering dark grey. Bedding is defined by layers and lenses of black limestone, and the same rusty weathering pale quartzite beds as seen throughout the section. Quartz sandstone beds are parallel laminated and range from 1 mm to 5 cm in thickness, typically 0.5 cm to 2 cm in thickness.

The limestones are black and silty in outcrop, and occur as both discontinuous beds and lenses. Thickness of the limestone beds varies from about 4 cm to 1 m thick, with a typical thickness of 4 to 10 cm. Lenses of limestone range from 10 to 20 cm in thickness, and vary from approximately 20 cm to several metres in extent. Coarse granular calcite and quartz are often concentrated along narrow bands, and may

Figure 7: Parallel laminated quartz sandstone defines bedding within unit 6b. The thin sandstones are prominent throughout unit 6.

outline original bedding within the limestone. Small, discontinuous, barren quartz veins are sometimes associated with the limestone beds, generally less than 4 cm thick, and often parallel or near parallel to bedding. Larger quartz veins are also observed, particularly within this section of the phyllites. The veins are frequently bedding parallel, and occur as discrete, discontinuous lenses 0.5 to 1 m thick, and up to several metres in extent.

2.2.2. Phyllites and tuffs

Map unit = Rb

The incorporation of a distinctive volcanic component in the sediments of unit 7 make it readily distinguishable from the underlying phyllite sequence. Unit 7 crops out continuously along the southern limb of the syncline and underlies much of the western portion of the area It extends to the west of the Horsefly River and contacts the overlying volcanics near the summit of Big Slide Mountain. In the core of the Eureka Peak syncline the sequence is capped by a volcaniclastic unit. The volcaniclastic unit is only locally preserved along the southern limb of the syncline, and is absent at the contact exposed on Big Slide Mountain (See Plate 1 - geologic map).

Unit 7a - Fissile phyllites and tuffs

Approximate thickness 50 m

The base of the unit is marked by a sharp fault contact, across which bedding is locally discordant (Fig. 8). Quartz lenses and veins, 5 cm to 0.5 m thick, containing clasts of the surrounding rock are observed at and near to the contact.

The phyllitic rocks weather rusty, dark grey to black, with a dark red hematite staining locally present. Within the lowermost 50 m of the unit the phyllites are fissile

(a)

(b)

Figure 8: a.) Sharp fault contact between unit 6 and 7. A light weathering tuff bed in the hanging wall is truncated against the fault. b.) Truncated bedding and quartz filled veins are prominent within fault zone.

and interbedded with thin, pale quartz sandstone beds averaging 1 cm thick, as observed in the underlying sequences. Interbedding of the quartz sandstone only occurs within a few metres of the contact and is absent from the upper portions of the unit. Tuffs occur as distinct beds weathering pale grey-green, and range in thickness from 6 cm to 4 m thick. Contacts between individual tuff beds and the surrounding phyllite appear to be conformable and locally interdigitated. At the very base of the unit, one tuff bed is particularly distinctive due to its very rusty weathering, pitted outcrop appearance. Thickness of this unit varies from 10 cm to 1 m. It is sharply truncated by the fault below and is associated with small buff coloured carbonate lenses averaging 4 cm thick by 20 cm to 30 cm in extent.

Unit 7b - Silty banded slates

Approximate thickness 200 m

Stratigraphically upsection the metasediments become more pelitic, and interbedded quartzites become predominant (Fig. 9). Dark grey limestones vary in thickness up to 4 m, and minor discontinuously interbedded black to brown limestone beds range in thickness from 5 cm to 1 m.

Very dark grey to black silty slates, 1 cm to 0.5 m thick, are interbedded with competent tuffs which range in thickness from 1 cm to 1 m. The grey to green tuffs are locally colour banded; individual colour bands range from 2 to 5 cm thick. Granular quartzites, pale grey to green in colour range in thickness from 10 cm to 1 m. The phyllites grade into well-banded slates, and the tuff beds become more massive and crystalline.

The tuffs weather buff to rusty and contrast sharply with the interbedded black silty slates (Fig. 10). a planar slaty cleavage is well-developed and cleavage refraction

Figure 9: Well bedded granular quartzites occur as distinct beds 1-10 cm thick within unit 7b.

is pronounced at the contact between individual tuff or quartzite beds and slates.

Unit 7b is well-exposed to the west of the lower Ptarmigan Lakes, along a large cliff exposure several hundred metres in extent. The Ptarmigan Lakes are the two lakes immediately to the east of Peak 6935'. It can be traced to the south and east where it crops out continuously along the main ridge of Peak 7367' in the hinge region of the Eureka Peak syncline. It reappears to the west of Peak 7352' and underlies the entire region extending west to Peak 6783', where it overlies unit 7a. Cross-cutting mafic dykes are common in this area. The composition of which appears to be equivalent to the main body of volcanics in the area. The contact between the two units is believed to occur at an elevation of 5500 to 6000 ft, to the west of Peak 6783', but is not exposed in this area.

Unit 7c - Graphitic phyllites

Approximate thickness 100 m

The uppermost 100 m of this tuff/phyllite unit in both the western and eastern sections is marked by an upward gradation back into the graphitic phyllites. Bedding is defined by interbedded tuffs, and locally by limestones and pale interbedded quartz sandstones. The phyllites are recessive weathering, black and sooty in outcrop. They are locally fissile, pyritiferous and weather rusty. The interbedded tuffs weather pale grey, speckled rusty and are commonly calcareous. An average bed thickness is 1 to 10 cm, with discontinuous lenses up to 1 m thick. The tuffaceous beds are locally strongly chloritized, weathering chalky. Limestone beds are commonly discontinuous and lensoid, with an average thickness of 0.5 m. These limestones weather black to brown with a very gritty outcrop appearance. Fresh surfaces reveal a characteristic medium grey colour and a coarse silty grain size. All rock units are locally pyritiferous. Pyrite

Figure 10: Colour laminated, interbedded black silty slates and buff weathering tuffs and siltstones within unit 7b.

cubes up to 1 cm square have been observed, with an average size of 1 to 3 mm. The bedded quartz sandstones are a very minor occurrence within this uppermost unit, and are typically very discontinuous and lensoid, weathering a pale, dull grey colour, and average less than 0.5 cm in thickness.

2.2.3. Volcaniclastic Breccia

Approximate thickness 0–75 m

Map unit = Rc

Locally overlying the tuff/phyllite sequence of unit 7 is a volcaniclastic breccia. This unit directly underlies the volcanics to the west of Eureka Peak. Previously this unit had been described by K.V. Campbell (1971) as an intraformational breccia. Petrographic studies indicate that this unit is not the product of primary brecciation of units adjacent to the contact as suggested by Campbell; but more likely represents a unit of pyroclastic origin.

The volcaniclastic breccia is medium grey on the fresh surface and weathers buff to pale grey. Recognizable clasts contained within the unit are angular and weather darker than the supporting matrix (Fig. 11). Frayed and flamelike terminations of the clasts are characteristic of pumice fragments in welded tuffs. Clasts vary in size from less than 0.5 cm to 4 cm in length. Cleavage is defined by a well-developed phyllitic foliation.

This volcaniclastic unit does not cap all exposures of the metasedimentary sequence. It does crop out as a continuous unit of measureable thickness at Peak 7352', and immediately to the southeast within the core of the Eureka Peak syncline. On the southern limb of the syncline it occurs as discontinuous slivers. Both the lower and upper contacts of the volcaniclastic with the phyllite/tuff sequence and the

Figure 11: Small, angular clasts within the volcaniclastic breccia weather darker than the supporting tuffaceous matrix.

volcanics, respectively, are faulted. The contact zone is marked by fault gouge, and slickenside surfaces within a zone 1 to 3 metres wide.

2.3. TAKLA GROUP

2.3.1. Crystal tuffs

Approximate thickness 0-50 m

Map unit = JTa

The basal member of the volcanic sequence is composed of a finely crystalline, variably cleaved, competent tuff. It is well-exposed in the vicinity of Ptarmigan Lakes, where it reaches a maximum thickness of 30 to 50 metres to the northeast of the lakes. To the west, and further to the northeast it thins, and is locally absent. It is observed in the western portion of the area, to the south of Peak 7352' where it overlies the metasediments in the core of the syncline, and attains a thickness of approximately 10 to 20 m.

Generally the tuff is massive and homogeneous in texture and composition; banding is locally observed. A pale green to grey fresh surface and buff weathering is characteristic of the tuff. Very fine grained, more siliceous horizons occur as disrupted and discontinuous layers, 1 to 4 cm thick. Minor green mafic phenocrysts, 2 to 3 mm in size, are commonly altered to chlorite and epidote. Parallel to the compositional layering are stylolitic solution surfaces along which insoluble organic material has been concentrated, and which may have been derived from the underlying sediments. Pyrite cubes up to 1 cm square have been observed, although commonly smaller, millimetre sized cubes are found concentrated within narrow zones.

At the base of the crystal tuff a thin, discontinuous breccia is observed near the contact with the underlying metasediments. The host rock is a vesicular, fine-grained, weakly banded flow supporting volcanic fragments of variable size, shape and composition. Flattened calcite-filled vesicles, and randomly oriented plagioclase

phenocrysts are present in addition to minor black, acicular to stubby pyroxene phenocrysts retrograding to hornblende and chlorite. The clasts are generally angular to sub-rounded amphibolitic clasts, and range in size from 2 to 30 cm in the longest dimension. Dark grey tuffaceous clasts are common within this unit and vary in size from 0.5 to 4 cm in length. This breccia has been observed in very limited exposures to the east of Ptarmigan Lakes, and also to the southeast of Peak 7352'.

2.3.2. Basaltic pillow lavas

Approximate thickness 5-10 m

Map unit = JTRa

Locally overlying the crystal tuff is a minor unit composed of basaltic pillow lavas. The pillow lavas are well-exposed along the ridge immediately to the west of Ptarmigan Lakes (Fig. 12). where they are underlain by approximately 5 m of crystal tuff which directly overlies unit 7. To the east of Peak 7352', along the western trending ridge of Eureka Peak, limited exposures of a massive, mafic volcanic unit lacking pillow structures is believed to represent the same unit.

The pillow lavas are pale grey to green weathering and dark greenish to blue-black on the fresh surface. The pillow structures generally appear flattened, with average dimensions of 50 to 60 cm for the long axis, and 20 to 30 cm for the short axis of the oblate pillow (Fig. 13). Average length of the third dimension of an individual pillow is estimated to be about 50 to 60 cm.

Figure 12: View to the east from Peak 6735' of the contact between the Quesnel River Group and overlying Takla Group rocks.

Figure 13: Massive appearance of pillow lavas.

2.3.3. Flows and flow breccias

Approximate thickness 300 m

Map unit = JTa

Overlying the pillow lavas is a thick sequence of porphyritic flows, and flow breccias (Parsons, 1969). The flows and flow breccias are pale green to grey, and weather pale grey to green. In outcrop, the flows grade upward from a brecciated base, to more massive, homogeneous, coarsely porphyritic flows (Fig. 14). Very porphyritic cobbles supported by an aphanitic to slightly porphyritic matrix texturally characterize the flow breccias. Phenocrysts of green pyroxene and amphibole are acicular to stubby, show variable degrees of alteration and range in size from less than 1 mm to 1 cm.

It is believed that the transition from flow breccia to massive volcanic represents a singular flow. Several of these transitions were observed; an average total thickness for an individual flow is estimated to be about 15–30 m.

The basal part of a single flow is characterized by the rubbly and lumpy outcrop appearance. It consists of distinct cobbles, usually well rounded and spheroidal with length to width ratios of approximately 2 to 1, and range from 10 to 15 cm in length. In outcrop, the cobbles appear compositionally equivalent to the matrix rock, but texturally differ. Most commonly, the cobbles are very porphyritic and the supporting matrix is fine grained, with fewer and smaller phenocrysts. To a lesser extent, the supporting matrix may be porphyritic while the cobbles tend to be finer grained and phaneritic in texture. Compositionally, individual flows vary little from bottom to top. The flows and flow breccias dominate the volcanic sequence underlying the Eureka Peak area, and crop out extensively in the core of the syncline.

(a)

(b)

Figure 14: Textural transitions within porphyritic flows. a.) flow breccia marks the base of the flow. b.) massive, more homogeneous appearance is characteristic of the upper part of the flow.

2.3.4. Volcanic flows and breccia

Map unit = JTb

In gradational contact with the flow breccias is a sequence of porphyritic flows, breccias and tuffs. The best exposure of this sequence is to the south and east of Eureka Peak. The flows are characteristically rusty and rotten. Within less altered outcrops, this unit weathers chalky grey to medium green. Locally extensive epidote alteration yields a yellowish green weathered surface. The fresh surface is pale green to greenish-grey.

The volcanic flows are coarsely porphyritic, with phenocrysts occupying approximately 20% to 50% of the rock volume. The groundmass is aphanitic, and pale green in colour. The occurrence of both black and green mafic phenocrysts is diagnostic of this unit. Black hornblende phenocrysts are almost always euhedral, varying in habit from acicular crystals to more elongate, prismatic crystals. The green pyroxene phenocrysts are commonly subhedral, and show greater alteration to chlorite than the hornblende. Average phenocryst size varies from 2 to 5 mm, but phenocrysts up to 2 cm in length and greater have been observed.

Locally, the flows support large clasts. In outcrop the clasts appear to be monomineralic and vary from glomeroporphyritic masses approximately 1-3 cm in size, to large irregularly shaped clasts tens of centimetres in diameter (Fig. 15). The clasts are composed of both pyroxene and amphibole. These brecciated zones are localized and in gradational contact with the surrounding flows. It is believed that the brecciated zones may be products of brecciation within or near to a vent zone. This interpretation is further supported by the associated flow breccias which may have formed during upwelling of a volcanic dome (Wright and Boyes, 1963).

Figure 15: Mafic clasts within volcanic breccia.

Associated with the porphyritic flows are interdigitated tuffs. The tuffs are medium to dark green in colour, weathering dark green to rusty, and vary in thickness from 1 to 10 m. This unit is consistently well cleaved, usually schistose in character, and is moderately to strongly calcareous. Small euhedral pyrites (1–2 mm or less) occur concentrated along individual horizons. Larger pyrites, range in size from 0.2 to 1 cm square, and occur randomly dispersed throughout the rock and often have well developed fibrous calcite pressure shadows.

2.4. REGIONAL CORRELATIONS

The Eureka Peak area is situated adjacent to the Omineca Belt - Intermontane Belt boundary (Monger, Price and Templeman-Kluit, 1982). The rocks underlying the Eureka Peak area are part of the Quesnel terrane of the Intermontane Belt (Struik, 1986).

In the area studied, the Quesnel terrane structurally overlies Hadrynian to lower Paleozoic meta-pelites belonging to the Snowshoe Formation of the Barkerville terrane within the Omineca Belt (Struik, 1986). Further to the north, the Slide Mountain terrane represented by the Antler Formation, of the Slide Mountain Group tectonically overlies rocks of the Barkerville terrane, and has yielded conodants that range in age from Mississippian to early Permian. The Slide Mountain terrane is in turn structurally overlain by the Quesnel terrane, composed of metasediments of the Quesnel River Group (Tipper, 1978; Campbell, 1978). Within the study area, the base of the Quesnel terrane is defined by the Eureka thrust, at the base of the Crooked Amphibolite, where present. The Crooked Amphibolite varies in thickness and is locally absent along the strike length of the terrane boundary. The Crooked Amphibolite may be correlative to the Antler Formation of the Slide Mountain Group. Ultramafic nodules within the

Crooked Amphibolite bear a definite Paleozoic mantle signature (Ross and Fillipone, 1986). Both formations maintain the same structural position with respect to the Barkerville terrane, however no physical link has been established between the two. Struik (1986) currently assigns the Crooked Amphibolite to the Quesnel terrane. Where the Crooked Amphibolite is absent, the Eureka thrust is positioned at the base of the Quesnel River Group sediments. The positioning of the basal thrust of the Quesnel terrane, either at the base of the Crooked Amphibolite or at the base of the Quesnel River Group has significant implications for the interpretation of the evolution of the terrane boundary, and the importance of the Crooked Amphibolite.

The lack of a physical link between the Crooked Amphibolite and the Slide Mountain Group, and the lack of fossil-bearing lithologies within the Crooked Amphibolite allows two feasible interpretations for its tectonic significance. If the Crooked Amphibolite is interpreted to be correlative to the Slide Mountain Group, as it has by previous workers, then the Eureka thrust must be placed at the base of the Quesnel River Group metasediments. The Crooked Amphibolite would therefore represent a sliver of the Permo-Carboniferous oceanic floor of the Slide Mountain terrane, which was obducted onto the continental slope and shelf sediments of the Barkerville and Cariboo terranes during the Mesozoic.

Conversely, the Crooked Amphibolite may represent Mesozoic oceanic basement upon which the Quesnel River Group sediments were deposited directly. If this is the case, the Crooked Amphibolite would be appropriately included within the Quesnel terrane. And, the entire Quesnel terrane, with the Crooked Amphibolite variably preserved along its strike length was obducted during Mesozoic time along the Eureka thrust.

Within the area studied, the Crooked Amphibolite lacks the sedimentary

component characteristic of the Antler Formation exposed further to the north, and is devoid of any known fossil-bearing localities. In addition, no physical link has been established between the Antler Formation and the Crooked Amphibolite to definitively assign it to the Slide Mountain terrane. Ophiolites observed in the Dunford Lake area are believed to be coorelative to the Crooked Amphibolite and may represent a portion of Paleozoic basement to the Quesnel terrane. A comparison of the geochemical characteristics of the Dunford Lake ophiolite, the Crooked Amphibolite, and the Antler Formation could provide some insight into the problem.

The metasediments which structurally overlie the Crooked Amphibolite have been informally referred to as the unnamed black phyllites of Triassic age by previous workers. It is here correlated with the Quesnel River Group as defined by Tipper (1978) and Campbell (1978). Fossil-bearing lithologies exposed north of Quesnel Lake have yielded conodants of Middle to Late Triassic age. Throughout the Quesnel terrane, the Quesnel River Group is structurally overlain by volcanic rocks assigned to the Takla Group volcanics. The Takla Group rocks have yielded fossils of Middle Triassic age and may range to early Jurassic (Campbell, 1978). The Takla Group volcanics underlie much of the area to the west of Quesnel Lake and are of variable thickness in the region. The Quesnel River Group and Takla Group are believed to represent the time equivalent western volcanic and eastern sedimentary facies of the evolving Quesnel basin or trough. During Mesozoic convergence the Quesnel terrane was thrust easterly over the Barkerville terrane towards the North American craton. Internal imbrication of the terrane during obduction resulted in overthrusting of the Takla Group volcanics upon the metasediments of the Quesnel River Group along low angle thrust faults.

3. IGNEOUS PETROGRAPHY AND GEOCHEMISTRY

The integration of petrography, major and minor element geochemistry and field relations has formed the basis from which the tectonic setting represented by the volcanic rocks of the Eureka Peak area can be interpreted. Samples selected were limited to Takla Group volcanics. Several samples representative of each lithologic unit defined by field mapping were selected and analyzed by XRF techniques for a suite of major and trace elements.

A total of 29 samples were chemically analyzed. Each sample selected for geochemical analysis was also examined petrographically. Petrographic studies involved determination of primary mineralogical and textural characteristics of individual lithologic units. The tectonic setting represented by the Takla Group rock is evaluated in terms of petrographic and geochemical criteria, and consideration of the lithologic relations established in the field. The petrographic characteristics of each lithology are evaluated first, according to the stratigraphic order established in chapter 2. Major and trace element diagrams are presented, followed by a discussion of the tectonic environment indicated by the discriminant diagrams, and compared to the field relations and petrographic observations.

3.1. IGNEOUS PETROGRAPHY

Petrographic studies focussed on establishing the primary igneous mineralogy and textures preserved within each lithologic unit. Pervasive overprinting by features related to deformation and metamorphism limited the extent to which the original character of the rock could be determined. Sample locations are illustrated in Plate 2.

3.1.1. Volcanic rocks east of Eureka Peak

3.1.1.1. Basal flows and tuffs

Basal flows and tuffs of the eastern section of the study area are similar compositionally but vary texturally from their western counterparts.

Clinopyroxene with or without hornblende comprises the primary phenocryst assemblage of the basal portion of the flows in the Ptarmigan Lakes area. The phenocrysts are dominantly euhedral. Plagioclase, approximately andesine (An 44–46) in composition, occurs in both the phenocryst and groundmass assemblages, and occurs in association with calcite, filling vesicles and cavities. In all occurrences albite twinning is well–developed and Carlsbad twinning is often present.

Primary pyroxene is well preserved and occurs as euhedral to subhedral phenocrysts varying in size from 0.01 to 3 mm. In figure 16, a primary augite phenocryst is completely enveloped by a rim of actinolite and biotite. Other pyroxenes show complete or nearly complete retrogression to chlorite and calcite (Fig. 17).

Hornblende is variably present as a primary phenocryst phase in the lowermost stratigraphic interval. The hornblende occurs as euhedral to subhedral, well–twinned cross–sections and tabular crystal forms (Fig. 17), varying in size from 0.01 mm to 1 cm. Generally, hornblende is present as a phenocryst phase in association with more abundant plagioclase phenocrysts. Metamorphic actinolite, occurring as fibrous needles and rhombic sections, and biotite are common replacements of hornblende. They are observed growing along cleavage planes of hornblende crystals or as rims or pressure shadows on the phenocryst phases.

Figure 16: Twinned pyroxene completely enveloped by a rim of actinolite and biotite. (Crossed polars)

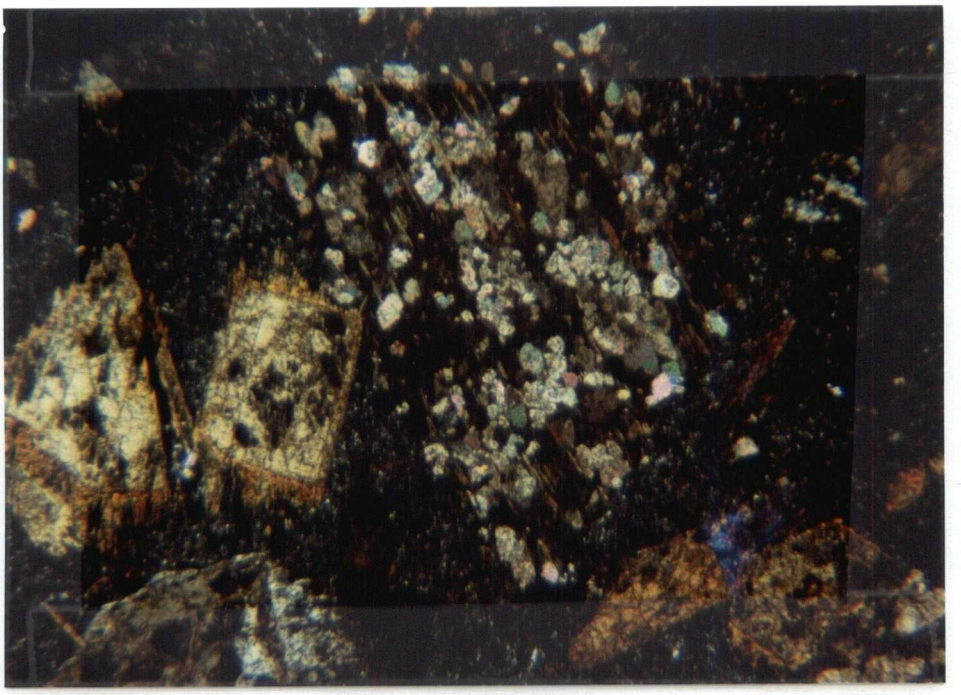

Figure 17: Primary pyroxene with retrograde replacement of chlorite and calcite. Euhedral hornblende phenocrysts show well-developed actinolite tails. (Crossed polars)

The groundmass assemblage consists of clinopyroxene, plagioclase, and hornblende in addition to quartz, clinozoisite, actinolite, epidote, sericite, chlorite and carbonate. Clinopyroxene, plagioclase and hornblende comprise the primary mineralogy of the groundmass. Sausseritization of plagioclase is variable. Accessory phases include apatite, opagues and sphene. Apatite occurs as euhedral grains up to 1 mm in size (Fig. 18). Texturally the flows are hypidiomorphic granular and variably vesicular.

The tuffaceous horizons associated with this stratigraphic interval vary both texturally and mineralogically. Samples adjacent to the contact between Unit 7 (see Stratigraphy) and the volcanics contain both porphyritic volcanic fragments and argillaceous clasts supported by a tuffaceous matrix (Fig. 19). At higher stratigraphic intervals the tuffs lack large lithic fragments and are dominated by small, stringy lenses and fragments composed entirely of chlorite and calcite (Fig. 20).

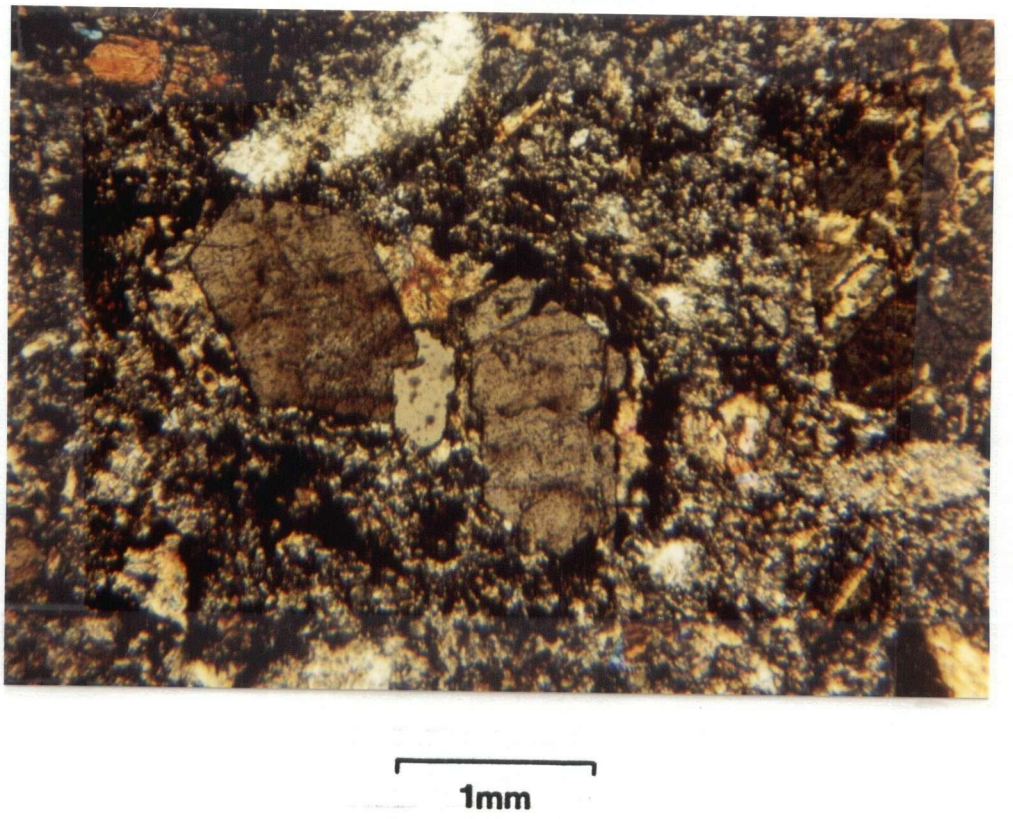

Figure 18: Euhedral apatite crystals with rims of fibrous epidote. (Crossed polars)

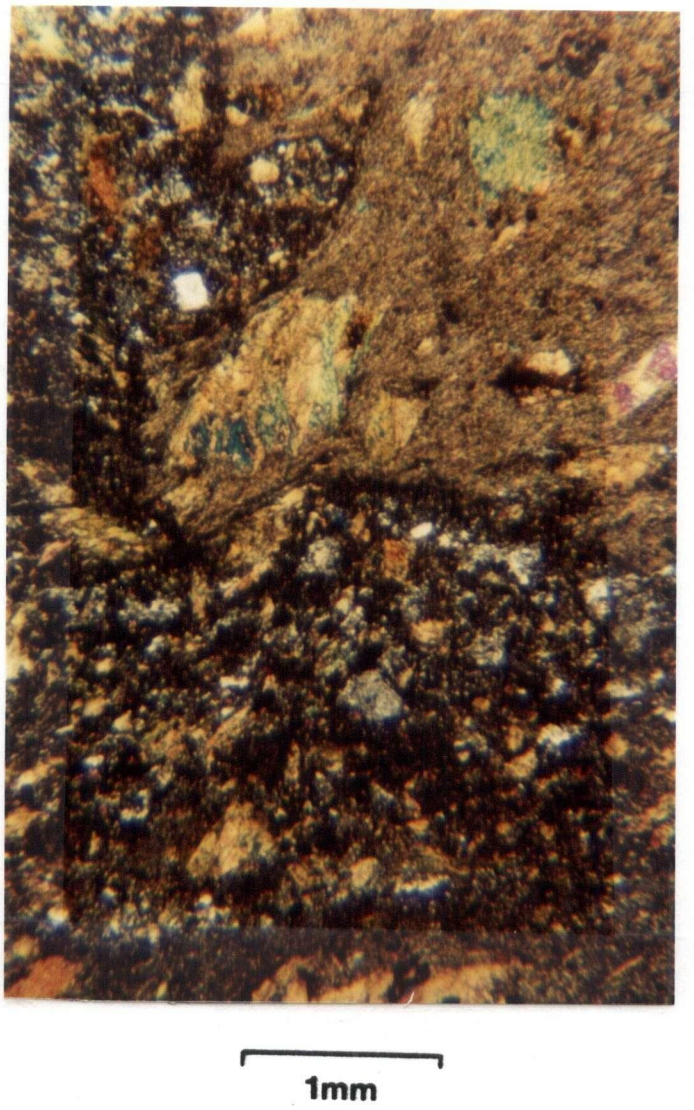

Figure 19: Porphyritic volcanic clast supported by a tuffaceous matrix. (Crossed polars)

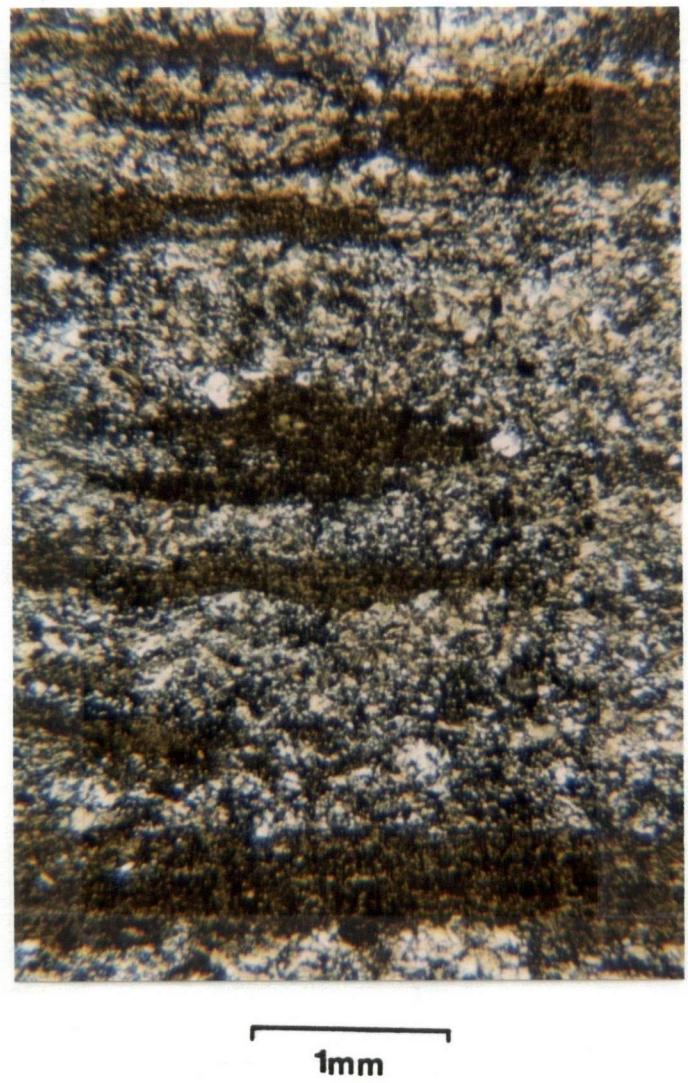

Figure 20: Photomicrograph of stringy, chloritic fragments within a calcareous tuff. Chlorite and calcite comprise the groundmass assemblage. (Crossed polars)

3.1.1.2. Volcanic flows and breccias

The volcanic flows and breccias to the south and east of Eureka Peak are characterized by coarsely porphyritic flows, fine grained tuffs, and local volcanic breccia. Tuffaceous horizons are more prevalent within this particular unit than within the adjacent volcanic flows and flow breccias.

The primary phenocryst assemblage of this unit consists of hornblende, pyroxene and plagioclase (An 44–46). Hornblende phenocrysts are euhedral to subhedral in form, twinned and well zoned (Fig. 21). Flow textures are well preserved in thin section and are probably enhanced by later tectonism. The groundmass assemblage consists of quartz, plagioclase, epidote, sericite and actinolite. Actinolite occurs as fine needles throughout the groundmass and partially enveloping hornblende crystals. Primary pyroxene phenocrysts are completely pseudomorphed by amphibole, probably tremolite–actinolite. Plagioclase phenocrysts of andesine composition are nearly completely replaced by retrograde sericite and epidote. In general, this stratigraphic unit is more enriched in quartz and feldspar than the volcanic flows and agglomerates adjacent to it.

Texturally the volcanic flows and breccias are hypidiomorphic granular to glomeroporphyritic in thin section. The large breccia fragments observed in outcrop (Fig. 15) occur as glomeroporphyritic clasts in thin section, and are composed of hornblende and pyroxene. As with the pyroxene phenocrysts, the pyroxene within the clasts have been pseudomorphed by amphibole. Retrograde chlorite is also present.

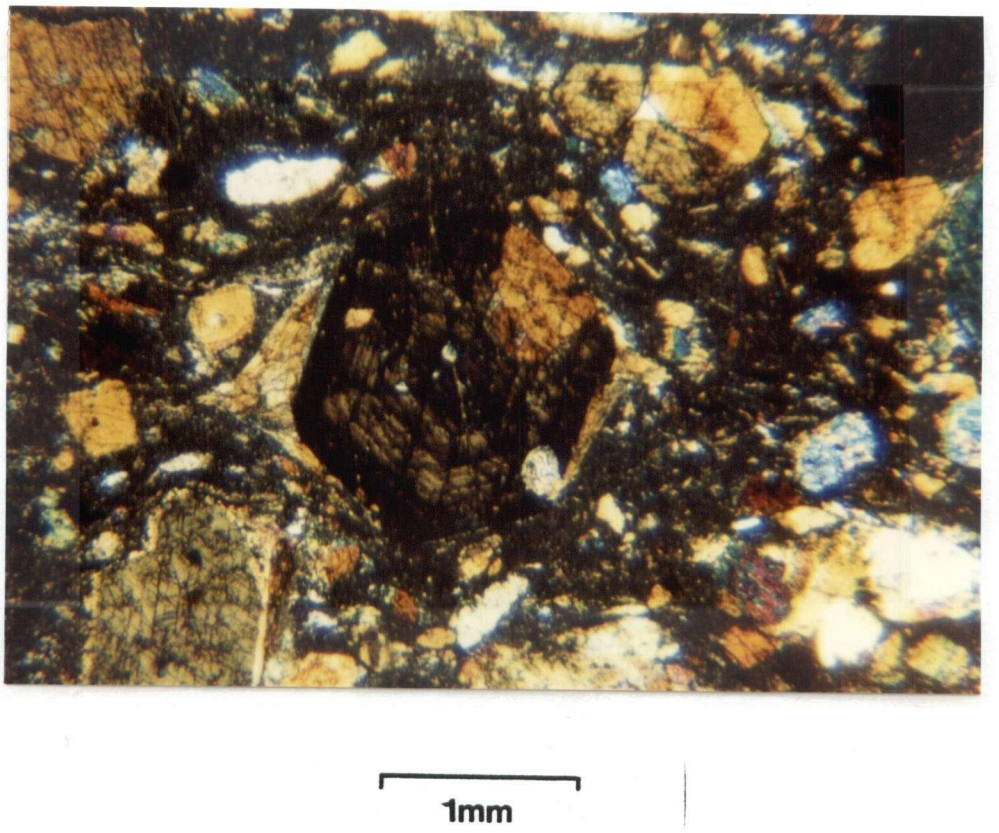

Figure 21: Photomicrograph of zoned, euhedral hornblende phenocryst in a coarsely porphyritic flow. A preferred fabric orientation may be a relict of original flow textures. (Crossed polars)

3.1.2. Volcanic rocks west of Eureka Peak

3.1.2.1. Volcaniclastic breccia

The volcaniclastic breccia is a very distinctive unit immediately underlying the volcanic flows exposed to the west of Eureka Peak. Petrographically, this unit is characterized by a fine grained tuffaceous matrix supporting angular lithic fragments and pumice fragments.

The mineralogy of the matrix is similar to the surrounding volcanic flows. Subhedral to anhedral plagioclase, clinopyroxene and minor hornblende comprise the phenocryst assemblage. The groundmass assemblage consists of primary plagioclase, quartz, epidote and actinolite. The lithic fragments are represented by pumice fragments, volcanic fragments and minor argillaceous fragments. All fragments are angular and range in size from less than 1 mm to 2 cm. Pumice fragments are now completely altered to fine grained micas (Fig. 22). Texturally the unit is very fragmental. Lithic fragments are supported by a matrix consisting of subhedral and fragmented phenocrysts and a fine grained groundmass.

3.1.2.2. Basal flows, tuffs and flow breccias

Mineralogically the flows and flow breccias in the western section of the study area are very similar to those in the eastern section. Texturally, however, the flows of the western section contain more abundant but smaller phenocrysts than their analogs to the east. Discontinuous tuffaceous horizons are also more prevalent to the west.

Primary phenocrysts are plagioclase (An 44–46), and clinopyroxene, plus or minus hornblende. Actinolite and biotite and/or chlorite are abundant, replacing both pyroxene and hornblende. Actinolite forms acicular to fibrous needles and rhombs

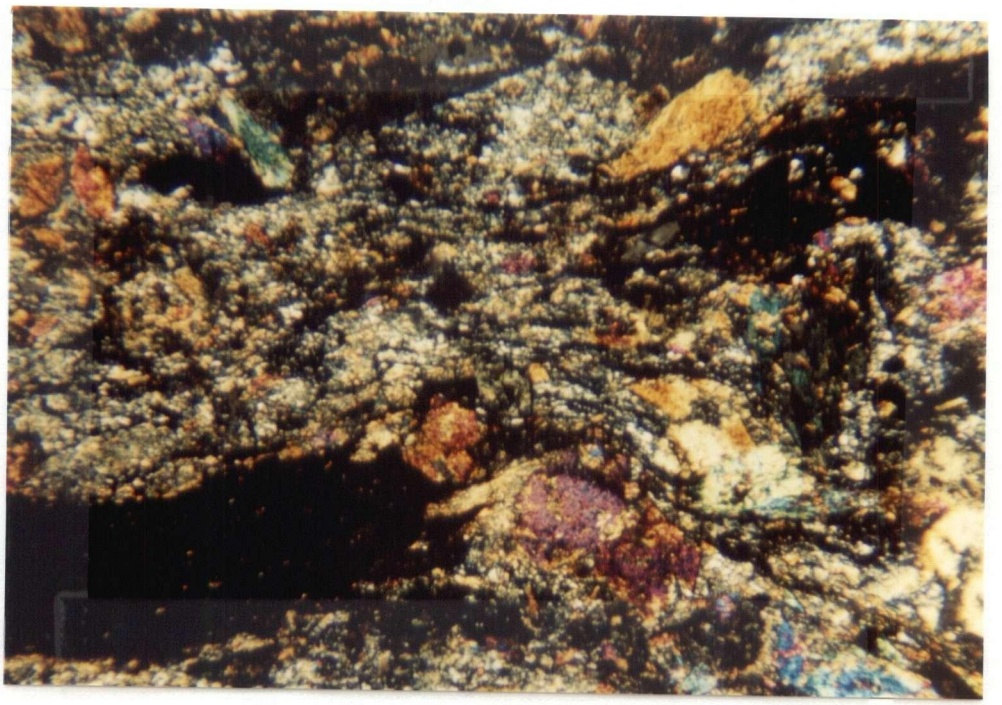

Figure 22: Photomicrograph of pumice fragment within the volcaniclastic unit, with characteristic frayed and flame–like terminations. (Crossed polars)

randomly oriented within the groundmass. Plagioclase and quartz occur as groundmass phases. Sericite, carbonate and clinozoisite are pervasive groundmass minerals produced during alteration of plagioclase. Fine, fibrous chlorite and sericite are associated with the replacement of small lithic fragments and pumice fragments. Accessory minerals include apatite, and opaques.

Tuffaceous horizons are similar mineralogically to the flows with which they are associated. Texturally however, the tuffs are fragmental and consist of broken, anhedral grains and lithic fragments supported by a fragmental groundmass. Groundmass mineralogy consists of quartz and plagioclase. Retrogression of plagioclase to epidote and carbonate is pervasive. In some samples the groundmass mineralogy is completely epidotized.

3.2. MAJOR AND TRACE ELEMENT GEOCHEMISTRY

Major and trace element geochemical analyses provide data which can be used to evaluate the chemical character of the rocks analyzed. Discriminant diagrams, in the form of binary and ternary plots emphasize chemical trends characteristic of particular volcanic suites. They are also used to differentiate rocks from specific tectonic environments (Irvine and Baragar, 1971; Pearce and and Cann, 1973; Miyashiro, 1974; Floyd and Winchester, 1975, 1978; Beccaluva et al. 1979; Shervais, 1982; Pearce 1982).

Samples were analyzed for major and trace element abundances by XRF analysis in the Department of Oceanography, at the University of British Columbia. Sample preparation and analytical procedures are detailed in Appendix 1. Reduced geochemical data is presented in Appendix 2. The objectives of performing major and trace element studies on the Takla Group volcanics were:

1. To geochemically characterize the major lithologic units within the volcanics differentiated by field studies.
2. To attempt to place the Takla Group rocks into a tectonic framework based on the use of discriminant diagrams.

3.2.1. Major element diagrams

Three major element diagrams have been chosen to distinguish the major volcanic suites. Each diagram is discussed with reference to the chemical trends observed. Interpretation of the diagrams with reference to petrography and field relations is discussed in section 3.3.1.

3.2.1.1. **Alkaline vs. subalkaline rocks:** *(K_2O + Na_2O) vs. SiO_2*

A plot of total alkalies versus silica was used to distinguish between rocks of alkaline and subalkaline compositions (Fig. 23). All samples plotted within the subalkaline field described by Irving and Baragar (1971), with the exception of one sample which plotted on the field boundary. According to the curve defined by MacDonald (1968), two samples plotted within the alkaline field. Petrographically, the samples show pervasive secondary alteration, and fractures filled by epidote, calcite, quartz and actinolite. In light of this, the anomalous points should probably be disregarded. In addition, K and Na are known to be relatively mobile, and therefore their concentrations can easily be influenced by alteration and metamorphism. The samples plotted follow a straight line trend over the range of silica values.

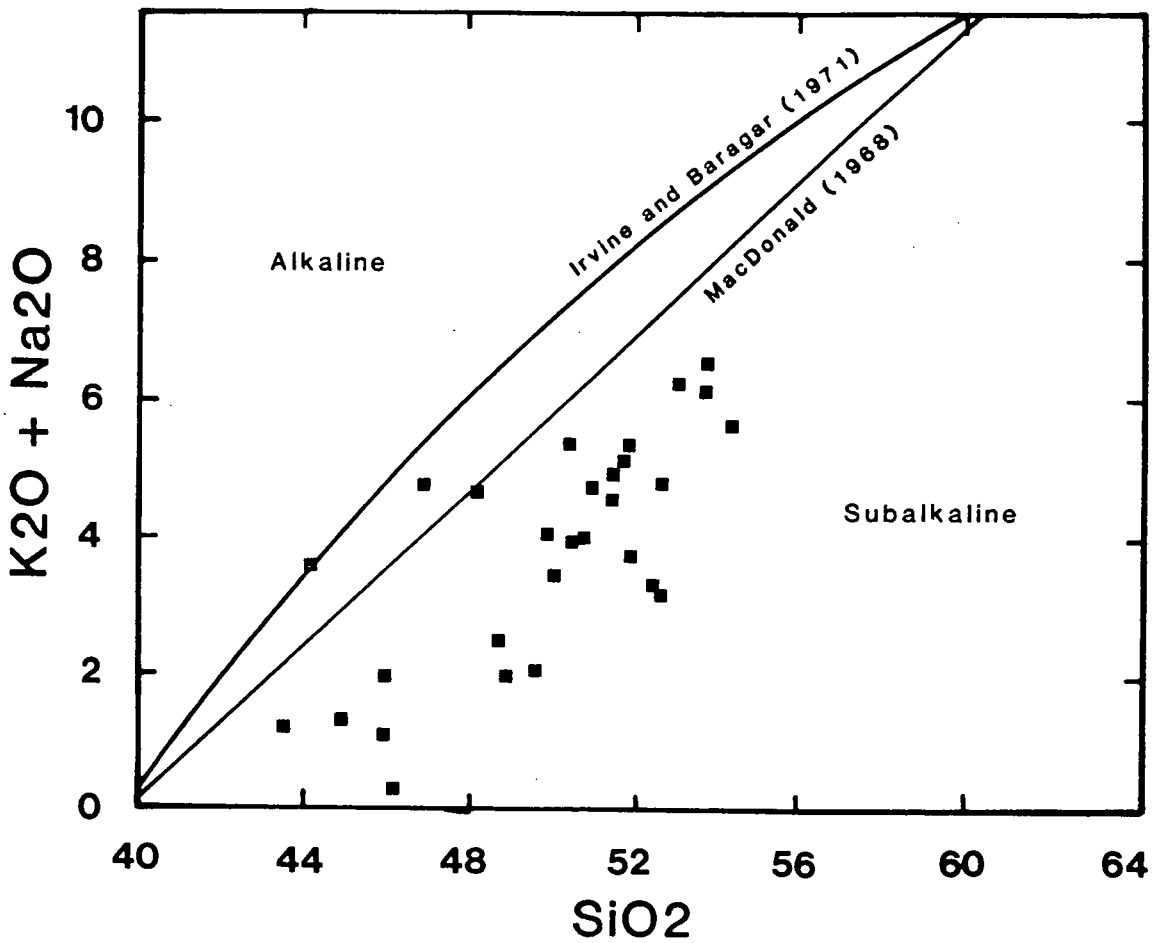

Figure 23: Plot of K_2O + Na_2O versus SiO_2 differentiating alkaline and subalkaline fields, after Irvine and Baragar (1971) and MacDonald (1968).

3.2.1.2. **Calcalkaline vs. tholeiitic:** *FeO/MgO vs. SiO_2; AFM*

Two diagrams were used to separate the calcalkaline and tholeiitic series of subalkaline rocks. The two fields are distinguished by iron enrichment trends during differentiation. Pronounced iron enrichment or lack of enrichment are characteristic of the tholeiitic and calcalkaline series, respectively.

Samples are almost equally divided between the two fields on the FeO/MgO vs. SiO_2 diagram of Miyashiro (1974) (Fig. 24). The iron enrichment trends observed in the samples seem to more closely follow that of the calcalkaline series as defined by Kuno (1968).

On the AFM (Fig. 25) diagram samples are almost equally divided between the two fields. Approximately 36% of the samples plot within the calcalkaline field and five samples plot on the boundary between the two fields as defined by Irvine and Baragar (1971). Irvine and Baragar (1971) also noted that the Al_2O_3 contents of tholeiitic and calcalkaline rocks differed systematically. Basalts and andesitic rocks of the tholeiitic series typically have Al_2O_3 contents of 12–16%, and calcalkaline rocks are more aluminous with average Al_2O_3 contents of 16–20wt%. All samples analyzed from the Eureka Peak area contain less than 16wt% Al_2O_3 with the exception of one sample which contains 16.45wt% Al_2O_3. Therefore, the rocks within the Eureka Peak area seem to be more tholeiitic in character.

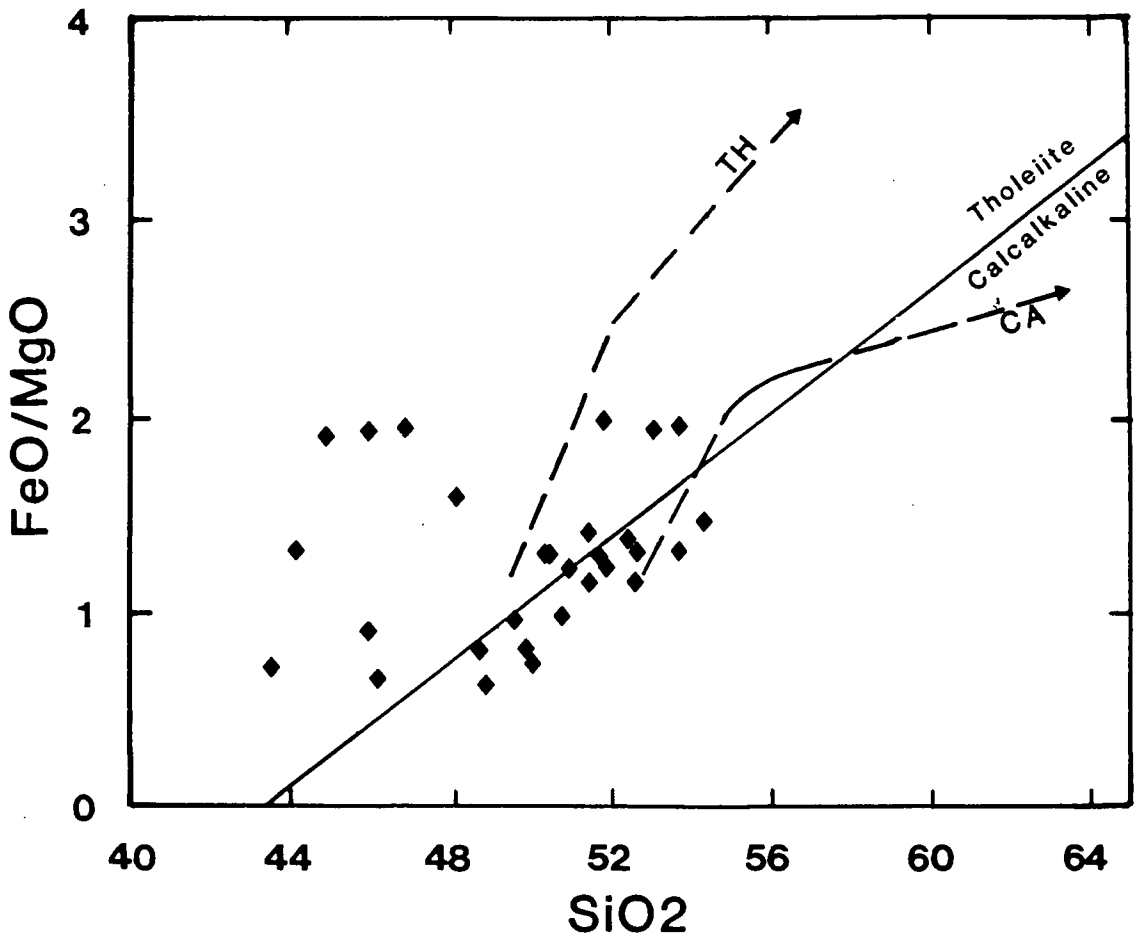

Figure 24: Plot of FeO/MgO versus SiO_2 diagram: the solid line defines the two fields (Miyashiro, 1974); dashed lines represent the differentiation trends of Fe, characteristic of each field, after Kuno (1968).

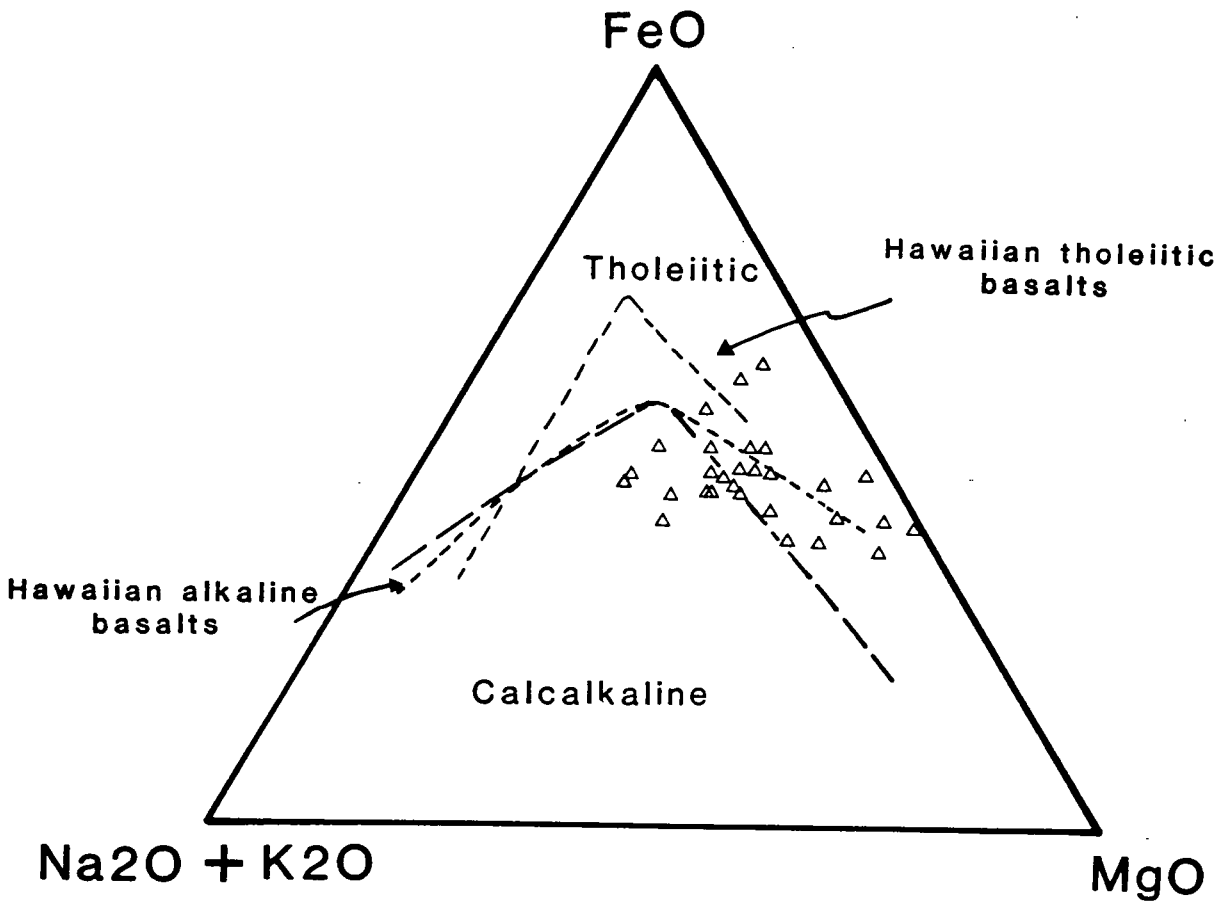

Figure 25: AFM plot distinguishing the tholeiitic and calcalkaline fields. Differentiation trends of Hawaiian tholeiitic and alkaline basalts are shown, after Irvine and Baragar (1971).

3.2.2. Trace element diagrams

Four discriminant diagrams have been chosen to evaluate the petrotectonic setting of the Takla Group volcanics. What follows is a presentation of the chemical trends observed on each plot. Interpretation of the data is presented in section 3.3.2.

3.2.2.1. TiO_2-ZR-Y

The TiO_2-Zr-Y diagram separates four tectonic environments (Pearce and Cann, 1973): 1.) WPB - within plate basalts, 2.) CAB - calcalkaline basalts, 3.) LKT - low K-tholeiites and 4.) MORB - mid-ocean ridge basalts.

The plot of TiO_2-Zr-Y (Fig. 26) reveals that most samples plot within the low K-tholeiite field. Nine points plot outside of the four defined fields, and one point plots on the upper boundary of the WPB field.

3.2.2.2. Ti vs. V

The plot of Ti vs. V (Shervais, 1982) discriminates between three different tectonic environments for tholeiitic and alkaline basalts (Fig. 27). Each field is bounded by the Ti/V ratio characteristic of each environment. Basalts of convergent margin affinity have Ti/V ratios in the range of 10-20; MORB have Ti/V ratios in the range of 20-50, and WPB have Ti/V ratios of 50-100.

Of the tholeiitic samples plotted, several plot within the ARC field, and the majority plot within the MORB field.

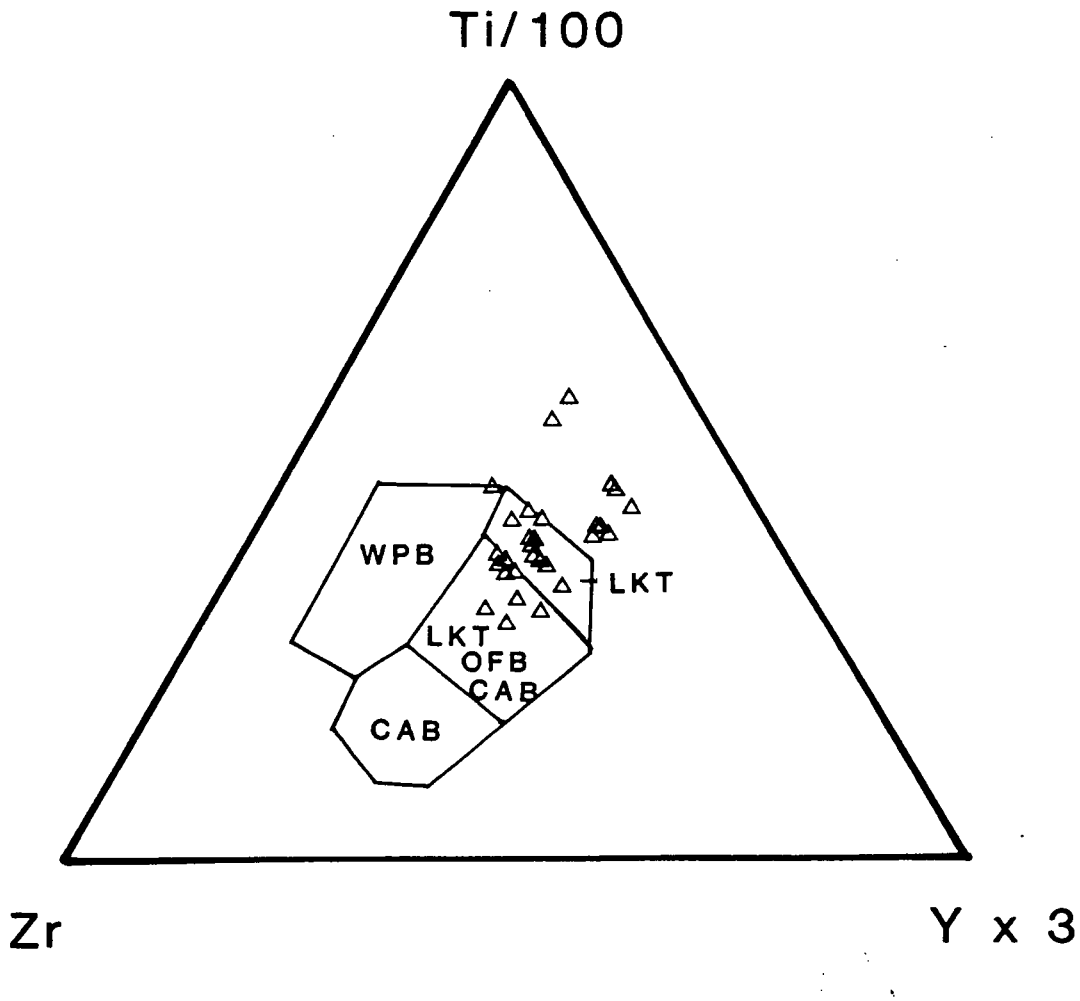

Figure 26: Ti - Y - Zr discriminant plot, distinguishing four separate tectonic environments. (Pearce and Cann, 1973)

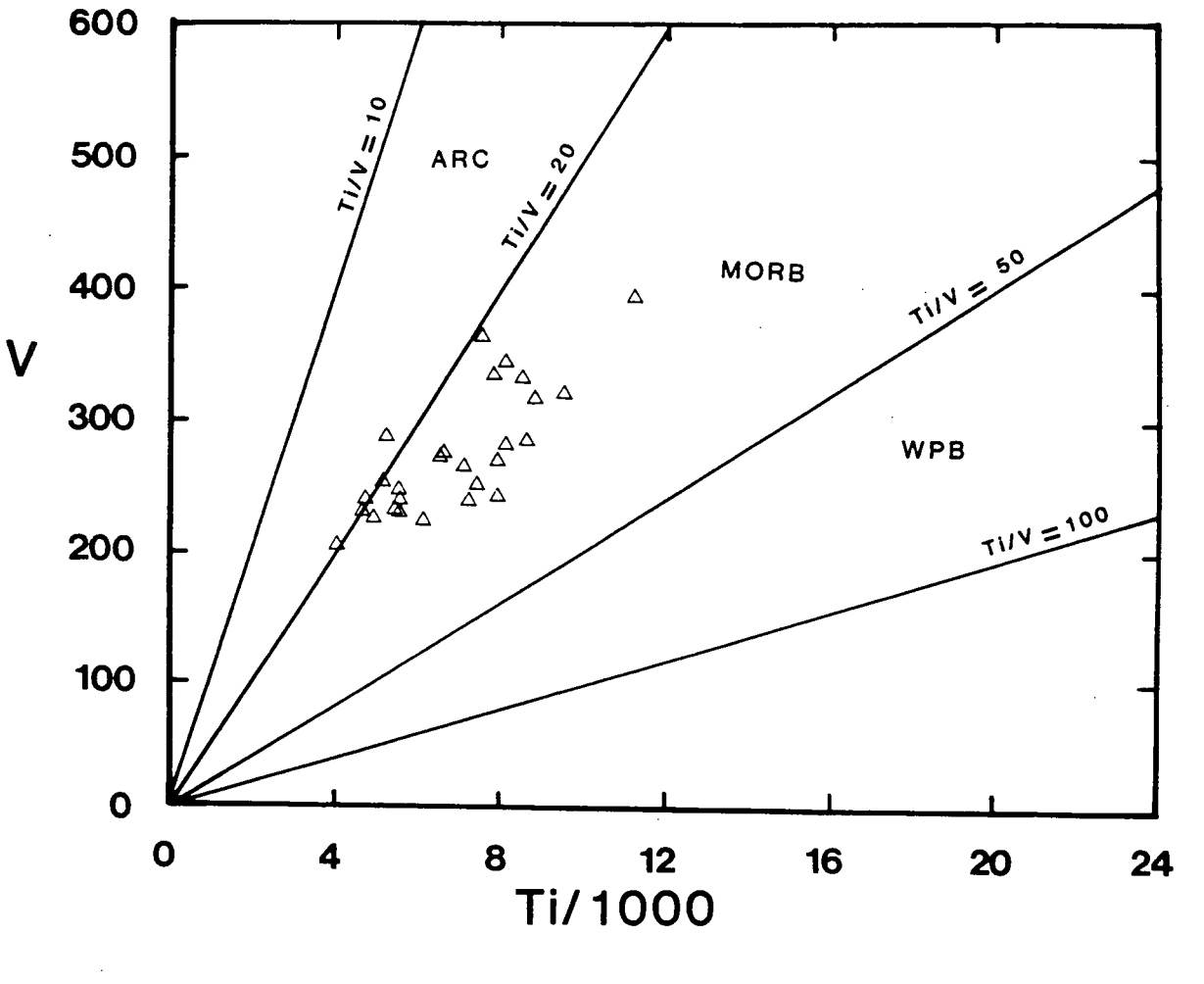

Figure 27: Discriminant plot of V versus Ti/1000 distinguishes arc, mid-ocean ridge basalts (MORB), and within plate basalts (WPB). (Shervais, 1982).

3.2.2.3. Ti/Cr vs. Ni

The plot of Ti/Cr vs. Ni differentiates island arc tholeiites from mid-ocean ridge basalts (Beccaluva et al. 1979). The distribution of samples plotted is along a line parallel to the boundary between the two fields (Fig. 28). The boundary itself is parallel to the trend of fractional crystallization, and increasing differentiation will tend to displace the data to the upper left with lower Ni contents and higher Ti/Cr ratios.

3.2.2.4. Cr vs. Y

The Cr vs. Y diagram distinguishes convergent margin from MORB and WPB (Fig. 29). The convergent margin field is well-defined although there is a region of overlap with the two latter fields and the high edge of the convergent margin field (Pearce, 1982). All points plot within the convergent margin field. And though some points plot close to the region of overlap, no points plot within that region.

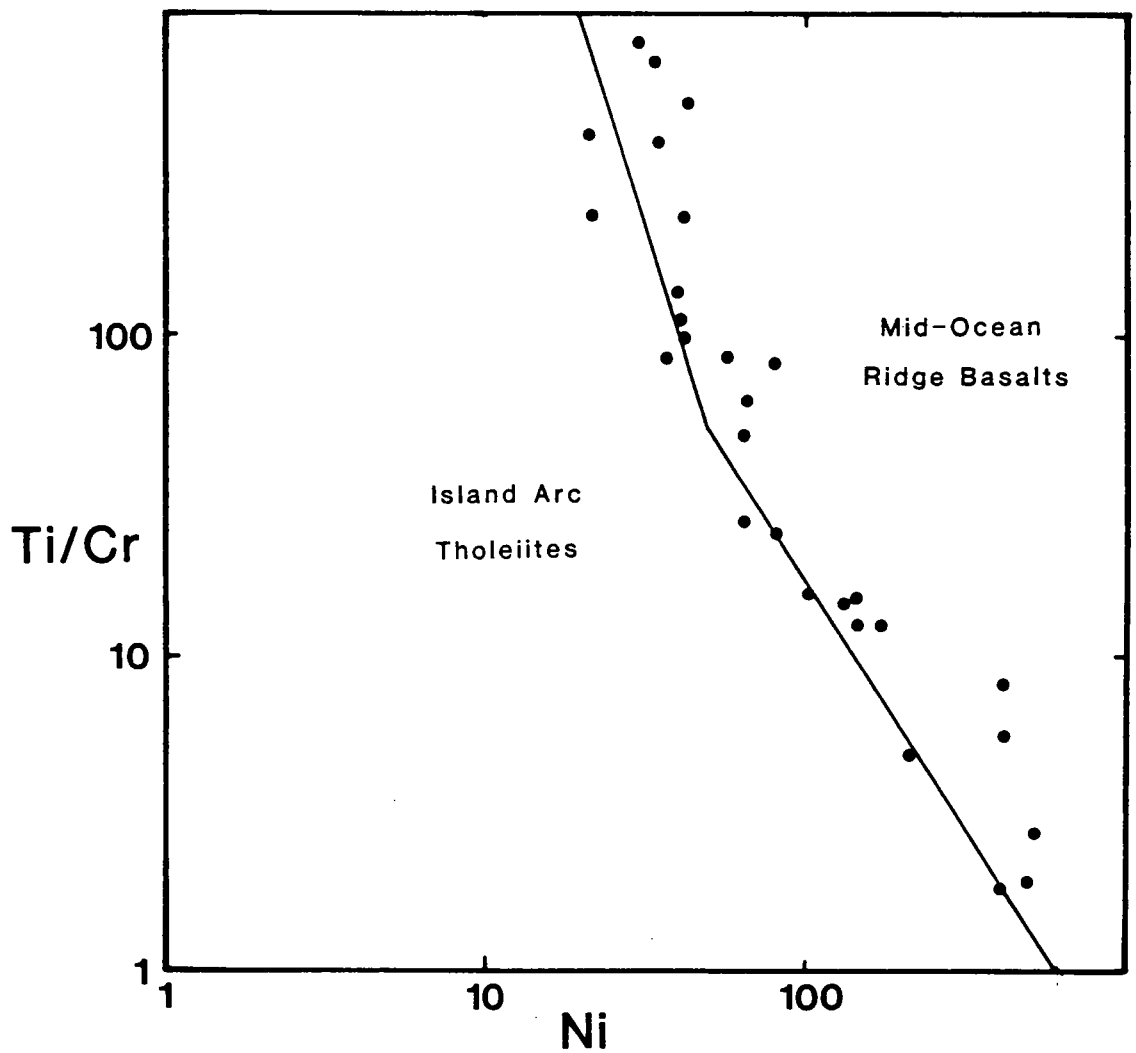

Figure 28: Discriminant plot of Ti/Cr versus Ni, distinguishing mid-ocean ridge basalts and island arc tholeiites. (Beccaluva, Ohnenstetter, and Ohnenstetter, 1979).

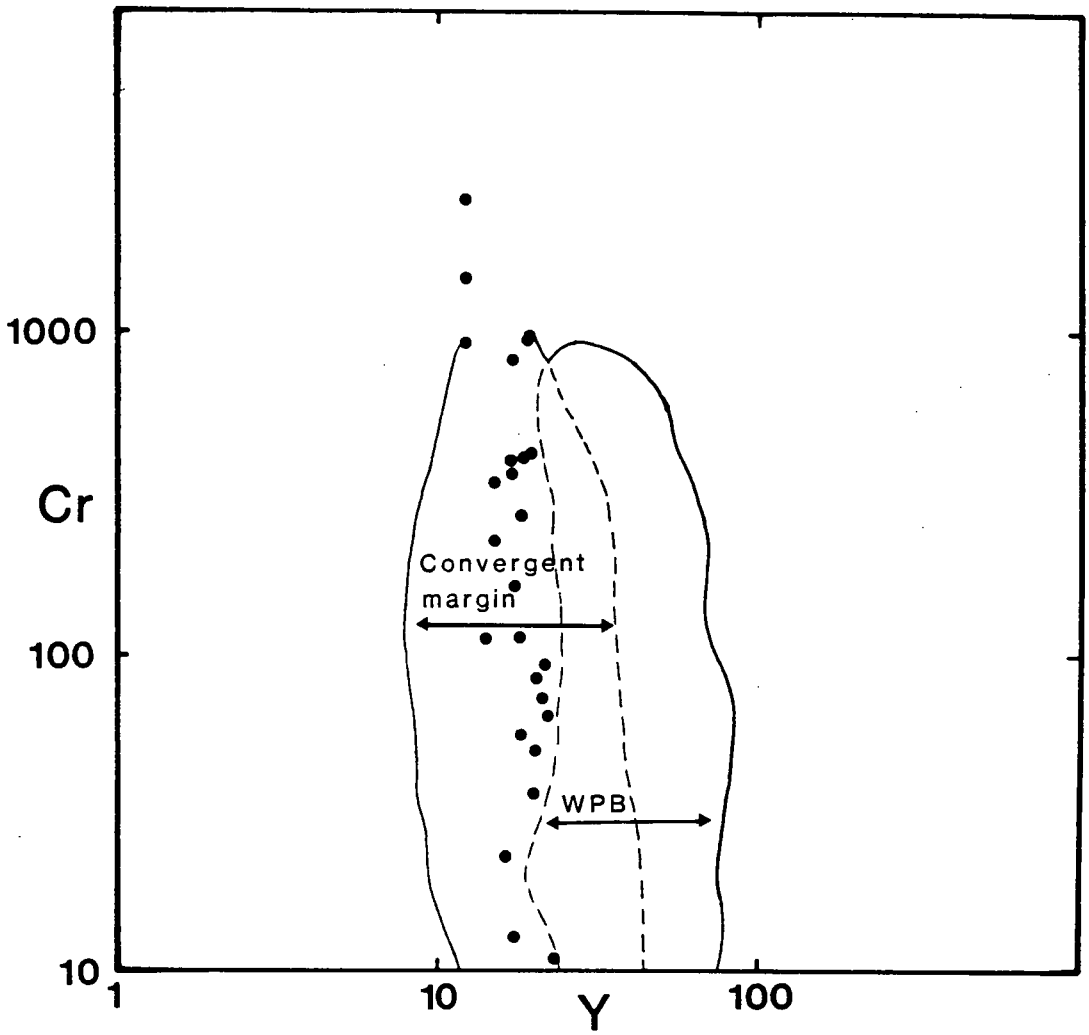

Figure 29: Discriminant plot of Cr versus Y distinguishing convergent margin basalts from within plate basalts. (Pearce, 1982).

3.3. DISCUSSION AND SUMMARY

3.3.1. Chemical distinction based on major elements

Major element diagrams are used to chemically distinguish between the major volcanic suites defined by Irvine and Baragar (1971). Plots of total alkalies versus silica distinguishes between the alkaline and subalkaline series. As shown in Figure 23, the majority of samples plot well within the subalkaline field of the diagram. This classification is supported by macroscopic and petrographic observation. The prevalence of quartz and associated silica-saturated minerals, such as plagioclase, amphibole, and pyroxene, is diagnostic of subalkaline rocks (Best, 1982). Relatively low concentrations of alkalies (Na + K) relative to silica also suggest subalkaline affinities. In addition, the subalkaline rocks are more characteristic of orogenic areas; alkaline volcanics are generally associated with more passive tectonic setting, such as interplate rifts.

Further distinction between the tholeiitic and calcalkaline series within the subalkaline suite is established by the FeO/MgO vs. SiO_2 diagram (Fig. 24) and by the AFM diagram (Fig. 25). Figure 24 shows the samples nearly equally divided between the two fields. Samples with relatively high or low Fe/Mg ratios show no correlation to particular lithologic units. Both the Fe and Mg ratios of the samples seem relatively high compared to published compositions of average tholeiitic and calcalkaline rocks (Wilkinson, 1986) and Mg content will have a significant effect on the plot. Petrographic studies suggest that the presence of abundant chlorite correlates positively with the elevated Mg concentrations. The effect of the higher Mg concentrations is to pull the samples downward for any given silica content, into the calcalkaline field. Alternatively, higher Fe concentrations might pull the samples toward the tholeiitic field. If the volcanics are believed to represent a relatively closed system

during metamorphism and alteration, it remains unclear why exactly the values remain higher than those expected for average tholeiites and calcalkaline rocks.

The AFM diagram shows a similar effect. Approximately 8 of the 29 samples plot distinctly within the calcalkaline field while the remainder plot inside the tholeiitic field with intermediate FeO/MgO ratios. Those samples which plot in the calcalkaline field contain a higher modal percent plagioclase suggesting possible plagioclase enrichment during differentiation. The effect of plagioclase enrichment will pull the samples toward the lower left of the ternary plot and into the calcalkaline field. Petrographically, the primary mineralogy of the volcanics seems more characteristic of the calcalkaline suite. Particularly, the relative abundance of primary hornblende suggests stronger calcalkaline affinities (Wilkinson, 1986; Cawthorn and O'Hara, 1976).

The major element diagrams alone do not conclusively differentiate the calcalkaline and tholeiitic fields of the samples plotted. A number of factors could contribute to the spread of data points between the two fields. A major factor is evaluating how closely the analyzed chemistry is to the original chemistry of the rock. The mobility of the elements during metamorphism and alteration is relatively unknown. It is possible that reactions are, at least in part isochemical, but this is certainly not true in all instances. Structural studies (Chapter 4) suggest that pore fluids played a prominent role in the structural and metamorphic history of the area. Such pore fluids could potentially remobilize elements, and effectively alter the original chemical character of the rock.

3.3.2. Chemical distinctions based on trace elements

Trace elements provide a potentially useful tool for determining petrotectonic environments of volcanic suites. Certain trace elements have been found to remain relatively immobile during alteration and low grade metamorphism, or to vary systematically depending upon environment of formation and subsequent conditions (i.e., metamorphism and/or alteration). Work by Floyd and Winchester (1975), Pearce (1982), and Pearce and Cann (1973) have investigated the relationships of the incompatible trace elements to establish which elements may be used to successfully discriminate between various tectonic environments. There are two important limitations to the application of the trace element discriminant diagrams are:

1. Though the elements are thought to be immobile, the behavior of each element is not well known under natural conditions of metamorphism and alteration.
2. Fields thought to be diagnostic of each particular tectonic environment are limited by the number of samples plotted to date in the published literature.

The diagrams chosen were selected on the basis of their ability to effectively discriminate the samples into a tectonic setting that could be supported by geologic and petrologic observations (Erdman, 1985). Previous workers in the Quesnel Lake region have proposed that the Takla Group rocks were derived from an island arc environment. Therefore the diagrams used are designed to identify rocks of arc-type affinity and to give some clues about particular settings within the arc environment.

The TiO_2-Zr-Y diagram includes 65.5% of the data within the low-K tholeiite field (Fig. 26). Low-K tholeiites are typical of the earliest volcanic activity of an arc (Jakes and Gill, 1970). This suggests that the volcanics within the Eureka Peak area may represent an immature arc sequence.

Recent work by Shervais (1982) has established a systematic variation of the

Ti/V ratio with tectonic environment. The plot is based on the crystal/liquid partition coefficients of vanadium and titanium. Figure 27 shows that the Ti/V ratios of the samples plotting in the 18–33 range, within the MORB field, or straddling the boundary between the ARC and MORB fields. Arc-type rocks generally have Ti/V ratios ranging from 10 to 20. In contrast, back arc basin basalts may have ratios ranging from 10 to 50. It is postulated that a spread such as observed in figure 27 may be diagnostic of a back arc setting (Shervais, 1982). This is particularly true if the samples are from a relatively small geographic area.

The plot of Ti/Cr vs. Ni (Fig. 28) also provides interesting results. Samples plot parallel to the boundary between the island arc tholeiites and mid-ocean ridge basalts. Island arc tholeiites are defined by the broad field with low Ti/Cr ratios for any given Ni content. From the work of Beccaluva et al. (1979), points lying parallel to the boundary but within the MORB field are typical of samples derived from marginal basin environments; whereas data plotting along the boundary are derived from known forearc settings. Generally the data support an island arc origin for the Takla Group rocks with a possible basin association.

The Cr vs. Y (Fig. 29) plot differentiates between two major tectonic environments: basalts associated with convergent margins versus those associated with continental volcanism. All data points plot within the convergent margin field. In addition to the chemical distinction, a within-plate origin for the Takla Group volcanics can be ruled out by field relations and particularly the association of the volcanics with the sediments of deep water affinity, such as turbidite sequences represented by the Quesnel River Group sediments.

3.3.3. Summary

Application of major and trace element geochemistry and the use of discriminant diagrams for rocks within the Eureka Peak area is limited by two important factors:

1. The effectiveness of the diagrams to accurately distinguish petrotectonic environments of rock samples is strongly related to the freshness of the samples. The Jurassic age of the Takla Group rocks therefore will certainly test the confidence limits of the diagrams.
2. The volcanics in the Eureka Peak area have been metamorphosed to lower greenschist facies. Although the elements used in the diagrams are thought to be relatively immobile during metamorphism and alteration, volcanic rocks of this grade are not adequately represented in the literature to confirm the effectiveness of the diagrams under these conditions.

It is apparent from this study that the diagrams alone are of limited reliability in differentiating the rock classifications. The trace element diagrams were more successful in placing the samples within the fields expected from field relations. However, those diagrams were chosen specifically because of their ability to distinguish rocks of island arc affinity. In conclusion, it is essential that the geochemical results are interpreted with regard to the geologic and petrologic observations. When considered in this manner discriminant diagrams can be a potentially useful and informative tool for determining tectonic settings for suites of older volcanic rocks. For the Takla Group rocks in the Eureka Peak area, geochemistry supports previous interpretations of an island arc origin, and suggests possible back arc basin or marginal basin affinities.

4. STRUCTURE

The Eureka Peak area is characterized by a complex deformational history, involving the folding and fracturing of a mechanically heterogeneous lithologic sequence. Structural investigations involved observations at the mesoscopic and microscopic scale. Field studies focussed on establishing the nature, orientation, and distribution of structural elements. The relationships of bedding, cleavage and linear structures to folds, fractures and faults were examined in detail to determine the relative timing of structural events, their geometry and kinematic history. Microscopic studies concentrated on determining the nature and development of cleavage and fractures, and evaluation of their relationship to the relative timing of the development of mesoscopic structures. Microscopic studies also focussed on establishing the relationship of the microstructures to metamorphic events.

Structural analysis of the Eureka Peak area in the following discussion is based upon the identification of the prominent structural elements and their manifestations at both the mesoscopic and microscopic scale. Both the orientation and the intensity of development of the structural elements is influenced by the relative competency of the lithology, in addition to position with respect to the major structure. Observations of overprinting relationships of the various structural elements is used to determine the relative timing of structural events. Careful examination of textural relationships observed in thin section allows inferences to be made regarding deformation mechanisms and partitioning of strain during the deformation history.

4.1. STRUCTURAL ELEMENTS

4.1.1. Bedding

Compositional layering is the dominant feature comprising bedding throughout the Quesnel River Group metasediments, and can be locally discerned within the Takla Group metavolcanics. Thin quartz sandstone beds (2 mm - 2 cm thick) comprise compositional layering within the black phyllite succession and are interbedded with fine grained argillaceous sediments. Grain size within the quartz sandstone beds varies from fine silts to sand-sized particles. A parallel colour lamination accentuates a stratification within individual sandstone beds, defined by subtle compositional variations. The interbedded argillaceous sediments are composed dominantly of muds, and fine silt-sized grains. Argillaceous sediments dominate the phyllitic succession; bed thickness ranges from a scale of centimetres to metres. Where the distinctive pale quartz sandstones are absent, bedding variations within the argillaceous sediments are defined by subtle changes in colour and/or grain size of the sediments.

Interbedding of argillaceous sediments with fine grained volcaniclastics, limestone and sandstone comprise the compositional layering within unit 7. Primary bedding structures include cross-bedding, loading structures, and grading (Fig. 30). Colour banding within the siliceous tuffs and within the slates of unit 7b is prominently developed locally. Bedding features within the Takla Group volcanics are represented by flow contacts and locally developed trachytic textures. The rare flow contacts observed are sharp and locally show loading structures. The lithologic contacts are only traceable over short distances due to rapid facies changes within the volcanics. Contacts between flows and tuffs are sharp.

(a)

(b)

Figure 30: Primary sedimentary structures observed in the field include: a.) cross-bedding within unit 7, and b.) small scale loading structures in unit 7.

4.1.2. Cleavage

Field studies have identified two types of cleavage: a penetrative and non-penetrative cleavage (Fig. 31). Cleavage is most prominently developed within the Quesnel River Group metasediments. A weakly developed foliation is observed within the Takla Group metavolcanics, that is penetrative locally, within very fine grained tuffs. The most prominent cleavage is defined by a penetrative slaty to phyllitic foliation. A second, non-penetrative cleavage occurs as a spaced cleavage, locally a crenulation cleavage. Concentration of insoluble materials along the cleavage planes indicate that they are dissolution-type cleavages. Limited dissolution has occurred along the crenulation cleavage surfaces, where crenulations are very tight and resemble the differentiated crenulation cleavage of Williams (1972).

The slaty to phyllitic cleavage within the black phyllite succession occurs as closely spaced planes. Spacing of individual cleavage planes varies from approximately 0.01 mm to 0.1 mm. They are defined by a fine micaceous to graphitic parting within the metasediments, and a chloritic parting in the volcanics. The cleavage is developed axial planar to mesoscopic and microscopic folds of bedding, striking to the northwest, and dipping variably to the northeast and southwest. Individual cleavage surfaces vary from planar surfaces to undulatory or anastomosing surfaces. A planar parting defines the cleavage within the more siliceous or slaty sediments. Within the finer grained sediments, the penetrative foliation occurs as more closely spaced anastomosing surfaces outlined by a micaceous to graphitic parting. Cleavage stripes are outlined by a darker colouration within and adjacent to the cleavage plane. In figure 32 subtle cleavage stripes are developed along the slaty cleavage and small scale folds of bedding outline rootless isoclines. These features are interpreted to be the result of extensive dissolution along the cleavage surface. Small quartz filled fractures occur parallel or subparallel to

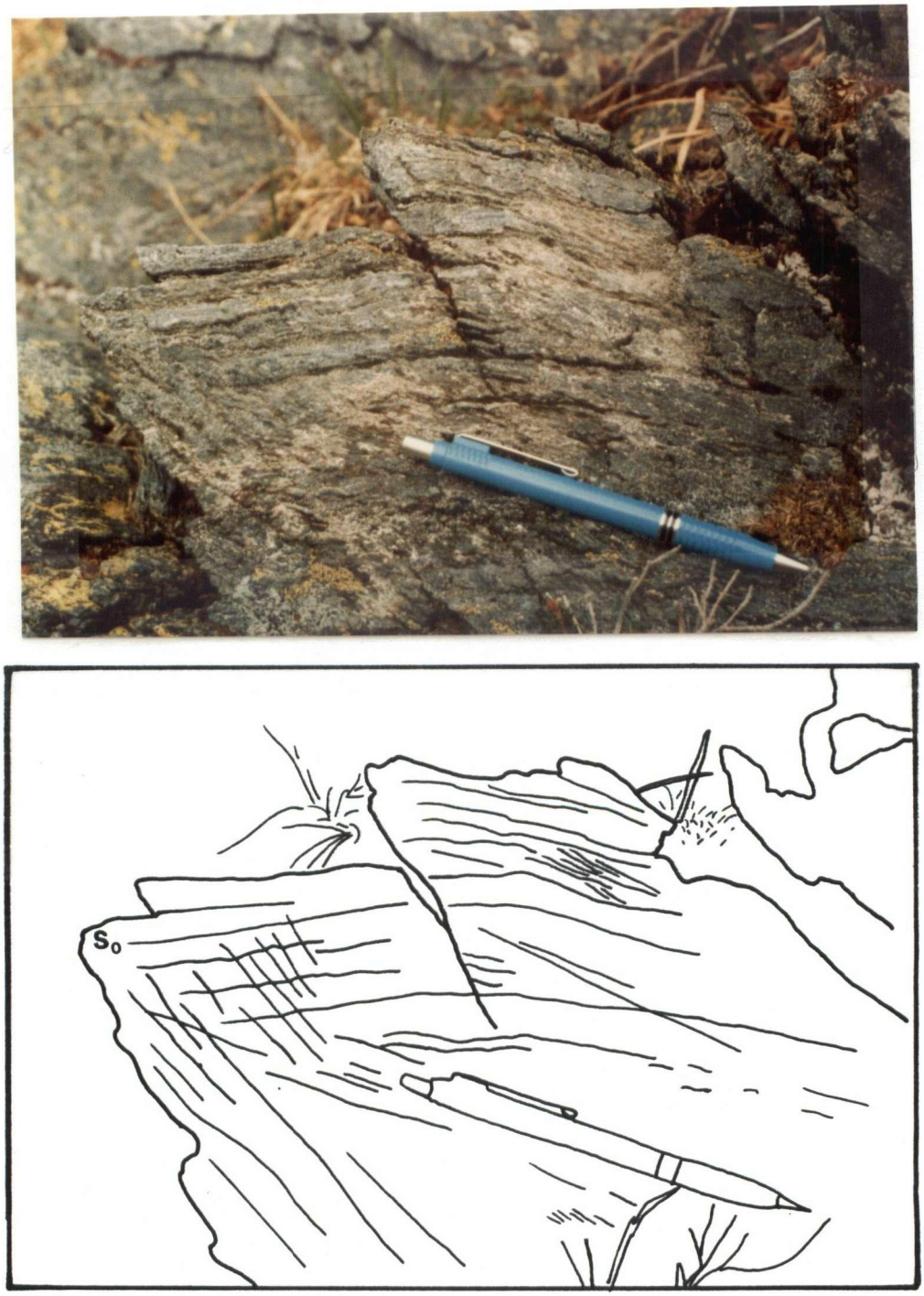

Figure 31: Two cleavage morphologies are recognized: a penetrative, slaty cleavage is developed subparallel to bedding (S_0), and parallel to the pencil. A spaced cleavage is oriented at a higher angle and crenulates bedding.

Figure 32: Development of fine cleavage stripes parallel to the axial plane of a small fold of bedding. Extensive pressure solution along the cleavage surface is responsible for the dissolution of bedding.

bedding and within the hinge region of folds, and may be indicative of material remobilized by pressure solution processes. The penetrative cleavage is most strongly developed within the argillaceous sediments of the black phyllite sequence, and is poorly developed or absent within the coarser lithologies, particularly the overlying metavolcanics.

The non-penetrative cleavage occurs throughout the lithologic sequence, within both the metasediments and the metavolcanics. This cleavage is a dissolution-type cleavage, characterized by the concentration of insoluble material along the cleavage surface which is evident on both the mesoscopic and microscopic scale. Throughout the area the cleavage is northwest striking, and dips moderately to steeply to the northeast and southwest. Spacing of cleavage varies according to lithology and position on mesoscopic structures. It is more closely spaced within the hinge region of mesoscopic structures, and less closely spaced on the limbs. In addition, the individual cleavage planes are more closely spaced within the metasediments than within the volcanics. Spacing of individual planes varies from 1 mm to approximately 1.5 cm within the metasediments.

Cleavage within the Takla Group volcanics is very weakly developed, striking to the northwest, dipping steeply to the northeast or southwest or vertical. Throughout the volcanics, the cleavage is defined by a fine chloritic parting, and cleavage spacing varies from approximately 1-3 mm in very fine grained tuffs, to 3-4 cm in the coarser grained volcanics.

Refraction of cleavage surfaces is observed, and is prominent within the interbedded banded slates and tuffs of unit 7b. Cleavage refraction is pronounced at the contact between beds of differing competencies, such as a mudstone and a very siliceous tuff. Fanning of cleavage within the hinge region of mesoscopic folds is also

observed, and generally converges toward the hinge of the fold.

4.1.3. Lineations

Linear structures observed within the study area occur as mineral elongation lineations and intersection lineations. All linear features recognized are consistently northwest or southeasterly plunging at shallow to moderate angles, and are parallel to fold axes of local mesoscopic structures. Mineral elongation lineations are defined primarily by elongate quartz grains. Quartz grains appear as fine, fibrous smears, up to several centimetres in length.

Intersection lineations are defined by the intersection of two planar structural elements, and are prominent within the well-bedded portions of the Quesnel River Group. The line defined by the intersection of bedding with either of the two cleavages, or the line defined by the intersection of the slaty cleavage with the spaced cleavage comprises the intersection lineation. The most prominent intersection lineation observed within the area is defined by the intersection of bedding with one of the cleavage surfaces. Intersections of the two cleavages is also recognized, but is less prominent.

In one locality, quartz rods approximately 1 cm in diameter, and a minimum of 1 m in length define the lineation. The mineral lineations and the lineation defined by the intersection of bedding and slaty cleavage are both curvilinear in form (Fig. 33).

Figure 33: Mineral lineation defined by quartz rods. A S_0/S_1 intersection lineation is visible in the lower part of the photo.

4.2. MESOSCOPIC STRUCTURES

4.2.1. Folds

Folds of bedding are recognized throughout the area. The sense of asymmetry of mesoscopic folds indicates the presence of a synform of regional scale, referred to as the Eureka Peak syncline (Plate 1-geologic map). An axial plane parallel cleavage is always present, either as a penetrative or non-penetrative cleavage. The axial plane to mesoscopic structures is consistently northwest striking, and dips variably to the northeast and southwest. A mineral lineation, defined by elongate quartz grains, and a bedding/cleavage intersection lineation is developed parallel to the fold axis, plunging shallowly to moderately to the NW and SE. Limb lengths of mesoscopic folds vary in scale from tens of centimetres, as observed in outcrops, up to approximately tens of metres in length.

At lower structural levels folds are tight to isoclinal (Fig. 34), with a highly variable amplitude to wavelength ratio. Generally the folds have very long limbs, with relatively small, tight hinge regions. Axial planar cleavage dips shallowly to moderately to the northeast. Transposition of layering and local mesoscopic stratigraphic inversions are a consequence of the extreme tightness of the structures observed at the lower structural levels. Without more prevalent sedimentary way-up indicators, it is impossible to determine facing directions within individual transposed packages. Despite the local structural inversions, there appears to be no overall inversion within the mapped stratigraphy. Transposition is particularly pronounced within several tens of metres of the upper and lower contacts of the Quesnel River Group sediments with the Crooked Amphibolite and Takla Group rocks, respectively. At the contacts, deformation has been largely accomodated by the phyllites due to the contrast in the competency of adjacent

Figure 34: Tight to isoclinal folding is observed at the lower structural levels.

units.

At higher structural levels, and within the hinge region of the Eureka Peak syncline, the axial plane cleavage is more steeply inclined and folding becomes more open and upright (Fig. 35). The amplitude to wavelength ratio is approximately 1 to 2, and the folds take on a class 1b geometry (Fig. 36), maintaining a near constant layer thickness around the folded surface. In contrast, at the lower structural levels, the folds display a class 1c geometry. Mesoscopic folds within the volcanics are poorly developed, and occur only locally as broad, open warps with amplitude to wavelength ratios of 1 to 6, or greater.

A structural transition has been documented, and is characterized by a variation in the style of folding with structural position. A schematic structural profile (Fig. 37) illustrates the gradation in structural style observed. Structures are tight to isoclinal, with shallowly dipping axial surfaces at lower structural levels, and gradually become more open and upright at higher structural levels, with progressively more steeply inclined axial surfaces. This gradation in structural style is influenced by both position with respect to the major structure, and the relative competence of the deforming lithology.

4.2.2. Fractures

Fractures are observed on all scales within the Eureka Peak area. Extensional fractures oriented at low angles to bedding and cleavage occur predominantly within the metasedimentary succession, and are almost exclusively filled by quartz. The fibrous nature of the quartz is sometimes apparent in outcrop exposures, particularly within the smaller veins. The filled fractures vary from approximately 1 mm to 2 cm in thickness and tens of centimetres in length, to approximately 1 m in thickness and several

(a)

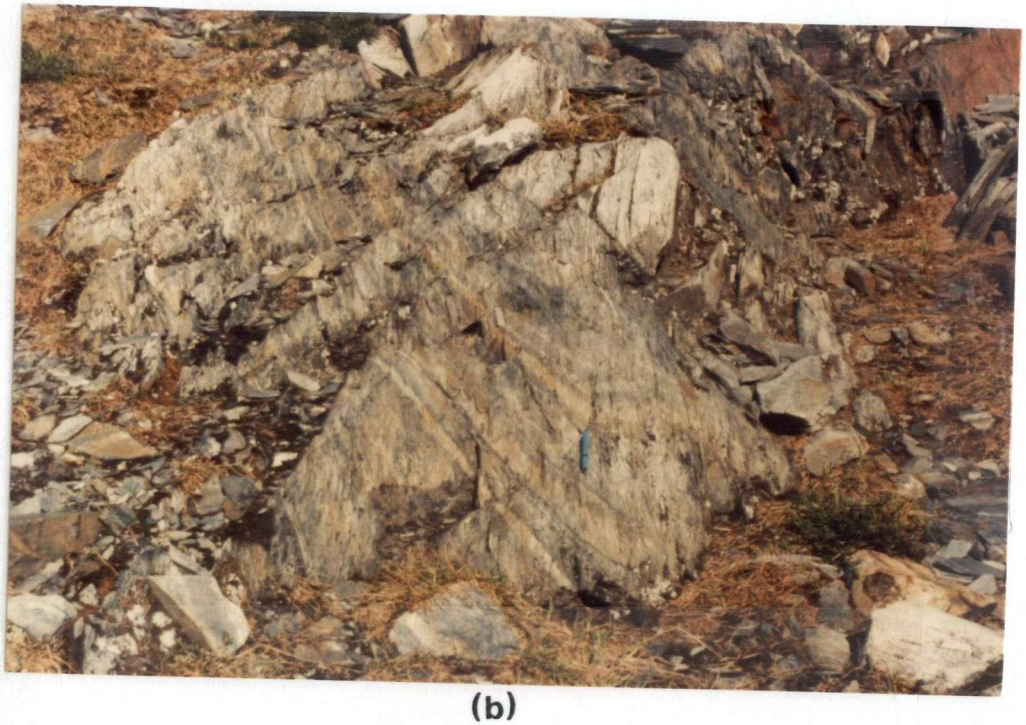

(b)

Figure 35: a.) at intermediate structural levels folds become more open and the axial plane more inclined. b.) folds are open and upright in the hinge region, at the highest structural levels.

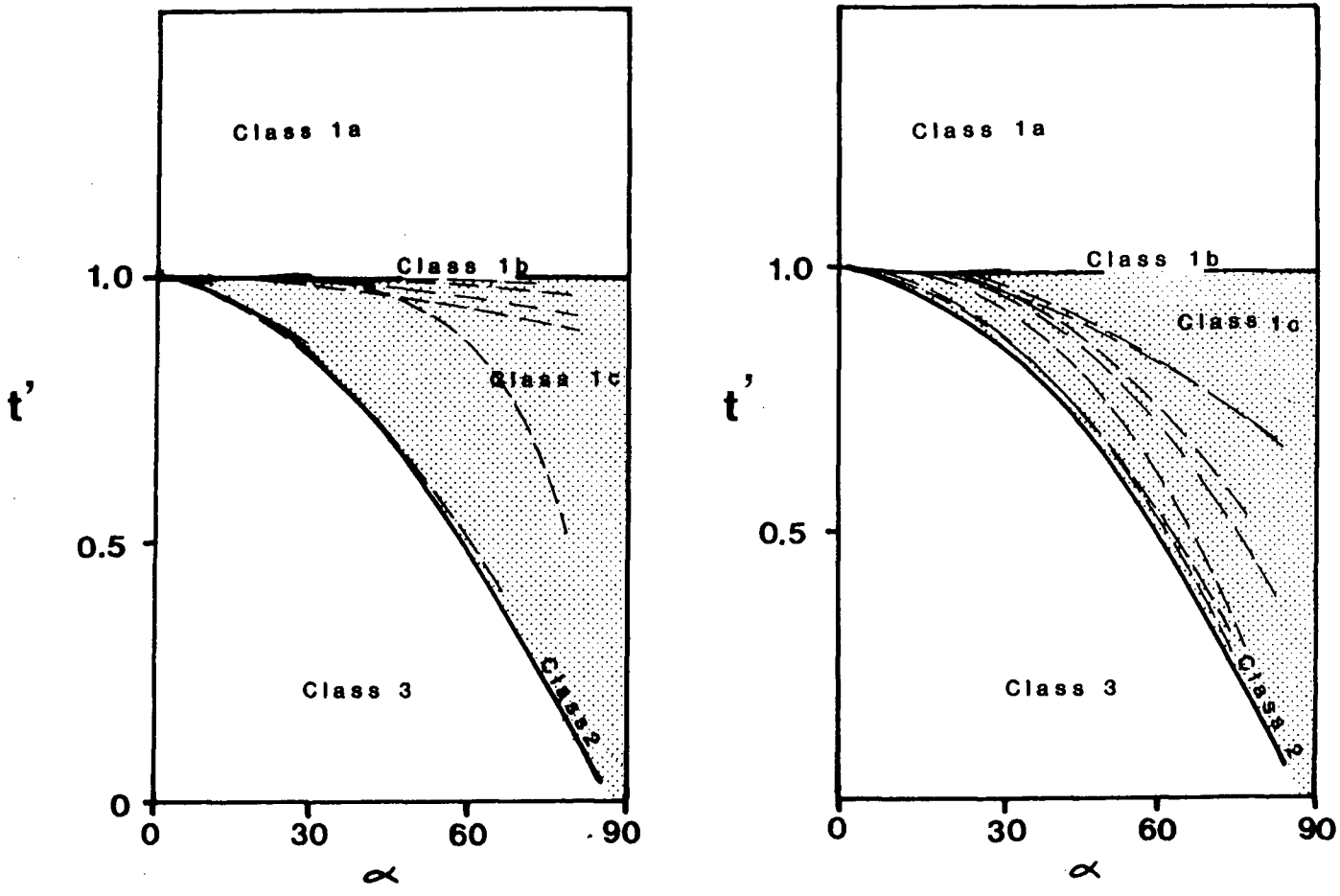

Figure 36: Geometric classification of fold style; folds at lower structural levels display a more class 1c geometry, folds at higher structural levels are closer to a 1b geometry.

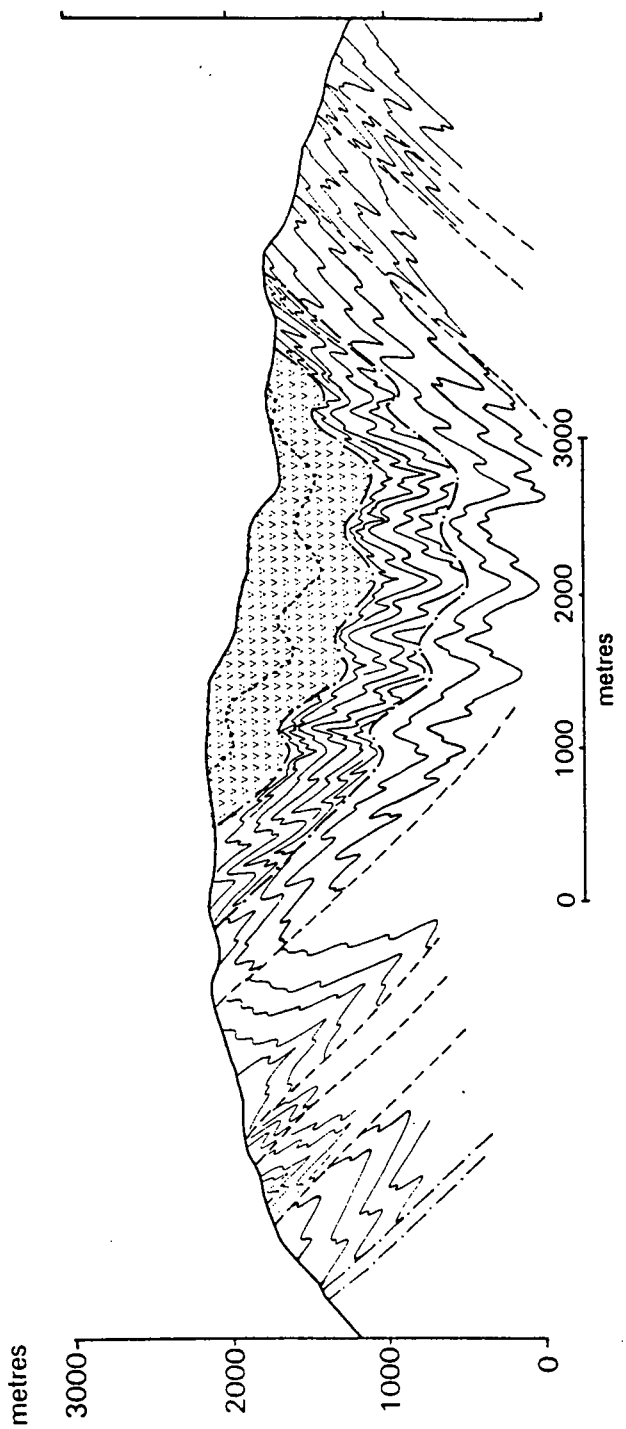

Figure 37: Schematic structural profile illustrating transition in structural style with structural level and lithology.

metres in length. The larger fractures are characterized by a much blockier quartz filling. Intensity of fracturing increases adjacent to fault contacts, and the fractures have an elliptical geometry in two dimensions. The quartz filled fractures occur at both high and low angles to bedding and cleavage. Both deformed and undeformed fractures are observed. Small, incipient quartz filled fractures outline rootless isoclinal folds, the limbs of which have been removed, likely as a result of pressure solution along the cleavage surface. Extension fractures with a sigmoidal geometry are also observed, oriented approximately perpendicular to the fold axis of mesoscopic folds of bedding. Deformed quartz veins occur on all scales, along the limbs of mesoscopic folds, and are commonly localized within the hinge region of mesoscopic folds. The relationship of quartz filled fractures to the mesoscopic structures indicates that fracturing was initiated early and continued throughout the deformational history. Figure 38 schematically represents the various vein geometries observed with respect to cleavage and bedding. Fractures initially formed in an orientation perpendicular to the direction of maximum compressive stress and strain, at a low angle to bedding, and high angle to cleavage. During progressive deformation, both bedding and fractures were deformed into mesoscopic fold forms. Fracturing is believed to have occurred throughout the deformational history, resulting in some fractures which are intensely deformed, while other fractures are completely undeformed.

A second type of fracture developed is manifest as a spaced fracture (Fig. 39). It is ubiquitous throughout the area and occurs in all lithologies. They are generally unfilled, open fractures which dip steeply to the north and south. Spacing of fractures varies with lithology, ranging from approximately 1 cm to 1 m. Within the Quesnel River Group spacing ranges from 1 to 50 cm; within the Takla Group volcanics, fracture spacing ranges from 20 cm to 2 m. As illustrated in figure 40, the fractures

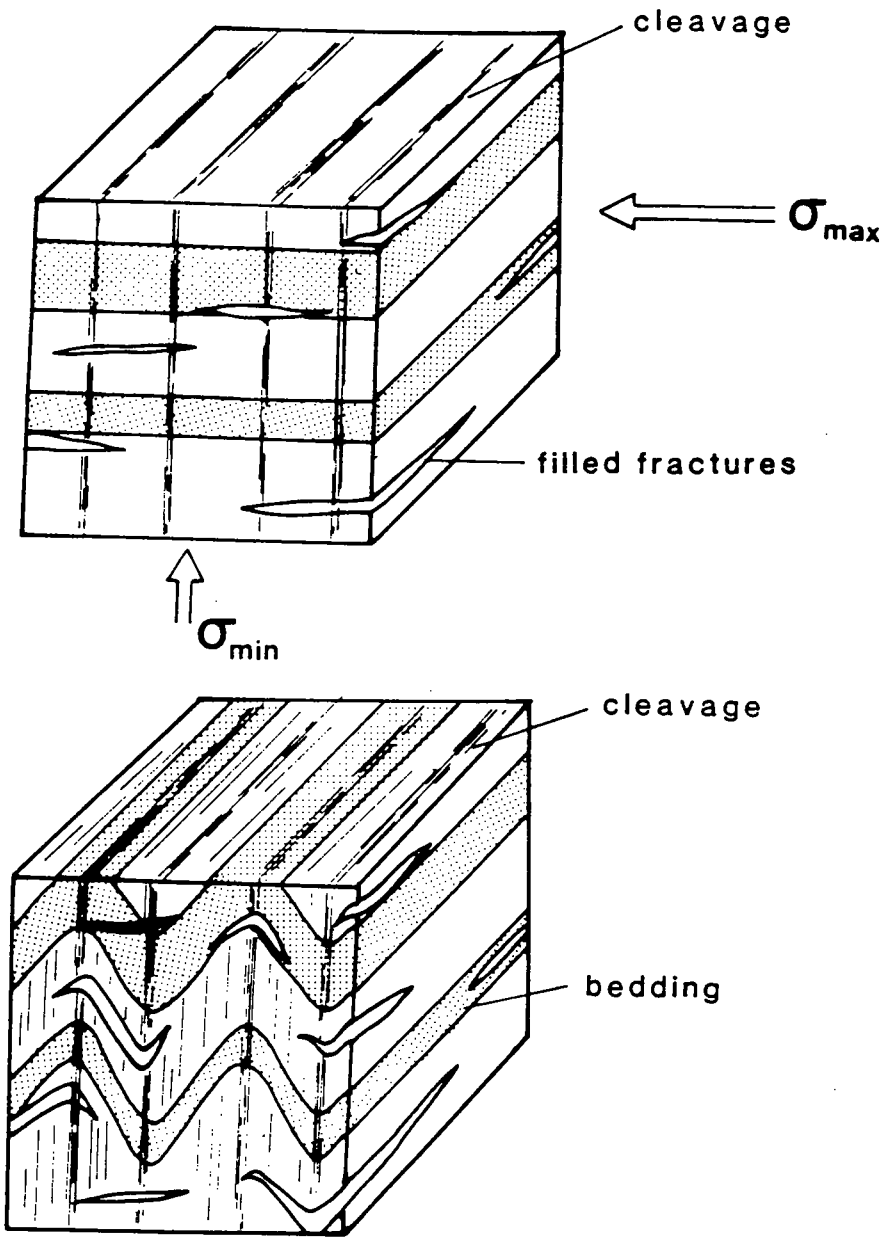

Figure 38: Geometry of fractures with respect to bedding and cleavage. Fractures initiated early and formed throughout the deformation history.

Figure 39: Spaced fractures are observed throughout the Eureka Peak area, and overprint all earlier formed structures.

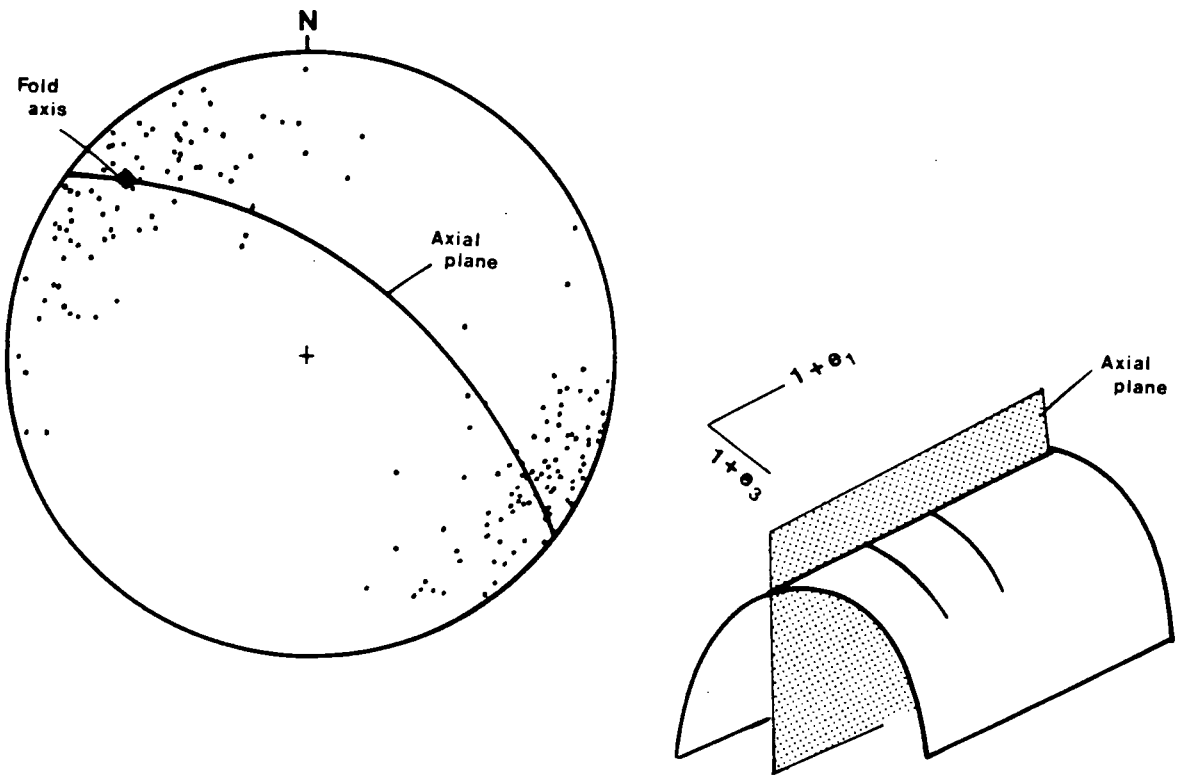

Figure 40: Equal area stereographic projection of fracture data. Fractures are oriented perpendicular to the axial plane and the fold axis of mesoscopic folds.

maintain a constant angular relationship to the mesoscopic folds of bedding, and are always oriented perpendicular to the fold axis and axial plane of the mesoscopic folds. The fractures show no evidence of a superimposed deformation, occurring as undeformed, planar fractures, and are believed to represent the latest structural event to be imposed upon the area.

4.2.3. Faulting

Faulting is concentrated along the major lithostratigraphic contacts. Four major faults have been identified:

1. at the base of the Crooked Amphibolite.
2. at the contact between the Crooked Amphibolite and the Quesnel River Group.
3. at the contact between units 6 and 7 of the Quesnel River Group.
4. at the contact between unit 7 and the overlying Takla Group.

The faults are parallel or near parallel to stratigraphic contacts, truncating bedding in some instances. They are overprinted by mesoscopic structures associated with crenulations and a non-penetrative cleavage, but are not intensely refolded. The amount of displacement along these faults is unknown. Along both the lower and upper contact of the Crooked Amphibolite with the Hadrynian Snowshoe Group and the Quesnel River Group rocks, respectively, concordant and discordant bedding relations have been observed (Campbell, 1971). Local mylonitization has been documented in the rocks adjacent to this contact (Elsby, 1985; Fillipone, 1985). The faulted nature of this contact has been documented further to the north as the Eureka thrust (Struik, 1986), and further to the south in the closure of the Eureka Peak syncline (Ross, pers. comm.).

Concordant and discordant bedding relations have been documented along the

sharply defined fault contact between units 6 and 7 of the Quesnel River Group (Fig. 8). Brecciation, slickensides and quartz filled fractures are common within the fault zone, which rarely exceeds 3 metres in width. Local imbrication along subsidiary splay faults is common proximal to the major fault zone. Figure 41 illustrates the geometry of the splay faults adjacent to the fault contact between units 6 and 7. Quartz filled fractures are prominent within and adjacent to the fault zones. Similar features mark the contact between the Quesnel River Group and Takla Group rocks. The fault contacts are interpreted to represent detachment surfaces. Deformation of the phyllites adjacent to the fault is intense, cleavage is strongly developed, and folding is extremely tight to isoclinal. In the Takla Group rocks, deformation is manifest as open warps of bedding. This discontinuity in structural style across the fault surface is interpreted in terms of a detachment or decollement surface, across which the strain is inhomogeneously accomodated. In each case, the less competent unit accomodates a greater proportion of the deformation, and is more intensely deformed than the more competent lithology.

The more competent unit controls the deformation and establishes the dominant wavelength of the enveloping surface to the folds developed within the less competent unit (Fig. 37). In each instance the more competent lithology occupies a higher structural position. The transition observed from tight, transposed structures at lower levels, to open, upright structures developed at higher levels is a combined effect of the control of structural position and lithologic competence on the development of structures.

Minor faults along the limbs of mesoscopic structures are observed in outcrop. The spaced or crenulation cleavage is often intensely developed within the fault zone, becoming nearly penetrative (Fig. 42). Minor faults of this type are also commonly

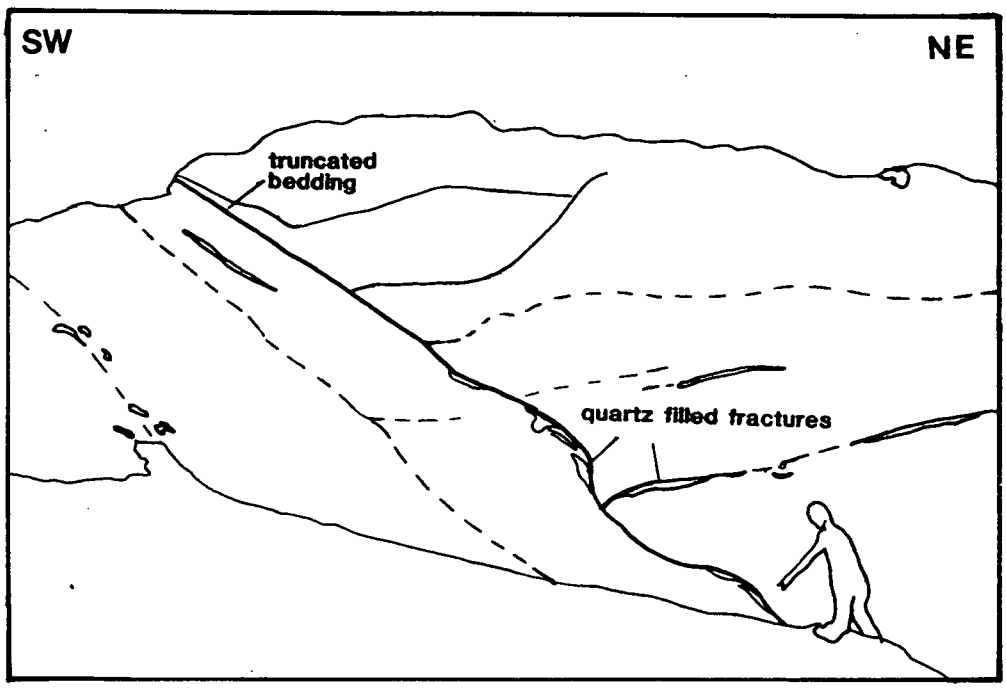

Figure 41: Numerous minor faults are developed in association with major fault contact between unit 6 and 7. (See also figure 8).

associated with the major faults along lithologic contacts.

High angle faults are developed at the higher structural and stratigraphic levels within the core of the Eureka Peak syncline, where they cut Takla Group rocks (see Plate 1 - geologic map). The faults are steeply inclined to the northeast, near parallel to the regional foliation. Displacements along the faults are not significant, but generally block movement seems to upwardly directed, out of the core of the syncline. The relative timing of the faults seems to post date all earlier structures, no effects of deformation are associated with these faults.

Figure 42: Strongly developed spaced cleavage adjacent to fault zone, parallel to pencil. Cleavage is locally penetrative, and here transects bedding at a high angle.

4.3. MICROSCOPIC STRUCTURES

4.3.1. Cleavage

Two cleavages are recognized in thin section, and are oriented axial planar to microscopic folds. One cleavage is outlined by the alignment of platy minerals, primarily muscovite and phengite. The second cleavage is associated with small scale crenulations, and is oriented axial planar to the crenulations. Both cleavages are dissolution-type cleavages, marked by the concentration of insoluble material along the cleavage planes.

Bedding within the black phyllite succession is composed of alternately interlayered quartz-rich and more argillaceous, phyllosilicate-rich domains which outline a well developed stratification or compositional layering. Quartz grains within the more quartz-rich horizons are generally small, and oblate with strongly sutured contacts and vary from 0.35 to 0.07 mm, with an average size of 0.04 mm. Grain boundaries vary from sharp and angular to irregular grain boundaries, marked by the development of subgrains. Filling the interstices, and along grain boundaries are blebs of organics, phyllosilicates and other insoluble material.

The cleavage selvages occur adjacent to grain boundaries and are defined by irregular, dark surfaces within which insoluble material and organics are concentrated (Fig. 43). Boundaries of grains adjacent to cleavage are often sharply truncated against the cleavage surface, and grain size reduction is apparent immediately adjacent to the cleavage surfaces. Truncation and minor offset of bedding against the cleavage is also observed. Such truncation of features indicate that soluble material (primarily quartz), has been preferentially dissolved and transported elsewhere in solution, probably eventually filling small extension fractures. Insoluble material left behind fills interstitial

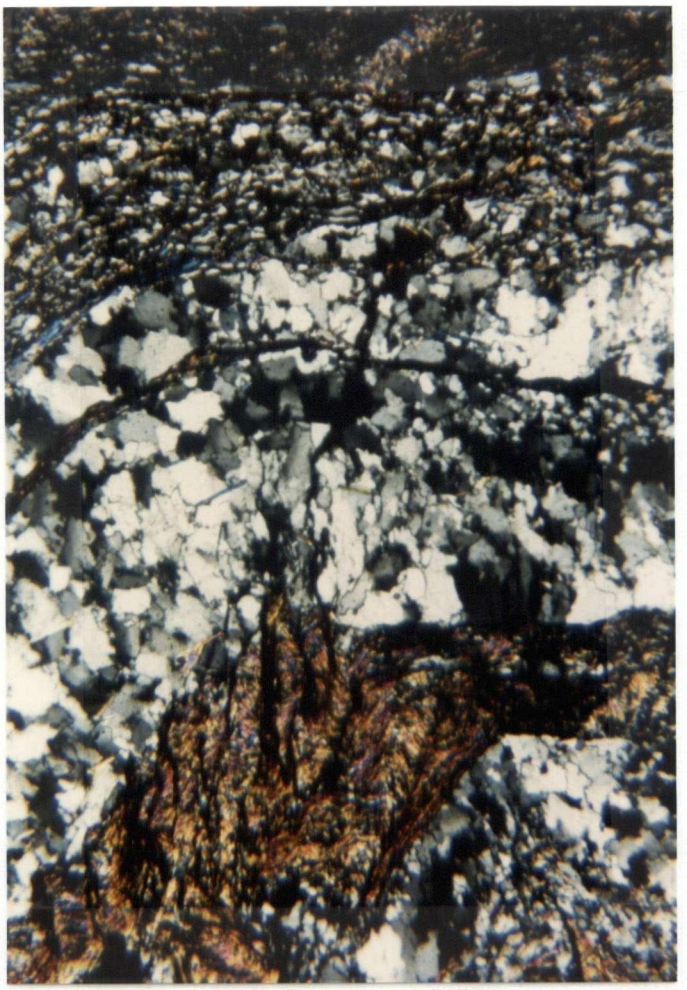

Figure 43: Photomicrograph of cleavage selvages. Cleavage is strongly developed along limbs of small crenulations. It partially crosscuts the quartz filled fracture and sharply truncates grains within the fracture.

voids around grains and is concentrated within the cleavage selvages. Intergranular relations adjacent to the cleavage selvages suggest that cleavage planes may have acted as a pathway along which extensive pressure solution occurred. The preferential dissolution of quartz has resulted in the oblate shape of the quartz grains, and the sutured nature of the grain contacts. Fibrous quartz and chlorite frequently occur as beards or pressure shadows on small quartz grains and are oriented parallel to the cleavage direction, and are likely the result of solution and deposition processes. Soluble material is dissolved at points of high stress concentration and redeposited in regions of lower stress concentration.

4.3.2. Fractures

Veins are observed at various angles to bedding and cleavage. In thin section, veins are frequently oriented at low angles to bedding, varying from 5 - 25°. They are lensoid in shape, with tapered or pinched terminations and are most prevalent in the Quesnel River Group metasediments, and adjacent to fault contacts. Within the metasedimentary sequence fractures are filled almost exclusively by quartz. Calcite and chlorite are present in lesser abundance. Chlorite, calcite and epidote are the most frequent vein filling minerals observed within the overlying metavolcanics.

In thin section, quartz grains are fibrous, elongate perpendicular to the vein wall, and display optical continuity along their length. This internal geometry suggests that the veins are filled extension fractures. As illustrated in figure 44, contacts between individual fibres are sharp. Individual grains are characterized by strongly sutured grain boundaries, wavy extinction, and the pervasive development of subgrains, indicating that the individual grains are highly strained. Quartz filled fractures can readily be distinguished from quartz rich compositional layering by the distinctive

Figure 44: Fibrous quartz filling fracture. Quartz fibres are optically continuous along their length, and elongate perpendicular to the vein wall. Grain size within fracture contrasts sharply with grain size within bedding.

mineralogy, composed almost exclusively of quartz, the fibrous nature of the fracture filling material as well as the optical continuity along the length of individual fibres. The quartz grains occuppying the fractures are markedly larger than the quartz grains comprising the compositional layering, and the discontinuous, lensoid geometry of the fractures contrasts with the more continuous nature of the bedding.

Both syntaxial and antitaxial filled fractures (Ramsay and and Durney, 1973; Ramsay, 1980) are observed in thin sections as inferred from intergranular relationships. Study of the grain to grain relationships within the veins indicates that multiple episodes of fracture opening and vein filling has occurred, and that both syntaxial and antitaxial veins are present. Textures within the veins suggest that deposition of new material has occurred along the centre of the vein as well as at the expense of the vein wall. Antitaxial veins characteristically show inclusions of wall rock fragments within the vein material (Fig. 45), which are symmetrically developed about the medial line within the fractures. Within some veins, newly added mineral fibres display a slightly different optical orientation than the fibres immediately adjacent to the vein wall, probably resulting from a slight change in orientation of the direction of maximum elongation. These veins generally have a much more diffuse medial plane than antitaxial veins, where the medial plane is marked by the presence of wall rock fragments. The lack of wall rock inclusions within these veins, and the slight reorientation of fibre growth from the wall to the centre of the vein is suggestive of a syntaxial geometry, and is characterized by vein material added along the central medial surface during sequential fracture filling episodes.

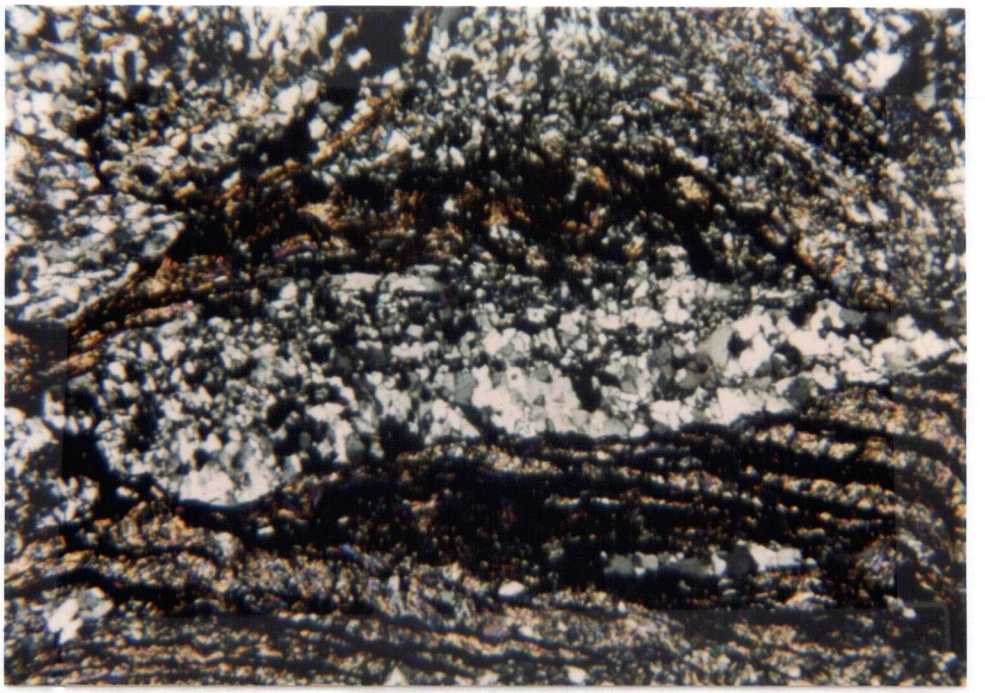

Figure 45: Discrete lines of wallrock inclusions symmetrically developed about the medial line of the fracture characterize antitaxial veins.

4.4. FOLD SETS

Overprinting relationships of structural elements indicate that two phases of deformation involving folding have occurred within the Eureka Peak area. The development of two cleavage morphologies and lineations is fundamental to the recognition of two phases of deformation. Separation of the two phases in the field is based upon the identification of the prominent structural elements, and their overprinting relationships at both the mesoscopic and microscopic scale. The discussion which follows examines the relationship of bedding, cleavage, and linear structures to the mesoscopic structures. The nature, orientation and distribution of the structural elements are considered in order to establish the relative timing of structural events, their geometry, and significance in the structural history of the area.

4.4.1. Phase 1 structures

Elements associated with first phase deformation (F_1) are the penetrative slaty cleavage (S_1), the lineation (L_1) defined by the intersection of bedding on the slaty cleavage surface, and the mineral lineation. Mesoscopic structures associated with F_1 are most strongly developed within the Quesnel River Group metasediments where a penetrative slaty to phyllitic foliation, S_1, is well developed axial planar to the F_1 folds. Within the Takla Group volcanics, an axial plane parallel cleavage is weakly to moderately developed, and mesoscopic folds are poorly developed, occurring locally as open warps.

As illustrated in figure 46, there is a consistent variation in the orientation of the first phase slaty cleavage, from the limb to the hinge region of the Eureka Peak syncline. At the lower structural levels, within the black phyllites, and on the limb of the Eureka Peak syncline, F_1 folds are tight to isoclinal in form. The axial planar

cleavage, S_1, is shallowly to moderately inclined to the northwest. At highest structural levels, within the volcanic succession, and in the hinge region of the syncline, S_1 becomes more steeply inclined, dipping to the northeast and southwest. Fold forms at this structural level are more open and upright. The change in orientation of the cleavage, and the transition in fold style is likely a result of higher flattening strains concentrated along the limb region of the syncline, and proximal to the faulted lithologic contacts. This interpretation is supported by the intensity of deformation within the phyllites in comparison to the volcanics. The more competent volcanics show little effects of the deformation in contrast to the phyllites, which are much less competent, and capable of accomodating a much greater proportion of the strain.

All structural elements associated with F_1 show the effects of subsequent deformation. The slaty cleavage in places is deformed, and transected by a spaced or crenulation cleavage (S_2). In the field, mineral lineations have been observed, completely distorted about the fold hinge of overprinting structures. Orientation analysis confirms the distorted nature of F_1 linear structures, and is presented in figure 47. The distribution of L_1 lineations plot along a great circle with some lateral spread. Such a distribution confirms that the lineations are distorted and suggests that a combination of flexural slip and simple shear folding may be responsible for the observed spread. The expected locus of distorted lineations produced by a flexural slip mechanism would lay along a small circle, with a constant angular relationship between L_1 and L_2. The relationship observed may be the result of simple shear modification of buckle folds originally formed by a flexural slip type mechanism. A simple shear deformation would produce a great circle distribution of distorted lineations.

No large scale, megascopic structures are recognized associated with F_1 deformation. The maximum limb length inferred from vergence changes of F_1

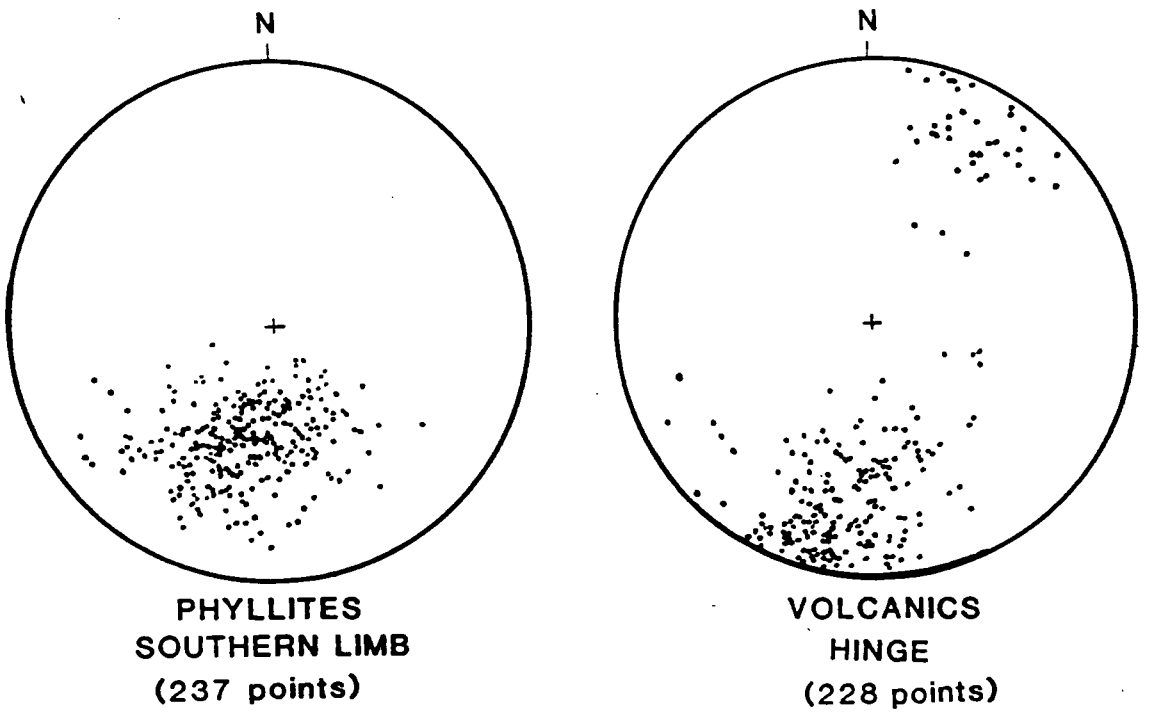

Figure 46: Equal area projection of poles to S_1. S_1 on the southern limb of the syncline dip shallowly to moderately to the northeast. S_1 in the hinge is steeper, dipping northeast and southwest.

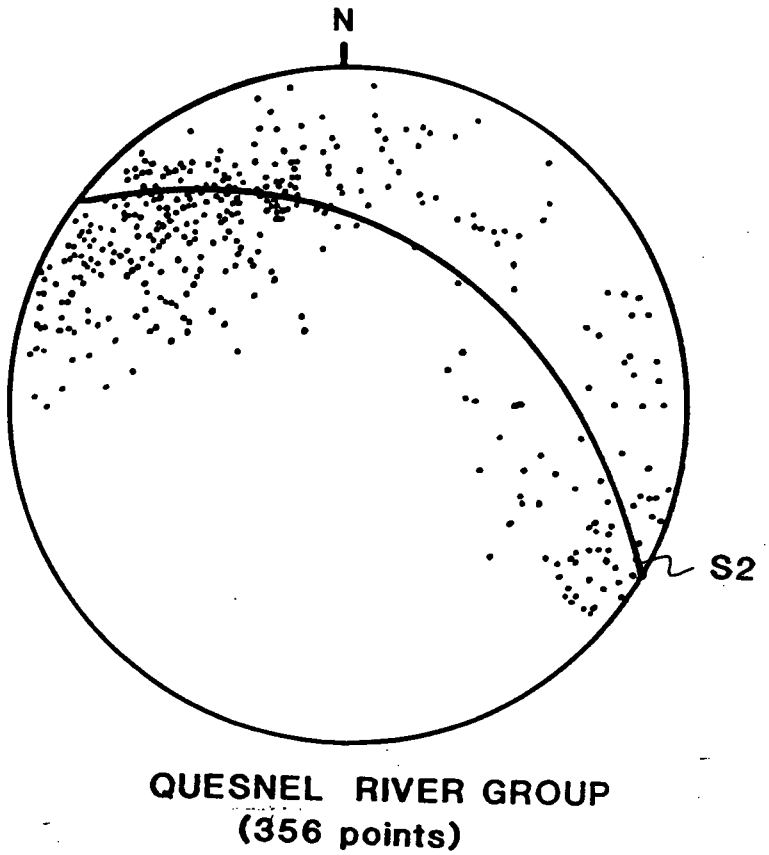

Figure 47: Equal area projection of L_1 for entire area. Distribution of lineations define a great circle locus corresponding to S_2.

mesoscopic structures is approximately 10 metres. The absence of any significant vergence change within the area can be interpreted in two ways:

1. location on a single limb of a very large scale F_1 structure.
2. F_1 mesoscopic structures are related to translation during the initial stages of accretion, and are not related to the formation of any regional scale structures in the area.

4.4.2. Phase 2 structures

Structural elements associated with F_2 deformation are the non-penetrative, spaced or crenulation cleavage (S_2), and the lineation (L_2) defined by the intersection of S_0/S_1 or S_1/S_2. The intersection lineation is parallel to the fold axis of mesoscopic F_2 folds, and S_2 is developed axial planar to F_2 mesoscopic structures which are recognized throughout the area. These structures show a change of vergence consistent with a megascopic second phase structure, the Eureka Peak syncline. F_2 structures maintain the same basic geometry as F_1 structures. Both phases are characterized by a NW - SE striking axial planar cleavage and a NW plunging fold axis. The orientation of S_2 shows little variation throughout the area as illustrated in figure 48. Poles to S_2 measured throughout the area are presented separately for the black phyllites (units 1-6), unit 7, and the volcanics. In contrast to S_1, S_2 shows no significant variation in orientation with respect to lithology. With regard to structural position, no significant variation is observed. The consistency of the orientation of S_2 throughout the area suggests that F_2 is the latest folding event to be observed in the Eureka Peak area. This conclusion is further supported by the examination of the stereonet distribution of L_2. Figure 49 is a stereoplot of F_2 fold axes and L_2 intersection lineations measured throughut the area; no significant spread is observed.

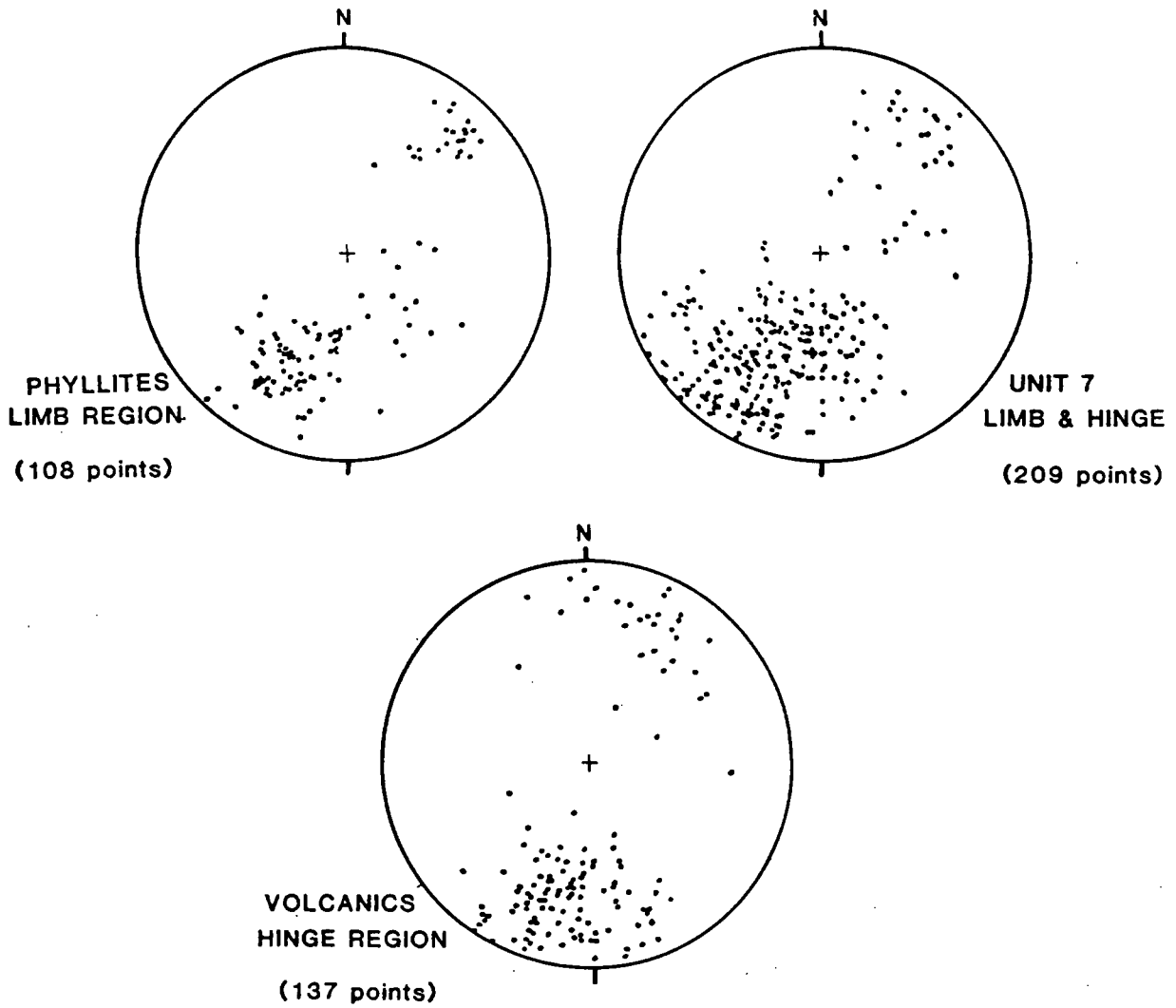

Figure 48: Equal area projection of poles to S_2. The orientation of S_2 varies little with respect to lithology or position on the major strucutre.

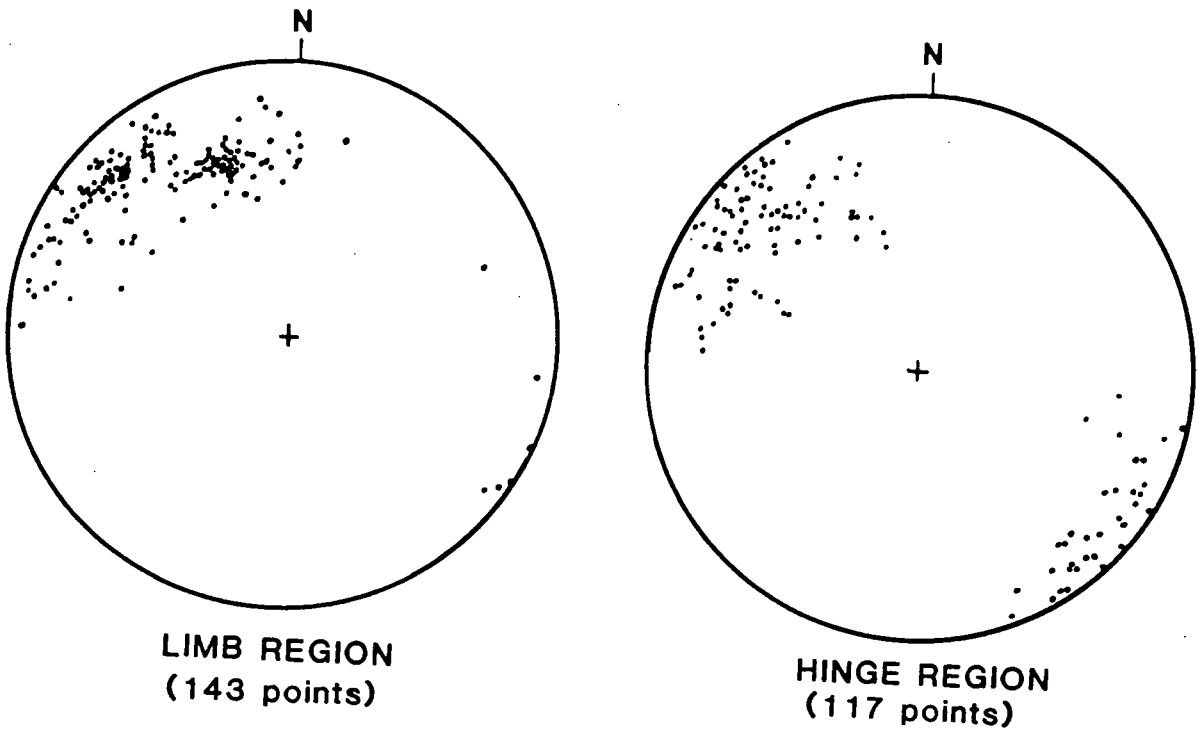

Figure 49: Equal area projection of F_2 fold axes, and intersection lineations measured in the hinge and limb region of the syncline.

Differentiation of the two phases in the field is often difficult unless unequivocal overprinting relations are observed. The structural elements associated with F_2 bear a close geometric relationship to F_1 structural elements. The development of F_2 mesoscopic folds is not always apparent in the field, however some overprinting relationship of the structural elements can be discerned in outcrop. At lower structural levels, the F_2 overprint serves to tighten and overturn the F_1 structures. At higher structural levels the F_2 overprint tightens F_1 folds, increasing the amplitude to wavelength ratio. Comparison of the orientation data for each phase suggests that folding was essentially coaxial throughout the deformation history. As a result of the similar orientation, F_1 structures are usually only modified by F_2, although complete refolding is sometimes observed. Figure 50 is an outcrop photo of a small F_1 synform, refolded and overprinted by strongly developed second phase crenulations.

Figure 50: Small F_1 fold immediately adjacent to the hammer is refolded and overprinted by strongly developed F_2 crenulations.

4.5. SUMMARY AND DISCUSSION

The structural analysis of the Eureka Peak area focussed upon the identification of the fundamental structural elements, both planar and linear, as observed in the field. Observations of the nature of bedding, cleavage and linear structures were made at both the mesoscopic and microscopic scale. Analysis of the nature of the structural features, the distribution, orientation and overprinting relationships were utilized to determine the geometry and the relative timing of structural events. Careful examination of textural features observed in thin section enabled inferences to be made regarding the mechanisms of deformation.

Particularly significant in the analysis of the structural evolution of the Eureka Peak area is the development of cleavage. Studies of cleavage morphology and the mechanical significance of cleavage are prevalent in the recent geologic literature (Powell, 1979; White and Knipe, 1979; Wood, 1974; Durney, 1972; Dietrich, 1969; Siddans, 1968). It is generally accepted that cleavage forms in an orientation perpendicular to the direction of maximum compressive strain, and is in the plane of flattening (Dietrich, 1969). Processes contributing most strongly to the development of a preferred planar orientation involve:

1. the mechanical rotation of platy minerals into the plane of flattening.
2. syntectonic recrystallization and the preferred growth of platy minerals parallel to the plane of flattening.
3. pressure solution transfer of soluble material, resulting in the formation of cleavage selvages defined by the concentration of insoluble material left behind.

From the microtextural features observed, it is inferred that the processes contributing to the formation of cleavage were initiated early in the deformational history. The intergranular relations adjacent to the cleavage selvages suggest that passive

rotation of phyllosilicate grains has occurred in response to the dissolution of quartz. Partially solved quartz grains have an oblate geometry with sutured grain boundaries. Phyllosilicates show a preferred orientation parallel to the long dimension of the quartz grains and are oriented parallel to the dissolution cleavage. Pressure solution processes, and the dissolution of more soluble minerals at points of high stress concentration enhance the process of mechanical rotation. As soluble material is removed, phyllosilicates will passively rotate into the plane of flattening. Syntectonic solution - deposition processes has resulted in the formation of pressure shadows of fibrous quartz, chlorite or mica which have grown at the ends of grains, and are oriented parallel to the cleavage direction. The pressure shadows grow away from the grain surface, within regions of low strain, in the plane of flattening.

It is evident from mesoscopic and microscopic structures that pressure solution has played a prominent role in the development of cleavage in the Eureka Peak area. Inherent to the dissolution process of pressure solution are episodic increases in pore fluid pressure. The effects of a high pressure fluid phase are both chemical and physical (Beach, 1974, 1982; Etheridge et al. 1983, 1984; De Boer, 1977; Robin, 1978). The chemical effects of a high pressure fluid have not been extensively evaluated in the Eureka Peak area, but essentially the fluid will act as a solute and transporting medium, in addition to acting as a reactant in metamorphic reactions. It may play an important role in the rheology of the deforming rocks by producing new grains of low dislocation densities, and thereby altering the deformation rate by initiating a period of relatively rapid creep (Etheridge et al. 1984). Secondly, it may enhance metamorphic reactions producing a reaction hardening or softening effect. The rate of subcritical crack growth will be enhanced in the presence of a chemically corrosive fluid (Anderson and Grew, 1984).

In terms of physical effects, the presence of a high pressure fluid phase tends to reduce effective stress, increasing porosity and permeability, and promoting fracturing on all scales, from the development of microfractures to large scale faulting (Hubbert and Ruby, 1959). It is likely that such a process may have facilitated faulting along the major lithologic contacts observed and the pervasive fracturing adjacent to the fault zones. This is particularly true of the contact between the Quesnel River Group and Takla Group rocks. It is believed that the relatively less permeable volcanics, compared to the more permeable sediments would provide an effective barrier to upward fluid flow, resulting in increased fluid pressures at, or below the contact. The elevated fluid pressure would promote the development of fractures in the vicinity of the fault, and could have a buoying effect on the volcanics, providing a buffer, and contributing to the general lack of pervasive deformation within the volcanics. The intensity of veining adjacent to the faulted zones would certainly support this interpretation. Although there is evidence for solution transfer within the volcanics, the degree to which fluid migration has occurred is negligible, and it appears that the model proposed is reasonable based on mesoscopic and microscopic evidence.

On the microscopic scale, hydraulic fracturing is pervasive within the Quesnel River Group sediments where a simple "source - path - sink" model (Etheridge et al. 1984) can be used to describe the inferred fluid path, and is modelled in figure 51. Pore fluid is generated by dissolution of soluble material at points of high stress concentration, and so soluble minerals such as quartz or calcite provide the "source" of pore fluid. Movement of the pore fluid is accompanied by grain boundary diffusion (Etheridge et al. 1984), and in thin section a film of insoluble residue along the grain boundaries of pressure solved quartz provides some indication that this mechanism was operative. When the pore presure is elevated to the tensile strength of the rock,

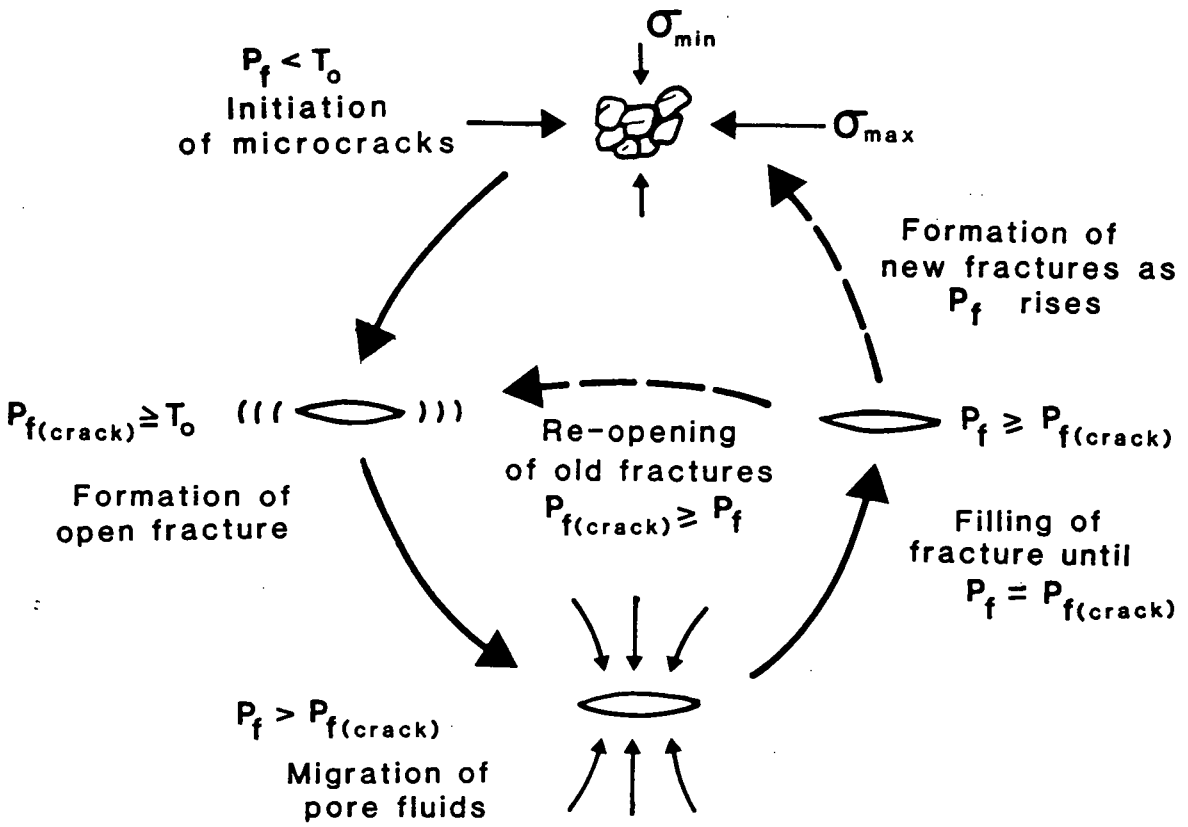

Figure 51: Fluid pump mechanism is responsible for the formation of fractures and fluctuations in pore fluid pressure.

fracturing occurs. The fractures provide the "sink" for the pressure solved material, and pore pressure decreases. Once the fracture is filled, pore pressure again begins to rise and the cycle is repeated. The fluctuations in the pore pressure become the driving force behind the pressure solution process. If additional fluids are generated by dewatering reactions during prograde metamorphism, the "source–sink" cycle becomes self–perpetuating, and gives rise to advective flow. Inherent to the cyclic fluctuations in fluid pressure and the repeated opening of fractures is the deposition of new vein material resulting in crack–seal textures (Ramsay, 1980) within the veins. Deposition of new vein material occurs either along the medial line of the vein (syntaxial veins) or at the expense of the vein wall (antitaxial veins). The evidence that such cyclic pressure variations has occurred, resulting in multiple fracture–opening events in the Eureka Peak area lies within the filled fractures which are interpreted in terms of a crack–seal mechanism involving multiple episodes of fracture opening and filling in response to the cyclic variations in pore fluid pressure. Addition of new vein material during the fracturing episode has resulted in the formation of both syntaxial and antitaxial veins in the area. The prevalence of mesoscopic quartz filled fractures is evidence that the fluid pump mechanism resulting from the cyclic variations in pore pressure has given rise to advective flow.

The structural evolution of the Eureka Peak area is interpreted in terms of a progressive deformation synchronous to metamorphism. Folding in the area is essentially coaxial, although structural elements characteristic of each of the phases of deformation can be recognized and differentiated where overprinting relationships are observed. The geometry of the folds observed suggest a simple buckling mechanism, with modifications due to higher flattening strains at the deeper structural levels, and proximal to the faulted lithologic contacts where accumulated strain energy is greater. Cleavage formation

is inferred to have been initiated early in the deformational history, and to be a result of both mechanical rotation of platy minerals into the plane of flattening, and solution–deposition processes associated with pressure solution. Pressure solution processes have had a significant influence on the development of structures on all scales. The dissolution of soluble material has enhanced the mechanical rotation of phyllosilicates into the cleavage plane in addition to concentrating insoluble material within the cleavage selvages. The cyclic fluctuations of fluid pressure inherent to the pressure solution process has facilitated fracturing on all scales, and may have contributed significantly to faulting along major stratigraphic contacts between lithologies of differing competency and permeabilities.

5. METAMORPHISM

The existence of a regional metamorphic event in the Crooked Lake area has been documented by numerous previous workers (Campbell, 1971; Fillipone, 1985; Elsby, 1985; Carye, 1985). Based on field evidence, isotope studies, mineralogical and microtextural studies regional metamorphism is believed to have been initiated during the Early–Middle to Late Jurassic orogenic event related to the convergence and eventual accretion of the Quesnel terrane to the North American cratonic margin. All lithologies within the Eureka Peak area have been affected by a regional metamorphism, interpreted to represent the same metamorphic event. Metamorphic isograds representing a basic Barrovian sequence have been mapped throughout the region (Campbell, 1978; Fillipone, 1985, Montgomery, 1985), based primarily on the first appearance of key mineral assemblages (Fig. 52). Textural evidence constrains the timing of the peak of metamorphism to syn– to post tectonic. Metamorphic grades cut across the tectonic boundary at a low angle and conform to the regional structures related to the the emplacement of the Quesnel terrane. Metamorphic mineral assemblages observed within the Eureka Peak area are characteristic of the greenschist facies, and vary from chlorite to garnet grade. The effects of metamorphism are most evident adjacent to the tectonic boundary, and particularly within the basal portion of the metasediments exposed to the north of Crooked Lake, where rocks of garnet grade are observed. Metamorphic grade seems to decrease rapidly away from the boundary, both stratigraphically and structurally upsection. Within the core region of the Eureka Peak syncline, rocks of chlorite grade prevail.

Investigations in the Eureka Peak area concentrated on field mapping and the first appearance of diagnostic metamorphic mineral assemblages. Study of the mineralogical and microtextural relationships focussed upon determining the grade of

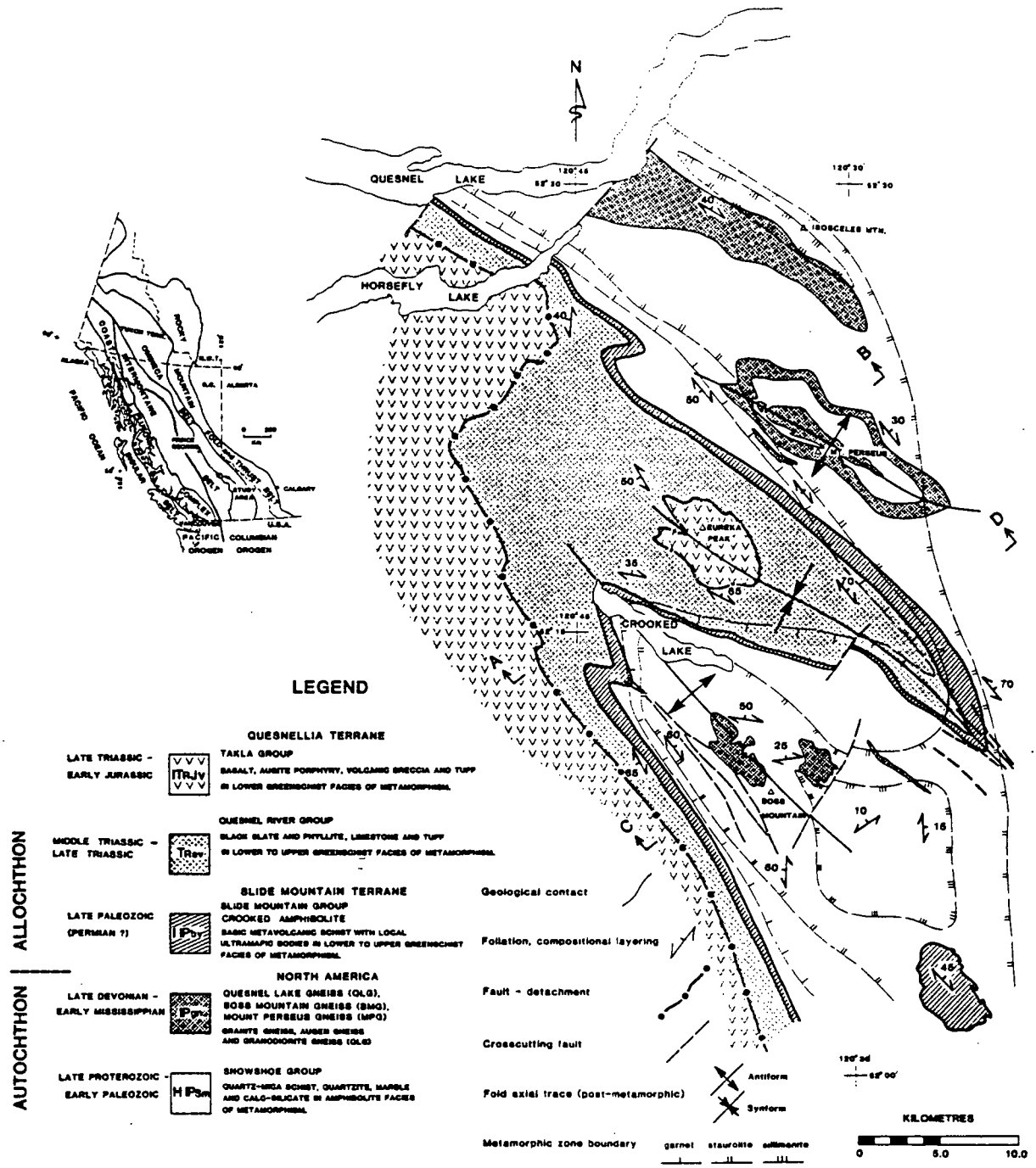

Figure 52: Distribution of metamorphic isograds throughout the Crooked Lake area.

metamorphism and the relative timing of metamorphism with respect to the structural events recognized in the area. Mineralogical evidence suggests that the rocks experienced one major episode of metamorphism resulting in the formation of minerals characteristic of greenschist facies metamorphism. Discussion of the nature of metamorphism in the Eureka Peak area is based upon the textural and mineralogical relationships observed in thin section. Characteristic mineralogy and microtextures are discussed for each major lithologic unit in the area. Microtextural relationships are examined to determine the relative timing of metamorphism with respect to major structural events discussed in chapter 4. Mineral reactions are inferred from the petrographic relationships observed. Temperature and pressure constraints are discussed based on what is known of the mineral parageneses from published experimental work.

5.1. METAMORPHIC MINERALOGY AND MICROTEXTURAL STUDIES

5.1.1. Crooked Amphibolite

Two lithologies comprise the Crooked Amphibolite along the northern shore of Crooked Lake: a fine grained chlorite–feldspar–amphibole schist, and a coarse grained actinolite schist or garbenschiefer. Metamorphic mineral assemblages comprising the Crooked Amphibolite are hornblende, actinolite, biotite, chlorite, talc, quartz and calcite.

Chlorite - Biotite

Within the chlorite–feldspar–amphibole schist, alternation of felsic and mafic layering comprise a compositional lamination which is parallel to S_1 A strongly developed schistose foliation (S_1) is parallel to compositional layering and is defined by planar alignment of coarse grained chlorite, and lesser biotite. Chlorite also grows as beards on quartz grains in an orientation parallel to the schistose foliation. Growth of

chlorite and biotite is synchronous to first phase deformation, and is crenulated by the second phase deformation. Examination of the chlorites shows continuous chlorite fibres bent around the hinge of crenulations indicating that growth of chlorite was still occurring synchronous to development of crenulations and therefore is synchronous to F_2 folding. Tabular biotite porphyroblasts cross-cut the S_1 foliation, (Fig. 53) but are not always aligned parallel to S_2 and may have developed sometime subsequent to F_1 deformation.

Hornblende

Large green pleochroic hornblende porphyroblasts are preferentially aligned parallel to the schistosity in the garbenschiefer. The growth of the hornblende may predate F_1, but must be at least synchronous to F_1, and probably outlasted first phase deformation because the porphyroblasts contain inclusion trails of opagues, quartz and plagioclase. Ilmenite comprises the opaques which occur as inclusion trails, either parallel or slightly rotated from parallelism with compositional layering and the main foliation. Hornblende porphyroblasts show irregular, wavy extinction indicative of post-crystallization strain. The porphyroblasts enclose biotite flakes that are optically continuous with the biotite external to the porphyroblast, and parallel to the S_1 foliation.

Epidote

Extremely embayed, inclusion-riddled epidote porphyroblasts occur throughout the matrix, and appear to have been originally oriented parallel to S_1 (Fig. 54). Epidote porphyroblasts are zoned and show a concentric extinction pattern. Quartz, plagioclase and opaques comprise the inclusion trails within the porphyroblasts and appear to outline rootless isoclines within a tranposed foliation. Growth of epidote porphyroblasts occurred relatively early in the deformational sequence. Individual inclusion trails are

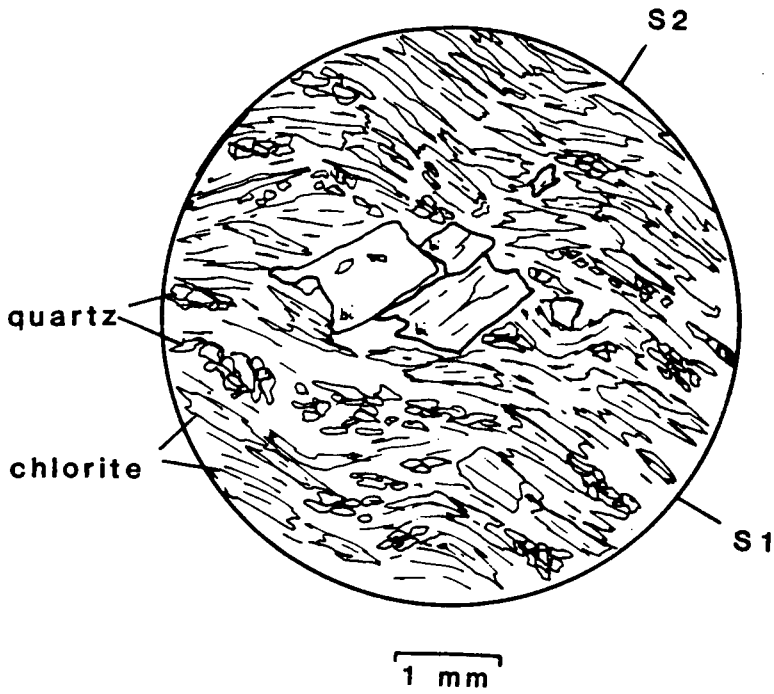

Figure 53: Biotite porphyroblast cross cutting the S_1 foliation, and oriented parallel to S_2. (Sample 522)

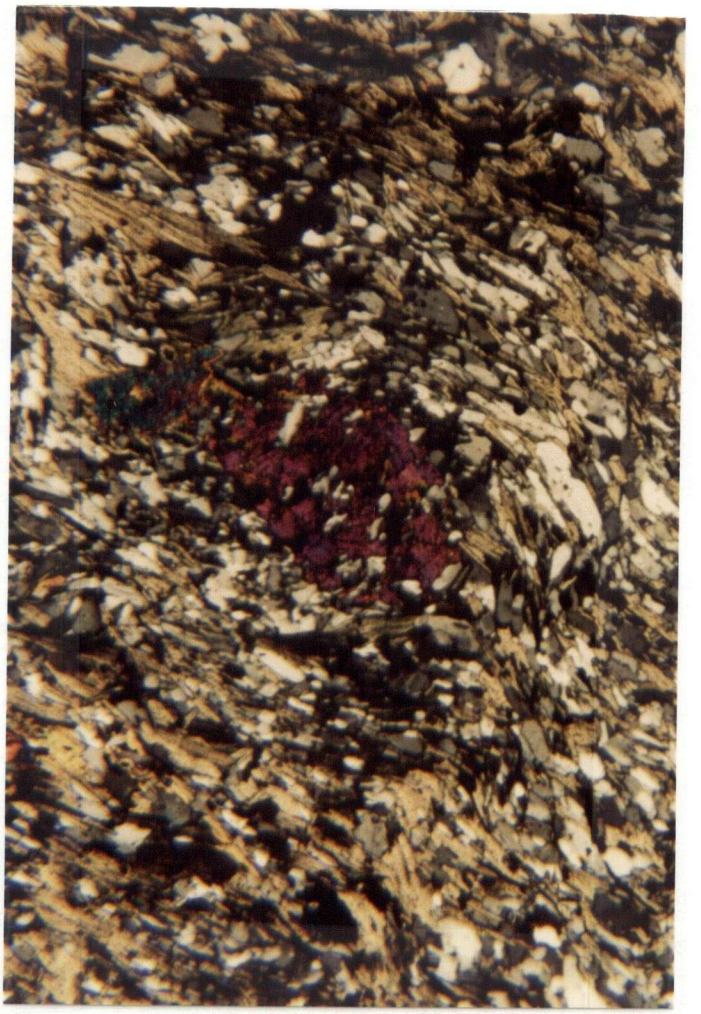

Figure 54: Poikiloblastic epidote porphyroblast containing inclusions of quartz, and opaques. Alignment of chlorite defines S_1. (Sample 522)

often not distinctive enough to determine if any rotation occurred during growth. Epidote porphyroblasts occur randomly and vary from small anhedral grains to moderately-sized grains, occassionally enveloped by actinolite porhyroblasts.

Opagues

Opaques occur as scaly masses and as fine blades or elliptical blebs of ilmenite parallel to the foliation and as inclusion trails within the porphyroblast phases (Fig. 55). Generally the inclusion trails show no effects of rotation during porphyroblast growth, and traverse the porphyroblast as a straight trail of inclusions. However, helicytic textures have been observed within one porphyroblast of hornblende indicating that some rotation of the porphyroblast within the plane of the foliation must have occurred during growth. Magnetite occurs as both corroded, anhedral porphyroblasts and as fine stringers parallel to S_1. Porphyroblast growth is probably syn- to post-F_1. The larger porphyroblasts seem to truncate the S_1 schistosity, but smaller porphyroblasts are often oriented parallel to the to the main foliation.

Microtextural evidence suggests that metamorphism within the Crooked Amphibolite was synchronous to deformation resulting in the development of the primary schistosity. The poikiloblastic nature of the hornblende and epidote suggest that the growth of these minerals was syn- to post- tectonic, because they enclose a metamorphic foliation. Growth of biotite porphyroblasts across the foliation and parallel to the axial plane to the microscopic kinks suggests that the metamorphism was still active during this latest phase of deformation.

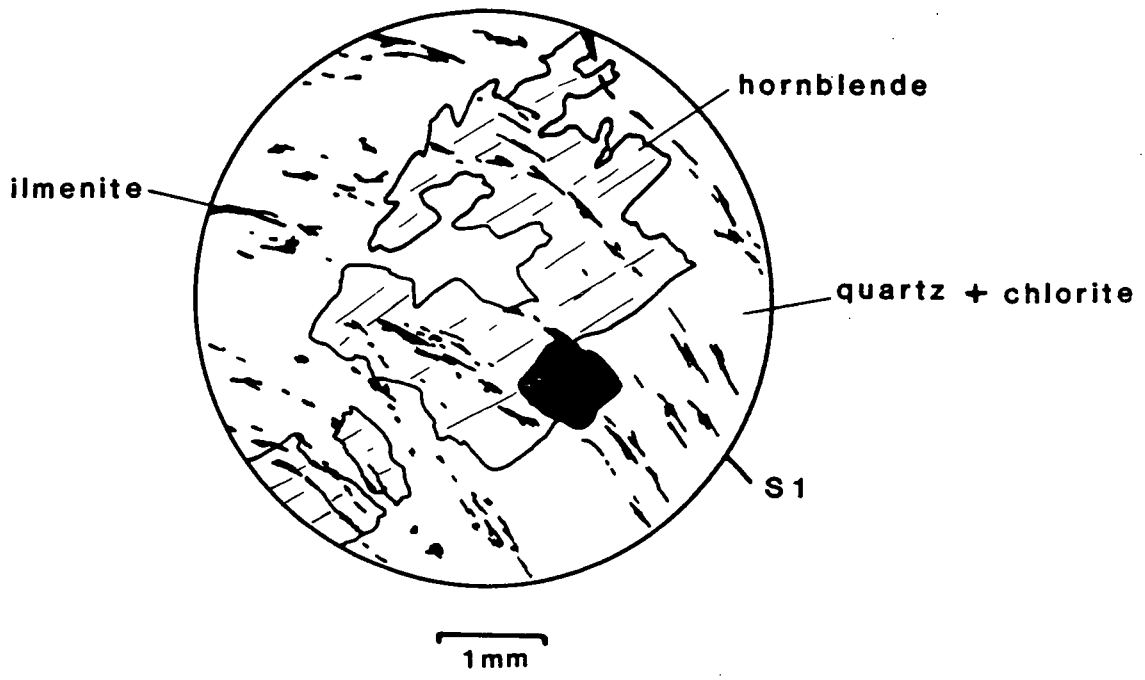

Figure 55: Ilmenite inclusion trails within hornblende porphyroblast. (Sample 520)

5.1.2. Phyllites

Textures associated with the growth of metamorphic minerals within the phyllites include porphyroblasts of garnet, albite, chloritoid, and ilmenite. A penetrative foliation (S_1) is defined by the planar alignment of muscovite and paragonite, with minor amounts of chlorite. Quartz-rich versus mica-rich domains comprise the compositional layering. Quartz-filled fractures are ubiquitous throughout the metasediments, and likely result from the remobilization of fluids generated during dehydration reactions and associated with pressure solution processes. There is a marked increase in the intensity of hydraulic fracturing at higher structural and stratigraphic levels which is marked by enhanced development of the pressure solution cleavage and the absence of ilmenite porhyroblasts. Veins are oriented parallel or subparallel to bedding and are variably deformed. The quartz filling is fibrous and highly strained. All porphyroblast phases are poikiloblastic, containing inclusions of quartz and opaques.

Garnet

All porphyroblast phases are poikiloblastic, containing inclusions of quartz and opaques. Garnets vary in form from very small, corroded porphyroblasts to relatively euhedral porphyroblasts, varying in size from 0.5 to 4 mm. Porphyroblasts contain inclusions dominantly of quartz or ilmenite, but sometimes are completely free of inclusions. Inclusion trails show no rotation internal to the garnets, indicating that no rotation occurred during growth. Superimposed flattening within the plane of the foliation is marked by an angular discordance between the foliation internal to the porphyroblast, and the foliation of the surrounding matrix.

Ilmenite

Small ilmenite porphyroblasts are oriented parallel to the main foliation and often contain quartz inclusions. Strain shadows of quartz and chlorite are associated

with ilmenite porphyroblasts that are oriented at low angles to the cleavage plane. Ilmenite also occurs as inclusions within garnet porphyroblasts.

Albite

Albite porphyroblasts vary in size from 0.55 mm to 2.5 mm. Porhyroblasts up to 7.5 mm in size have been observed in the field. Inclusion trails of quartz within the albite porphyroblasts sometimes comprise up to 50% of the porphyroblast (Fig. 56). An angular discordance of up to 20° is observed between the external foliation and the foliation contained within the porphyroblasts. However, no curved inclusion trails are observed. This lack of helicytic textures indicates that the orientation of the principal strain axes were constant during the period of growth of the porphyroblast. Pressure shadows of quartz and chlorite occur in association with all porphyroblast phases. In some areas, the phyllite is so coarsely porphyroblastic that strain shadows develop an almost anastomosing texture.

Chloritoid

Coarse, tabular chloritoid porphyroblasts grow in a variety of orientations, sometimes within the pressure shadows of albite porphyroblasts or parallel to the main schistosity, but also at high angles to the S_1 foliation, either parallel to S_2 crenulations or at a random orientation, unrelated to the prominent foliations. On the north limb of the Eureka Peak syncline, chloritoid occurs as coarse tabular porphyroblasts, showing no preferred orientation, and occur as intergrown, radiating masses (Fig. 57). Chloritoid varies from idiomorphic porphyroblasts to strongly poikiloblastic porphyroblasts containing the S_1 foliation. Inclusion trails within the porphyroblasts show no evidence of rotation during growth. An angular discordance between the foliation of up to 70° is observed resulting from post crystallization flattening within the plane of the foliation .

Metamorphic grade seems to decrease stratigraphically upsection within the

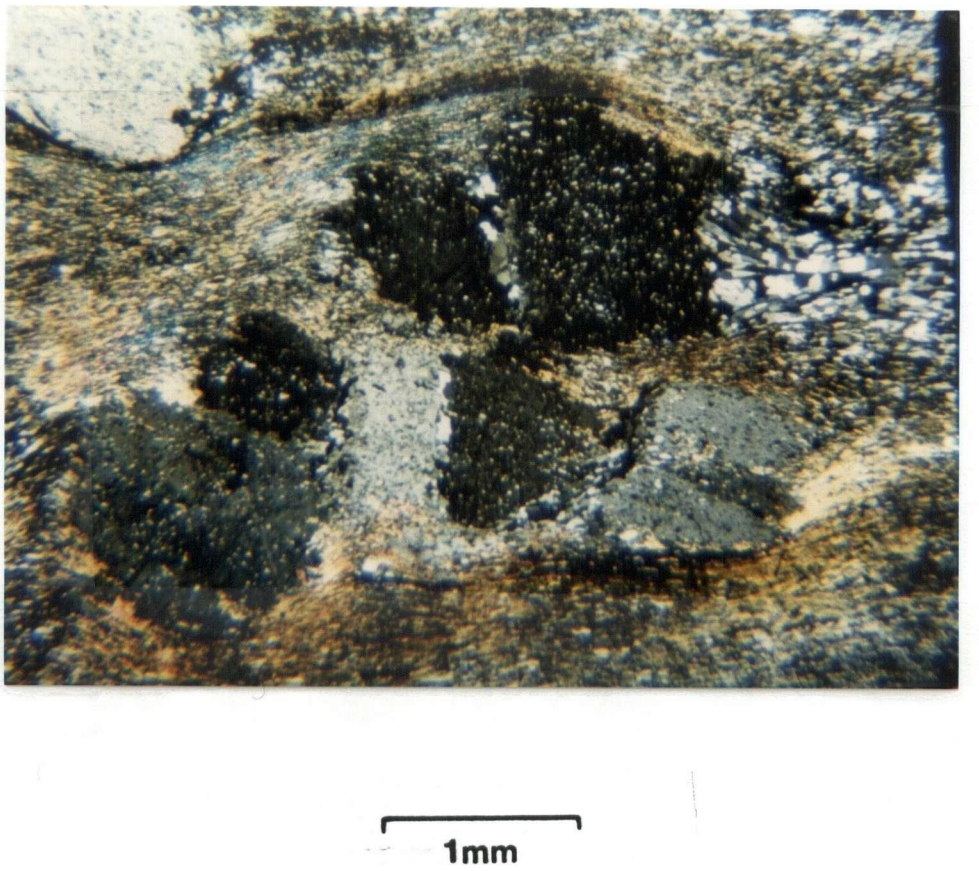

Figure 56: Quartz inclusions within albite porphyroblasts. Pressure shadows of quartz, chlorite and mica at the ends of the grains are parallel to S_1.

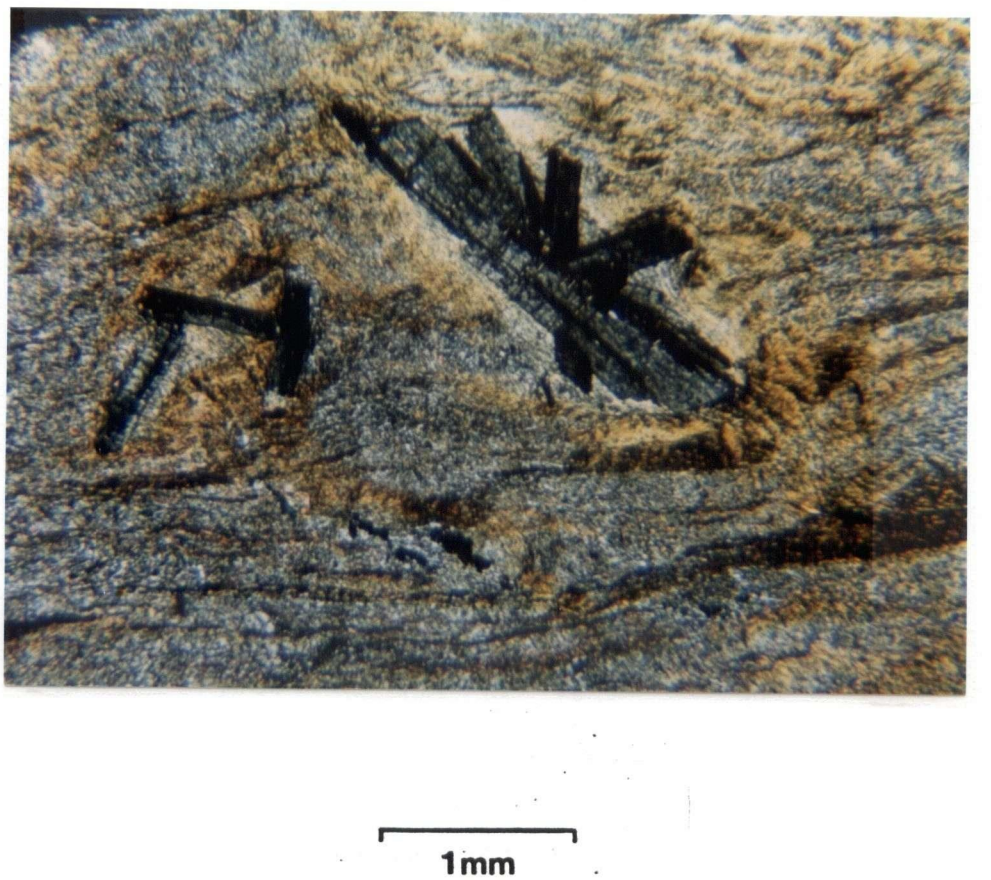

Figure 57: Chloritoid porphyroblasts are variably oriented with respect to the foliation.

phyllites, and away from the tectonic boundary. Garnets are very small, and strongly riddled by quartz before their complete dissappearance. The disappearance of all porphyroblast phases within the phyllites occurs above the 6300 ft topographic contour, immediately south of Peak 6735', and is probably a result of bulk compositional changes and decreasing metamorphic grade at higher structural and stratigraphic levels. A strongly developed foliation is ubiquitous throughout the metasedimentary sequence, outlined by fibrous muscovite and paragonite. Crenulation of the foliation (S_1) is pervasive, and micas show evidence of kinking in addition to growth parallel to the axial plane of the crenulations (S_2).

5.1.3. Takla Group Metavolcanics

All rocks within the Takla Group in the Eureka Peak area lie within the albite–actinolite–chlorite zone as defined by Winkler (1979). Metamorphic minerals characterizing the volcanics are actinolite–albite–chlorite–biotite and epidote.

Actinolite

Actinolite occurs as rhombic porphyroblasts throughout the volcanic sequence, and as fine acicular needles randomly oriented throughout the groundmass. Actinolite overgrowths are particularly pronounced on pyroxene phenocrysts, growing preferentially along cleavage planes, and as fibrous tails oriented parallel to the cleavage traces. Actinolite fibres also occur as fracture filling internal to fractured phenocrysts. Composition of the fracture filling changes abruptly at the phenocryst margin, and is usually filled by fibrous quartz external to the fractured phenocryst. Metamorphic actinolite replacing primary hornblende occurs as scaly intergrowths concentrated along cleavage planes and along the rims of phenocrysts (Fig. 58).

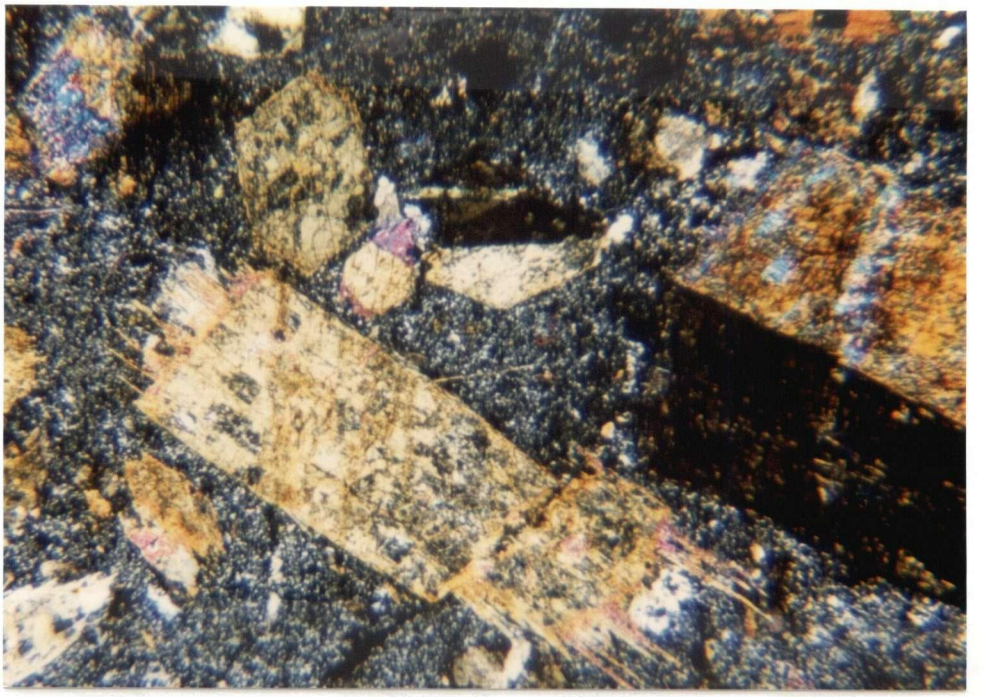

Figure 58: Fractured pyroxene phencrysts with overgrowths of actinolite. The actinolite fibres grow parallel to the cleavage within the pyroxene. (Sample 02)

Albite

Abite is primarily restricted to fibrous growths within fractures and vesicles. It is frequently associated with calcite, and may have resulted from the prograde metamorphism of analcime and quartz. Well developed twinning is associated with the albite which often displays a radially symmetric growth within the vesicles.

Biotite

Biotite occurs as overgrowths of mafic minerals, usually in association with actinolite, replacing primary pyroxene. The biotite more frequently occurs as stubby, tabular crystals as opposed to fine fibres. It seems to show no preferred directional orientation, Occurrence of biotite seems restricted to replacement of mafic minerals and does not occur freely within the groundmass. In one thin section, fibrous intergrowth of biotite and chlorite have completely replaced a primary amphibole, the original euhedral crystal outline being the only relict of the original mineralogy.

Chlorite

Chlorite is most predominant in those specimens lacking biotite. Chlorite in association with actinolite and/or epidote, usually occurs as fine fibres and is particularly concentrated along the cleavage traces within primary hornblende, corroding the original phenocryst. Chlorite also occurs as dull green-pleochroic fibres throughout the groundmass, outlining the primary metamorphic foliation. Kinking of chlorite occurs in the few specimens where crenulation of the foliation is evident, and growth of some chlorite appears to be synchronous to kinking. Kinked chlorite also occurs in strain shadows, sometimes in association with biotite (Fig. 59).

Epidote - Clinozoisite

Epidote and clinozoisite occur pervasively throughout the metavolcanic sequence. Fine, euhedral crystals of clinozoisite (0.01-0.05 mm) occur throughout the groundmass,

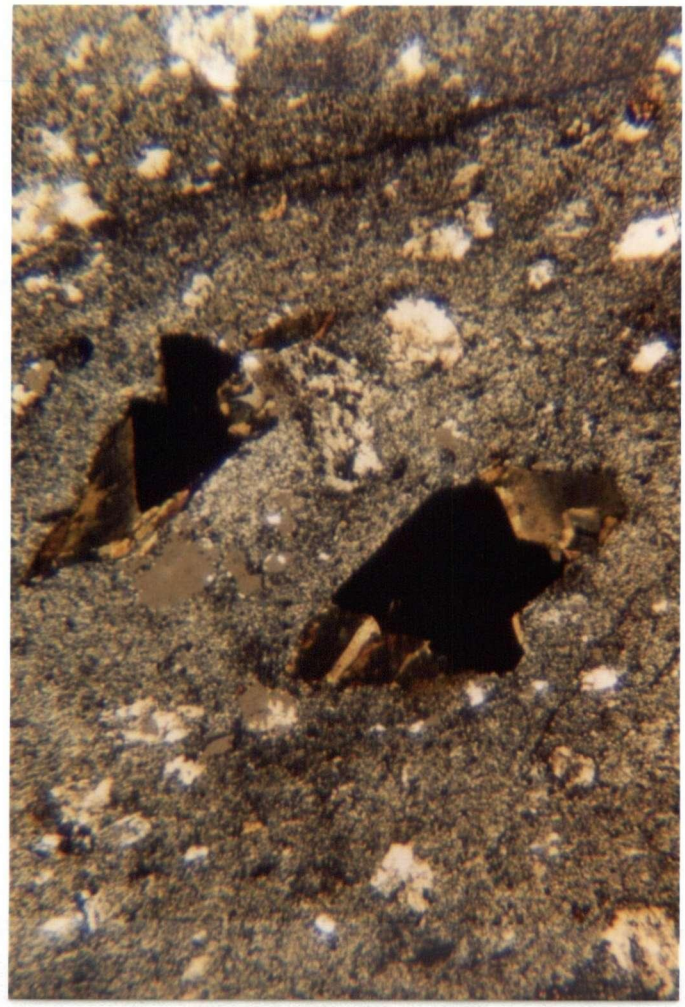

Figure 59: Photomicrograph of kinked chlorite in pressure shadow around pyrite. The kinking indicates that a rotation in the orientation of the principal strain axes occurred subsequent to the growth of the chlorite.

and as coarse crystals (0.1-0.5 mm) within vesicles and fractures. Coarse euhedral to subhedral clinozoisite is often intimately intergrown with fibrous epidote in cross-cutting fractures and open-space fillings (vugs and vesicles). Epidote is also associated with the alteration of primary plagioclase and occurs in association with calcite and sericite.

The relative timing of the growth of individual mineral phases within the volcanics is more difficult to constrain than the metasediments due to the general lack of the development of features associated with pervasive deformation. Where a foliation is observed, it is generally defined by the preferential growth of chlorite. In many samples the foliation is strictly a tectonic foliation, outlined by parallel alignment of metamorphic actinolite or chlorite. In several samples however, the tectonic foliation is closely aligned to what appears to be a primary igneous flow foliation defined by parallel alignment of microphenocrysts within the groundmass, outlining a weakly developed trachytic foliation. Biotite is generally not abundant enough within the volcanics to define a foliation, and is more frequently associated with replacement of mafic minerals. The preferred crystallographic orientation of metamorphic minerals, such as actinolite is not observed within the volcanics although in some specimens fine actinolite needles within the groundmass may show a weakly developed preferred alignment parallel to S_1. Timing of the growth of metamorphic minerals within the volcanics is believed to be synchronous to the underlying metasediments, and the biotite isograd seems to traverse the contact between the two units. Growth of metamorphic mica parallel to the foliation and at high angles to it indicate that metamorphism within the volcanics outlasted first phase deformation.

5.2. CONDITIONS OF METAMORPHISM

Evaluation of the conditions of metamorphism within the Eureka Peak area incorporate evidence from:

1. the relative timing of metamorphic mineral growth based upon structural correlations to the development of folds and foliations.
2. identification of metamorphic mineral assemblages that may be used to distinguish metamorphic zones.

Metamorphic isograds representing the first appearance of garnet are illustrated in figure 53. The assemblages observed are characteristic of greenschist facies metamorphism. Metamorphic reactions are inferred on the basis of mineral associations observed in thin section. Definite mineral reactions cannot be deduced without more extensive sampling of the area and chemical analyses of individual minerals.

The Crooked Amphibolite is inferred to lie within the higher temperature part of low grade metamorphic conditions, due to the presence of metamorphic hornblende. Mineral assemblages observed are characteristic of metamorphosed mafic rocks at greenschist facies (Winkler, 1979). At lower temperatures hornblende becomes unstable; actinolite, chlorite, clinozoisite and epidote replace the hornblende, and coexist with albite, quartz, muscovite and calcite (Winkler, 1979). From the textural features observed, it appears that hornblende is quite stable with only minor retrograde alteration to actinolite, chlorite, and talc. Chlorite is pervasive in the Crooked Amphibolite, defining the schistose foliation, and is considered to be diagnostic of low grade metamorphism. Metamorphic hornblende, containing inclusions of crystallographically continuous epidote may have formed at the expense of actinolite and epidote during prograde reactions. Inclusion trails within the hornblende either traverse straight across the crystal, or show only minor rotation.

In terms of relative timing, it appears that chlorite, biotite and epidote were the earliest phases to form, synchronous to first phase deformation. Hornblende porphyroblasts containing optically continuous inclusions of these minerals indicates that the hornblende porphyroblasts developed slightly later. Little data is available concerning the metamorphic changes in mafic rocks at these conditions. But on the basis of field evidence, it is postulated that the change from actinolite to hornblende occurs at approximately the same P-T conditions as the appearance of almandine garnet, in metapelitic rocks, at about 500°C (Winkler, 1979). This is consistent with the field observations in the Eureka Peak area, where garnet-bearing phyllites are located adjacent to the Crooked Amphibolite.

Within the metapelitic black phyllite sequence it is apparent that the bulk composition of the rocks significantly affects the mineral parageneses observed, particularly the presence of chloritoid. The formation of chloritoid requires a special bulk composition, characterized by a large Fe/Mg ratio, a reltively high Al content, and low K, Na, and Ca. Two reactions have been proposed for the formation of chloritoid:

(pyrophyllite + Fe-rich chlorite) = (chloritoid + quartz + H_2O)

(hematite + Fe-rich chlorite) = (chloritoid + magnetite + quartz + H_2O)

The first reaction has been proposed for the first appearance of chloritoid (Frey, 1978), and based on the mineral assemblages observed, it is preferred over the second reaction (Thompson and Norton, 1968) for the development of chloritoid. The lack of hematite and magnetite in the observed assemblages tends to favor the first reaction.

The mineral assemblages characterizing the porphyroblastic phyllites are almandine, chlorite, chloritoid, albite, muscovite and quartz. Formation of almandine-rich garnet is characteristic of the higher temperature part of greenschist facies

metamorphism. Temperature and pressure constraints on the first appearance of garnet are dependant on its composition. Experimental work by Hirschberg and Winkler (1968) suggests that garnet can be produced at a temperature of 500°C, with pressures in excess of 4kb. The coexistence of albite and chloritoid is relatively rare, but implies definite temperature constraints. The albite - chloritoid pair has been reported in the Wissahickon schist of Maryland (Hietanenm, 1941, 1951) where the reaction:

(chlorite + paragonite + quartz) = (chloritoid + albite + H_2O)

From the mineral assemblages observed, this seems like a feasible reaction. Experimental work by Hoschek (1969) using this same reaction found that chloritoid and albite coexisted over a very limited temperature range of 510–575°C, but was not so greatly constrained by pressure. The proximity of the reaction to the upper boundary of the greenschist facies, and the limited stability of chloritoid in that range probably in part accounts for the relative rarity of the observed assemblage.

The assemblages characterizing the Takla Group volcanics are actinolite, chlorite, epidote, albite, biotite, quartz and calcite. The effect of metamorphism within the volcanics is limited primarily to secondary overgrowths of the primary igneous mineralogy, and the variable development of a preferred planar fabric outlined by fine chlorite. The occurrence of actinolite as rhombic porphyroblasts, and fine acicular needles is ubiquitous throughout the sequence. The presence of biotite is pervasive within the lower portion of the volcanic stratigraphy, south of Eureka Peak. To the west of Eureka Peak and within the core of the syncline, chlorite dominates the assemblage. Textures associated with the alteration of the primary igneous mineralogy are fairly consistent throughout the region. Primary hornblende is frequently replaced by actinolite and chlorite, or biotite and chlorite. Pyroxene shows secondary alteration to chlorite and calcite, and is sometimes enveloped by actinolite and biotite.

Sausseritization of plagioclase is variable. In some samples, replacement of plagioclase by epidote, calcite and sericite is complete, and in other specimens alteration is less pronounced.

Study of the mineralogical and microtextural evidence suggests that prograde metamorphism within the Eureka Peak area was initiated early in the deformational history, and was associated with Jurassic convergence. The textural relationships within the Quesnel River Group sediments yield the most information about the relative timing of metamorphic events due to the pervasive development of structural features, particularly the penetrative and non-penetrative cleavages. Correlation with structural features, such as foliations, allows the relative timing of the metamorphic mineral growth to be inferred.

The growth of metamorphic minerals as porphyroblast phases occurred during and outlasted phase one deformation. The first phase foliation is evident in all lithologies, and is defined by the growth of metamorphic biotite and chlorite in the Crooked Amphibolite; muscovite and phengite or paragonite in the Quesnel River Group sediments; and chlorite in the Takla Group volcanics. Porphyroblast phases within the Crooked Amphibolite developed synchronous to post- F_1. Most porphyroblasts contain inclusions of the S_1 foliation which traverse the porphyroblasts as straight lines, and rarely show any curvature internal to the porphyroblast. From this textural relationship, it can be inferred that the porphyroblasts developed synchronous to post- F_1.

Without conducting geothermometric and geobarometric studies, temperature and pressure conditions of metamorphism can only be postulated, based upon the application of published experimental work to mineral assemblages and textures observed in thin section. A narrow temperature range of 510°C to 575°C has been established for the

coexistence of albite and chloritoid, based upon experimental work of Hoschek (1969). Pressure constraints on this assemblage have not been specifically determined. Chloritoid has a limited stability at the upper boundary of the greenschist facies, which partially accounts for the relative rarity of the observed assemblage, in addition to the special bulk composition required for the formation of chloritoid (Zen, 1960).

The temperature conditions necessary for the coexistence of albite and chloritoid inferred from experimental work is consistent with field observations in the Eureka Peak area. The presence of metamorphic hornblende as a stable phase is also indicative of the higher temperature boundary of the greenschist facies. It is postulated, based on field evidence, that the transition from metamorphic actinolite to hornblende as a stable phase occurs at about 500°C; the same P-T conditions as the first appearance of garnet in metapelites (Winkler, 1979). The presence of garnet bearing phyllites immediately adjacent to the Crooked Amphibolite supports this inference.

The predominance of filled fractures on all scales throughout the Eureka Peak area is indicative of the presence of a high pressure, mobile fluid phase. The pore fluids are generated by dewatering reactions accompanying prograde metamorphism and by the dissolution processes of pressure solution, as discussed in chapter 4. Pore fluid pressures during regional metamorphism tend to lower the effective stresses, thereby increasing porosity and permeability (Etheridge et al. 1983, 1984) . Fluid migration is a natural consequence of the enhanced porosity and permeability, and is in part due to the large pressure gradients induced during the hydraulic fracturing process. Dominant transport mechanisms are advection and diffusion (Etheridge et al. 1984). Solute diffusion (Nabarro-Herring creep and Coble creep) generally occurs on the scale of centimetres and is restricted to chemical potential gradients. Advection is the mass transport mechanism operative at the regional scale and is responsible for extensive

fluid circulation and heat transfer. The driving forces behind advective flow are:

1. the large scale thermal buoyancy arising from an enhanced thermal gradient inherent to regional metamorphism.
2. local gradients in pore fluid pressure in the bulk rock mass, and the pore fluid pressure in dilatant zones such as hydraulic fractures on all scales, faults, or any other zones characterized by a high strain rate (Etheridge et al. 1983).

Advective processes also seem to play a dominant role in pressure solution processes. The significant volume loss during foliation development is indicative of a substantial fluid flux through the rock and removal of soluble material. Dewatering reactions accompanying prograde metamorphism are capable of contributing significantly to the pore fluid "budget" of the rocks, and maintaining high fluid pressures. The pervasive development of dissolution cleavages, and quartz filled fractures on all scales suggest that the fluids were mobile. Mobilization of pore fluids by advective flow is favored to diffusional processes. Diffusion, a temperature dependant process, only becomes active on the large scale at high temperatures. Advective flow is more likely operational at the prevailing temperature conditions of the Eureka Peak area. Field evidence suggests that the dissipation of heat from the underlying rocks was accomplished by large scale circulation of fluids inherent to the process of advective flow, resulting in the rapid decrease in metamorphic grade observed across the tectonic boundary and the dominance of veins filled with minerals reflective of the prevailing temperature and pressure conditions.

6. DISCUSSION - TECTONIC INTERPRETATION

The Eureka Peak area lies within the Quesnel terrane of the Intermontane Belt (Monger et al. 1982), and is adjacent to the Omineca Belt-Intermontane Belt tectonic boundary. The map area is underlain by sedimentary and volcanic rocks which comprise the easternmost facies of the Quesnel terrane. The terrane boundary is defined by the Eureka thrust. Three phases of deformation and one episode of regional metamorphism have been documented within the study area.

Detailed geologic mapping has established the stratigraphic succession underlying the map-area. Three major lithostratigraphic units are recognized, representing sedimentary and volcanic rocks of the Quesnel terrane correlative to the Crooked Amphibolite, the Quesnel River Group, and the Takla Group.

In recent years, the geologic setting of the area has been interpreted in terms of a convergent zone between the island arc related Quesnel terrane and the Barkerville terrane (Struik, 1986). The Quesnel terrane is represented by an allochthonous succession of sedimentary and volcanic rocks thrust eastwards over rocks of continental affinity, represented by the Hadrynian to early Paleozoic Snowshoe Group of the Barkerville terrane. The basal thrust of the Quesnel terrane is the Eureka thrust at the base of the Crooked Amphibolite (Fig. 2). The Crooked Amphibolite occurs as a discontinuous unit along the terrane boundary. It may be correlative to the Antler Fm of the Slide Mtn Group which comprises the Slide Mtn terrane exposed further to the north, structurally overlying the Barkerville terrane (Struik, 1986). Where the Crooked Amphibolite is absent, the Eureka thrust occurs at the base of the Quesnel River Group rocks, structurally overlying the Snowshoe Group rocks. If the Crooked Amphibolite is correlative to the Antler Fm of the Slide Mtn Group, it may represent an imbricate sliver of the Slide Mtn terrane, and therefore

should not be included within the Quesnel terrane, as it has by Struik (1986). Alternatively, the Crooked Amphibolite may represent a portion of oceanic crust upon which the Quesnel River Group sediments were directly deposited, and thus represent the basal member of the Quesnel terrane. The positioning of the Eureka thrust, either at the base of the Crooked Amphibolite or at the base of the Quesnel River Group has significant implications for the role of the Crooked Amphibolite in the tectonic evolution of the terrane boundary. At the present time, the origin of the Crooked Amphibolite is unknown. Although the Crooked Amphibolite in the Eureka Peak area occupies the same structural position with respect to the Barkerville terrane as the Slide Mtn Group exposed further to the north, no physical link between the two has been established. Ophiolites exposed in the Dunford Lake area appear to be correlative to the Crooked Amphibolite, and may represent remnants of oceanic basement upon which the Triassic Quesnel River Group sediments were deposited. However, no direct correlations can be made based on physical relationships. A detailed study of the petrologic and geochemical characteristics of the volcanic rocks from the three locations may provide additional information to resolve the problem.

Petrologic and geochemical studies of the Takla Group volcanics suggest protoliths of island arc and marginal basin affinities. Convergence along the plate margin is believed to have initiated during the Jurassic, when rocks of island arc affinity were accreted to the cratonal margin of North America. At least three distinct phases of deformation have been recognized within the Quesnel terrane in the Eureka Peak area. Correlation of features observed across the plate boundary has established the structural continuity in the region and recognition of structural phases common to both the Barkerville and Quesnel terranes, which developed in response to plate convergence. A transition in structural style with structural level has been documented

within the region at the deeper structural levels (Elsby, 1985; Fillipone, 1985; Montgomery, 1985; Ross et al. 1985). A similar variation is observed within the Eureka Peak area where structural style is influenced by structural level and lithology.

During the initial stages of convergence deformation is accomodated by folding accompanied by the development of a penetrative, axial plane parallel slaty cleavage. Inhomogeneous accomodation of strain during deformation has resulted in the development of detachment surfaces along stratigraphic contacts resulting from extreme viscosity contrasts of adjacent lithologies. Localized zones of higher strain are evidenced within tens of metres of the faults where tightening of first phase structures is extreme, causing local transposition. The effects of regional metamorphism accompanying deformation are evidenced by the growth of mineral assemblages characteristic of the greenschist facies of metamorphism. Dissipation of heat from the underlying Barkerville terrane into the Quesnel terrane is suggested by the rapid transition in metamorphic grade across the boundary (Fillipone, 1985), where contrasting amphibolite facies rocks of the Barkerville terrane are adjacent to greenschist facies rocks of the Quesnel terrane. Mobilization of metamorphic fluid is indicated by the presence of veins and quartz filled fractures at various orientations to S_1. In addition, the slaty cleavage surface has acted as a locus along which pressure solution has occurred, providing a pathway for the escape of fluids generated during metamorphism. Deposition of material within extensional fractures is prominent adjacent to the contact between the Quesnel River Group sediments and the overlying Takla Group volcanics, where the viscosity contrast between the two lithologies provides a barrier to extensive fluid flow. Concentration of fluids along the contact may have had a buoying effect on the volcanics, allowing further eastward translation during deformation.

Progressive deformation during continued convergence led to the eventual

"locking-up" of the terrane boundary, which was buckled into the cuspate form of the Eureka Peak syncline. Mesoscopic features related to this deformational event are evidenced by the extreme flattening of F_1 folds adjacent to the lithologic boundaries. Second phase southwesterly verging folds are associated with a non-penetrative spaced or crenulation cleavage that overprints all earlier-formed structures and deforms the low-angle thrust contacts. The growth of metamorphic minerals parallel or subparallel to S_2 suggests that metamorphism outlasted first phase deformation. Lower temperature assemblages associated with F_2 (muscovite-chlorite) suggest that metamorphism was waning. Pressure solution along S_2 indicates that fluid transfer from the underlying sequences was still active at this time.

A tectonic model has been proposed for the evolution of the Crooked Lake area (Ross et. al 1985), based on this and related projects (Elsby, 1985; Fillipone, 1985; Montgomery, 1985), and is illustrated in figure 60. Convergence between the Quesnel terrane and Barkerville terrane involves the deformation of two tectonic packages of contrasting rheological properties resulting in a systematic transition in structural style with structural level (Campbell, 1973; Fillipone, 1985). Within the Quesnel terrane a similar transition in structural style with structural level is observed. At lower structural levels, folds are tight to isoclinal with extensive flattening resulting in transposition of early structures, particularly close to lithologic boundaries. At higher structural levels, fold forms become more open and upright.

Initiation of convergence along the plate margin is interpreted to have occurred in pre- to mid-Jurassic time (Ross et. al 1985). Amalgamation of the Quesnel terrane with other smaller terranes of the Intermontane Belt probably occurred prior to Jurassic time. Translation and eventual obduction of the Quesnel terrane over the Barkerville terrane may have been facilitated by a regional topographic and structural slope

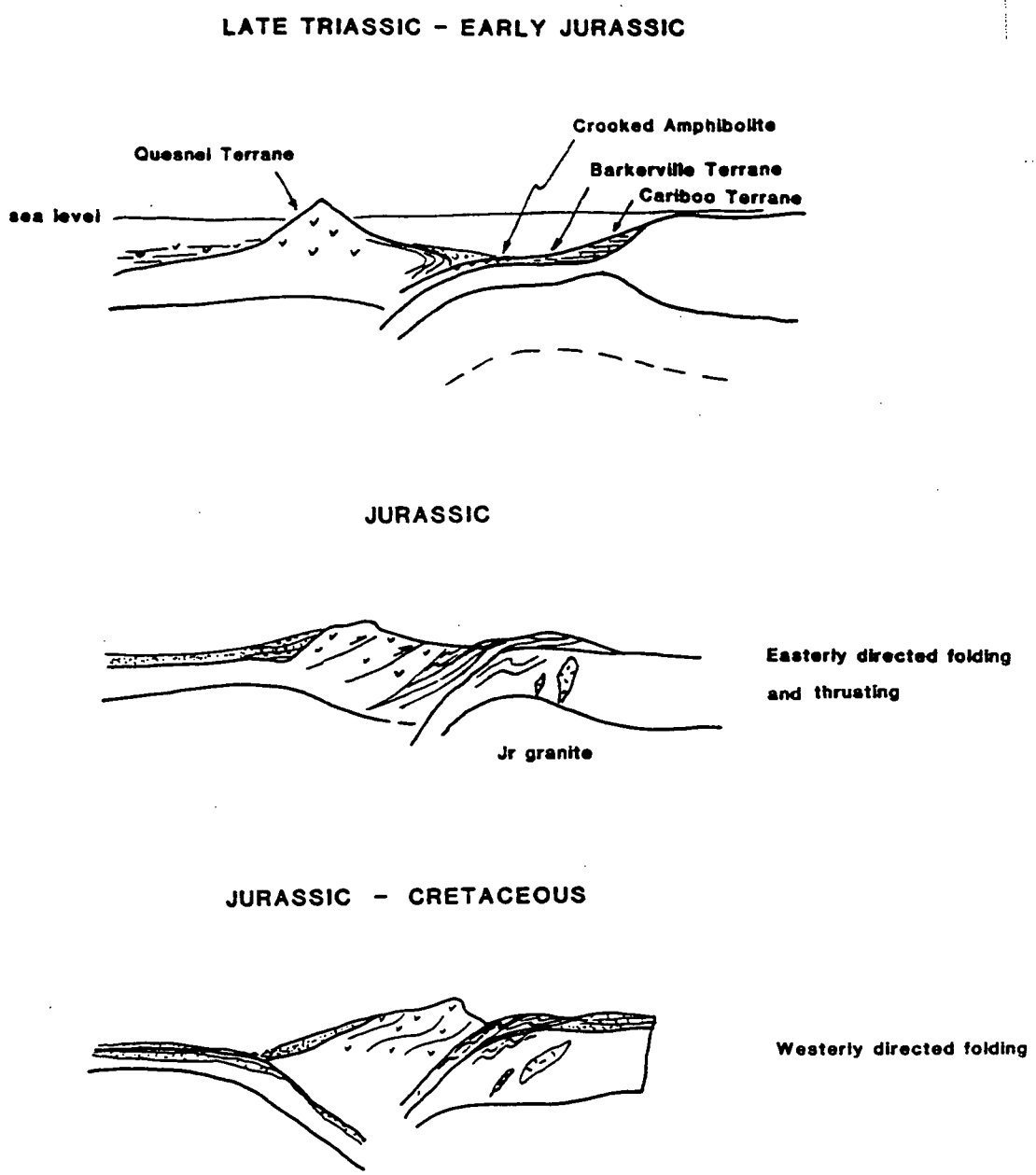

Figure 60: Interpretive tectonic model illustrating the evolution of the plate boundary throughout the Mesozoic.

associated with the Triassic marginal basin situated to the west of the craton. Eastward directed thrusting of the Quesnel terrane over a westwardly dipping subduction zone was followed by obduction of the Quesnel terrane over the Barkerville terrrane. Subsequent tectonic burial of the Barkerville terrane resulted in a regional metamorphism reflected by high grade assemblages within the metasediments of the Barkerville terrane and greenschist facies assemblages within the metasedimentary and metavolcanic sequences of the Quesnel terrane. Metamorphism is synchronous to the first phase of deformation within the Quesnel terrane, and is associated with the growth of metamorphic minerals, extensive pressure solution along cleavage surfaces and remobilization of metamorphic fluids within extensional veins and fractures at the higher structural levels. Continuing metamorphism during phase 2 deformation is indicated by the development of pressure solution surfaces, and the continued growth of metamorphic minerals parallel to S_2. Second phase deformation involves folding of the tectonic boundary, establishing the regional map pattern, and producing southwesterly verging folds. Tightening of first phase, convergence related folds and extreme flattening localized along the terrane boundary and lithologic contacts are the result of inhomogeneous strain accomodation during deformation.

7. REFERENCES

Anderson, O.L. and Grew, P.C. 1977. Stress corrosion theory of crack propogation with applications to geophysics. Reviews of Geophysics and Space Physics, 15, pp. 77–104.

Beach, A. 1974. A geochemical investigation of pressure solution and the formation of veins in deformed greywacke. Contributions to Mineralogy and Petrology, 46, pp. 61–68.

Beach, A. 1982. Chemical processes in deformation at low metamorphic grades: pressure solution and hyraulic fracturing. Episodes, no. 4, pp. 22–25.

Beccaluva, L., Ohnenstetter, D., and Ohnenstetter, M. 1979. Geochemical distribution between ocean floor and island arc tholeiites, applications to some ophiolites. Canadian Journal of Earth Sciences, v. 16, pp. 1874–1882.

Best, M.G. 1982. Igneous and metamorphic petrology. W.H. Freeman and Company, San Francisco, 630 pages.

Bloodgood, M.A. 1987. Geology of the Triassic black phyllite in the Eureka Peak area, central British Columbia. BC Ministry of Energy, Mines and Petroleum Resources, Geological Fieldwork 1986. Paper 1987–1. pp.135–142.

Campbell, K.V. 1971. Metamorphic petrology and structural geology of the Crooked Lake area, Cariboo Mountains, British Columbia. Ph.D. thesis, University of Washington, Seattle, Washington, 192 pages.

Campbell, K.V. and Campbell, R.B. 1970. Quesnel Lake map area, British Columbia. In report of activities, part A. Geological Survey of Canada, Paper 70–1, pp. 32–35.

Campbell, R.B. 1970. Structural and metamorphic transitions from infrastructure to suprastructure, Cariboo Mountains, British Columbia. The Geological Association of Canada, Special Paper No. 6, pp. 67-72.

Campbell, R.B. 1973. Structural cross-section and tectonic model of the southeastern Canadian Cordillera. Canadian Journal of Earth Sciences, 10, pp. 1607-1620.

Campbell, R.B. 1978. Quesnel Lake (93A) map area, British Columbia. Geological Survey of Canada, Open File map 574.

Campbell, R.B., Mountjoy, E.W. and Young, F.G. 1973. Geology of the McBride map area, British Columbia (93H). Geological Survey of Canada, Paper 72-35, 104 pages.

Carye, J.A. 1985. Structural geology of part of the Crooked Lake area, Quesnel Highlands, British Columbia. Unpublished M.Sc. University of British Columbia. Vancouver, British Columbia, 185 pages.

Cawthorn, R.G. and O'Hara, M.J. 1976. Amphibole fractionation in calcalkaline magma genesis. America Journal of Science, 276, pp. 309-329.

Coney, P.J., Jones, D.L. and Monger, J.W.H. 1980. Cordilleran suspect terranes. Nature, 288, pp. 329-333.

deBoer, R.B. 1977. On the thermodynamics of pressure solution - interaction between chemical and mechanical forces. Geochimica et Cosmochimica Acta, 41, pp. 249-256.

Dieterich, J.H. 1969. Origin of cleavage in folded rocks. American Journal of Science, 267, pp. 155-165.

Durney, D.W. 1972. Solution-transfer, an important geological deformation mechanism. Nature, 235, pp. 315-317.

Elsby, D.C. 1985. Structure and deformation across the Quesnellia- Omineca terrane boundary, Mt. Perseus area, east-central British Columbia, Unpublished M.Sc., University of British Columbia. Vancouver, British Columbia, 178 pages.

Etheridge, M.A. 1983. Differential stress magnitudes during regional deformation and metamorphism: upper bound imposed by tensile fracturing. Geology, 11, pp. 231-234.

Etheridge, M.A., Wall, V.J., Cox, S.F. and Vernon, R.H. 1984. High fluid pressure during regional metamorphism and deformation: Implications for mass transport and deformation mechanisms. Journal of Geophysical Research, 89, pp. 4344-4358.

Etheridge, M.A., Wall, V.J. and Vernon, R.H. 1983. The role of the fluid phase during regional deformation and metamorphism. Journal of Metamorphic Geology, 1, pp. 205-226.

Fillipone, J.A. 1985. Structure and metamorphism at the Intermontane - Omineca boundary, near Boss Mountain, east central British Columbia, Unpublished M.Sc. University of British Columbia. Vancouver, British Columbia, 156 pages.

Floyd, P.A., and Winchester, J.A. 1975. Magma type and tectonic setting discrimination using immobile elements. Earth and Planetary Science Letters, 27, pp. 211-218.

Gray, D.R. and Durney, D.W. 1979. Investigations on the mechanical significance of crenulation cleavage. Tectonophysics, 58, pp. 35-79.

Grove, T.L. and M.L. Baker 1984. Phase equilibrium controls on the tholeiitic versus calcalkaline differentiation trends. Journal of Geophysical Research, 89, pp. 3253-3274.

Hietanemn, A. and Cloos, E. 1941. Geology of the Martie overthrust and the Glenarm series in Pennsylvania and Maryland. Geological Society of America Special Papers, 35, 207 pages.

Hietanemn, A. 1951. Chloritoid from Rawlinsville, Lancaster County, Pennsylvania. American Mineralogist, 36, pp. 859-868.

Hirschberg, A. and Winkler, H.G.F. 1968. Contributions to Mineralogy and Petrology, 18, pp. 17-42.

Hobbs, B.E., Means, W.D. and Williams, P.F. 1976. An outline of structural geology. John Wiley and Sons, 571 pages.

Hoschek, G. 1969. The stability of staurolite and chloritoid and their significance in metamorphism of pelitic rocks. Contributions to Mineralogy and Petrology, 22, pp. 208-232.

Hubbert, M.K. and Rubey, W.W. 1959. Role of fluid pressure in mechanics of overthrust faulting. Geological Society of America Bulletin, 70, pp. 115-166.

Irvine, T.N., and Baragar, W.R. 1971. A guide to the chemical classification of the common volcanic rocks. Canadian Journal of Earth Sciences, 8, 523-548.

Jakes, J.P., and Gill, J. 1970. Rare earth element abundances and the island arc tholeiitic series. Earth and Planetary Science Letters, 9, 17-28.

Jakes, J.P. and White, A.J.R. 1972. Major and trace element abundances in volcanic

rocks of orogenic areas. Geological Society of America Bulletin, 83, pp. 29–40.

Miyashiro, A. 1974. Volcanic rock series in island arcs and active continental margins. American Journal of Science, 274, pp. 321–355.

Monger, J.W.H., Price, R.A. and Tempelman–Kluit, D. 1982. Tectonic accretion and the origin of two major metamorphic and plutonic welts in the Canadian Cordillera. Geology, 10, pp. 70–75.

Montgomery, J.R. 1985. Structural relations of the southern Quesnel Lake Gneiss, Isoceles Mountain area, central British Columbia. MSc. thesis, University of British Columbia, Vancouver, British Columbia.

Montgomery, S.L. 1978. Structural and metamorphic history of the Dunford Lake map area, Cariboo Mountains, British Columbia. M.S. thesis, Cornell University, Ithaca, New York.

Norris, R.J. and Henley, R.W. 1976. Dewatering of a metamorphic pile. Geology, 4, pp. 333–336.

Orchard, M.J. and Struik, L.C. 1985. Conodants and stratigraphy of upper Paleozoic limestones in Cariboo gold belt, east–central British Columbia. Canadian Journal of Earth Sciences, 22, pp. 538–552.

Pearce, J.A. 1975. Basalt geochemistry used to investigate past tectonic environments of Cyprus: Volcanic rock suites – Geochemical fingerprint. Tectonophysics, 25, pp. 41–67.

Pearce, J.A., and Cann, J.R. 1973. Tectonic setting of basic volcanic rocks determined using trace element analyses. Earth and Planetary Science Letters, 19, 290–300.

Pearce, J.A. and Norry, M.J. 1979. Petrogenetic implications of Ti, Zr, Y, and Nb variations in volcanic rocks. Contributions to Mineralogy and Petrology, 69, pp. 33-47.

Powell, C.McA. 1979. A morphological classification of rock cleavage. Tectonophysics, 58, pp. 22-35.

Ramsay, J.G. 1967. Folding and fracturing of rocks. McGraw-Hill, New York, N.Y., 568 pages.

Ramsay, J.G. 1980. The crack-seal mechanism of rock deformation. Nature, 284, pp. 135-139.

Ramsay, J.G. and Huber, M.I. 1983. The techniques of modern structural geology, volume 1,: strain analysis. Academic Press, New York, N.Y., 307 pages.

Rees, C.J. 1981. Western margin of the Omineca Belt at Quesnel Lake, British Columbia. In Current Research, Part A., Geological Survey of Canada, Paper 81-1A, pp. 223-226.

Robin, P.F. 1978. Pressure solution at grain to grain contacts. Geochimica et Cosmochimica Acta, 42, pp. 1383-1389.

Ross, J.V., Fillipone, J.A., Montgomery, J.R., Elsby, D.C. and Bloodgood, M.A. 1985. Geometry of a convergent zone, central British Columbia, Canada. Tectonophysics, in press.

Ross, J.V. and Fillipone, J.A. 1986. Configuration of upper continental lithosphere at a convergent margin, central British Columbia, Canada. (abstract) EOS, 67, no. 44, pp. 1190.

Shervais, J.W. 1982. Ti - V plots and the petrogenesis of modern and ophiolitic lavas. Earth and Planetary Science Letters, 59, 101-118.

Siddans, A.W.B. 1972. Slaty cleavage - a review of research since 1815. Earth Science Reviews, 8, pp. 205-232.

Smith, R.E. and Smith, S.E. 1976. Comments on the use of Ti, Zr, Y, Sr, K, P, and Nb in classification of basaltic magmas. Earth and Planetary Science Letters, 32, pp. 114-120.

Sorby, H.C. 1853. On the origin of slaty cleavage. New Philosophical Journal, Edinburgh, 55, pp. 137-148.

Struik, L.C. 1984. Geology of Quesnel Lake and part of Mitchell Lake, British Columbia. Geological Survey of Canada, Open File Map, 962.

Struik, L.C. and Orchard, M.J. 1985. Late Paleozoic conodants from ribbon chert delineate imbricate thrusts within the Antler Formation of the Slide Mountain terrane, central British Columbia. Geology, 13, pp. 749-798.

Struik, L.C. 1986. Imbricated terranes of the Cariboo gold belt with correlations and implications for tectonics in souteastern British Columbia. Canadian Journal of Earth Sciences, 23, pp. 1047-1061.

Sutherland Brown, A. 1963. Geology of the Cariboo River area, British Columbia. British Columbia Department of Mines, Bulletin 47.

Tipper, H.W. 1961. Prince George map area, Cariboo District, British Columbia. Geological Survey of Canada Map 49-1960.

Tipper, H.W. 1978. Northeastern part of the Quesnel (93B) map-area, British Columbia. Current Research, Part A. Geological Survey of Canada, Paper 78-1A, pp. 67-68.

Tipper, H.W., Woodsworth, G.J. and Gabrielse, H. 1978. Tectonic assemblage map of the Canadian Cordillera and adjacent parts of the United States of America. Geological Survey of Canada, Map 1505A.

Tipper, H.W., Campbell, R.B., Taylor, G.S., and Stott, D.F. 1979. Parsnip River, British Columbia (Sheet 93). Geological Survey of Canada, Map 1424A (1:1,000,000).

Wheeler, J.O. and Gabrielse, H. 1972. The Cordilleran structural province. Geological Association of Canada, Special Paper 11, pp. 1-81.

White, S.H. and R.J. Knipe 1979. Microstructure and cleavage development in selected slates. Contributions to Mineralogy and Petrology, 66, pp. 165-177.

Wilkinson, J.F.G. 1986. Classification and average chemical compositions of common basalts and andesites. Journal of Petrology, 27, pp. 31-62.

Williams, P.F. 1972. Development of metamorphic layering and cleavage in low grade metamorphic rocks at Bermagui, Australia. American Journal of Science, 272, pp. 1-47.

Williams, P.F. 1976. Relationships between axial plane foliations and strain. Tectonophysics, 30, pp. 181-196.

Winkler, H.J.F. 1979. Petrogenesis of metamorphic rocks. Springer Verlag, New York, N.Y., fifth edition, 348 pages.

Wood, D.S. 1974. Current views of the development of slaty cleavage. Annual Reviews of Earth and Planetary Sciences, 2, pp. 369-401.

Wright, A.E. and Boyes, D.R. 1963. Classification of volcanic breccias: a discussion. Geological Society of America Bulletin, 74, pp. 79–86.

Zen, E-an 1960. Metamorphism of lower Paleozoic rocks in the vicinity of the Taconic Range in west-central Vermont. The American Mineralogist, 45, pp.129–175.

8. APPENDIX 1

MINERAL NAME	ABBREVIATION
Actinolite	Act
Albite	Ab
Amphibole	Amp
Apatite	Ap
Augite	Ag
Biotite	Bi
Calcite	Cc
Chlorite	Ch
Chloritoid	Ctd
Clinozoisite	Cl
Epidote	Ep
Garnet	Gt
Hematite	He
Hornblende	Hb
Ilmenite	Im
Muscovite	Ms
Magnetite	Mg
Plagioclase	Pl
Pyrite	Py
Pyroxene	Pxn
Quartz	Qz
Sericite	Sc
Sphene	Sp
Tourmaline	To

8.1. METAMORPHIC MINERAL ASSEMBLAGES

CROOKED AMPHIBOLITE:

Sample	Metamorphic Assemblage
522	Ep-Ch-Bi-Im
520	Ch-Ep-Bi-Im

QUESNEL RIVER GROUP:

Sample	Metamorphic Assemblage
519	Gt-Al-Ctd-Ch
450	Al-Ctd-Im
447	Gt-Ms-Im
102	Ms
140	Ch-Ep-Cc
76	Act-Ms-Ch
30	Ch-Cc-Bi
93	Act-Cc-Ch
43	Ch-Cc
46	Ch-Ep-Py
48	Ch-Cc
55	Cc
57	Act-Ep-Ch
159	Ch-Act-Sc-Ep
267	Act-Ch-Ep-Ms
250	Act-Ch
252	Act-Sc-Ch-Cc
260	Act-Ch-Cc
282	Ch-Ms
285	Cc-Ch
293	Act-Cc
300	Act-Ch-Sc
311	Ch-Bi
327	Bi-Ch
332	Act-Ep-Ch

TAKLA GROUP VOLCANICS:

Sample	Metamorphic Assemblage
01	Ch-Act-Cc
02	Ch-Act-Cc
05	Act-Bi-Cc-Ep
13	Act-Bi-Cc-Ep
15	Act-Bi
16	Act-Bi-Ch
25	Cc-Act-Ch
26	Act-Ch
98	Act-Cc
121	Act-Bi-Ep
185	Bi-Act
216	Act-Bi-Ep
218	Act-Bi-Ep-Ch
219	Act-Bi-Ep
221	Act-Bi-Ep
347	Act-Cc-Ms
352	Act-Bi
358	Act-Bi-Ch-Ep
395	Act-Bi-Ch-Ep
399	Ch-Cc-Sc
361	Cc-Ch-Ep
363	Act-Ep-Ch-Cc-Sc
374	Act-Ch-Cc-Ep
375	Ch-Sc-Ep-Act
380	Act-Ep-Ch
407	Act-Bi-Ch
409	Act-Ch-Ep
412	Act-Ch-Ep-Cc

8.2. IGNEOUS PETROGRAPHY

SAMPLE	IGNEOUS MINERALS	SECONDARY MINERALS	ACCESSORY MINERALS	FRAGMENTS	VESICLES
274	Ag-Pl	Act-Bi-Ep-Qz-Ch-Cc	Mt-Sc		Pl-Cc-Act
218	Pxn-Amp-Pl	Act-Ep-Bi-Sc	Qz-Sp	lithic	Pl-Ca-Ch
252	Pxn-Pl	Act-Qz-Pl-Ch-Ep-Sc	Cc-Sp		
05	Pxn-Hb-Pl	Act-Bi-Cc-Pl	Ep-Cc-Qz		Pl-Cc-Ep
02	Pxn-Hb	Ch-Cc-Act-Ep	Pl-Op		
219	Pxn-Pl	Act-Bi-Ep-Qz-Ch	Pl-Sc-Op		
275	Pxn-Pl	Act-Ep-Ch-Sc	Qz-Sp	lithic	
260	Pxn-Hb	Act-Ch-Cc-Ep	Qz-Pl-Sp-Sc		
293	Pxn-Hb	Act-Bi-Ch-Ep	Sc-Ep		
409	Hb-Pxn-Pl	Act-Ep-Bi-Qz	Cc-Cl		
395	Hb-Pl-Pxn	Act-Bi-Cl-Ep	Py-Qz		Cl
16	Hb-Pl-Pxn	Act-Bi-Ep-Cc-Sc	Qz-Op-Cl		Pl-Cl-Cc-Qz
15	Hb-Pl Pxn	Act-Bi-Ep-Cc	Sc-Op-Ap		Pl-Ep
185	Pxn-Amp	Act-Bi-Ep-Sc-Ch	Op-Qz	lithic	
172	Hb-Pl-Pxn	Act-Bi-Ep	Ap-Sp		
WS86	Hb-Pxn-Pl	Act-Bi-Ep	Qz-Sp	lithic	

SAMPLE	IGNEOUS MINERALS	SECONDARY MINERALS	ACCESSORY MINERALS	FRAGMENTS	VESICLES
01		Act-Cc-Ch-Ep-Sc-Qz		lithic	
332	Pxn-Pl-Qz	Act-Ep-Ch-Cl			
25	Pl-Qz	Act-Bi-Ch-Cc			
WS41	Ag-Pl-Qz	Act-Ep-Ch-Cl			
407	Hb-Pxn	Act-Ep-Ch-Bi	Sp-Cc-Ms		
358a	Hb-Pl	Act-Bi-Ep-Cc	Ap-Sp-Py		
WS70	Pl-Hb-Pxn-Qz	Act-Bi-Ep-Ch	Py-Ap-Sc		
300	Amp-Pl	Act-Ch-Ep-Qz-Cc-Sc	Sp-Py		
374	Pxn-Hb-Pl	Act-Ep-Ch	Sc-Qz		
358b	Pl-Amp	Act-Bi-Ep-Cc-Ch-Cl	To-Sc.		Cc-Act
269	Pxn	Act-Ch-Ep	Ms-Cc		
358c	Pxn-Amp	Act-Bi-Cl-Cc	Op-Sc		Qz-Cc-Ch
46		Qz-Ch-Ep-Cc-Act	Py-Pl		

9. APPENDIX 2

9.1. MAJOR AND TRACE ELEMENT ANALYSES BY XRF

All samples selected for analyses were prepared by the author according to the procedures outlined below. Rock specimens were first crushed in a chipmunk jaw crusher in the UBC sample preparation lab. Samples were then reduced to approximately 200 mesh powder by hand grinding in a small agate mortar, followed by 4 to 5 minutes in a mechanical agate mortar. This procedure was followed in order to minimize contamination introduced by the machinery used in sample preparation (Hickson and Juras, in press). The powder samples were then pressed into powder pellets for XRF analysis.

9.1.1. Major Element Analysis

A total of 29 samples were analysed as unknowns with 14 standards for which major element concentrations are reported as oxides. Analyses for H_2O and CO_2 were not performed. The analysis was carried out by x-ray fluoresence spectroscopy on an automated Phillips spectrometer. The analyses were performed on the pressed powder samples by B. Cousens in the department of Oceanography at the University of British Columbia, according to the procedures of Armstrong(1985).

9.1.2. Trace Element Analyses

Concentrations of Ba, Cr, Nb, Ni, Rb, Sr, V, Y, and Zr were determined by XRF analysis. The 29 pressed powder pellets were used for both major and trace element analyses. All analyses were analyzed by B. Cousens at UBC, department of Oceanography. Data was reduced using a computer program produced by C. Hickson (1986).

9.2. REDUCED GEOCHEMICAL DATA

SAMPLE		(274)		(218)		(252)		(05)		(02)		(219)		
Wt. %	σ_C †													Det.
SiO2(w	3.26	51.45 ± 0.0		50.75 ± 0.0		49.87 ± 0.0		52.67 ± 0.0		44.13 ± 0.0		51.45 ± 0.0		0.201
TiO2	0.03	0.71 ± 0.0		0.66 ± 0.0		0.55 ± 0.0		0.81 ± 0.0		1.12 ± 0.0		0.55 ± 0.0		0.006
AL2O3	0.79	13.68 ± 0.0		12.38 ± 0.0		14.46 ± 0.0		10.85 ± 0.0		15.59 ± 0.0		12.87 ± 0.0		0.180
FE2O3	0.42	11.37 ± 0.0		10.38 ± 0.0		9.56 ± 0.0		11.51 ± 0.0		13.98 ± 0.0		10.84 ± 0.0		0.008
						0.0 ± 0.0		0.0 ± 0.0		0.0 ± 0.0		0.0 ± 0.0		0.007
MNO	0.80	0.16 ± 0.0		0.17 ± 0.0		0.17 ± 0.0		0.18 ± 0.0		0.21 ± 0.0		0.18 ± 0.0		0.050
MGO	0.42	8.00 ± 0.0		10.50 ± 0.0		11.61 ± 0.0		8.84 ± 0.0		10.51 ± 0.0		9.28 ± 0.0		0.015
CAO	0.27	9.29 ± 0.0		10.80 ± 0.0		9.42 ± 0.0		10.42 ± 0.0		10.51 ± 0.0		9.75 ± 0.0		0.106
NA2O	0.12	2.39 ± 0.0		2.31 ± 0.0		1.32 ± 0.0		3.40 ± 0.0		3.00 ± 0.0		2.56 ± 0 0		0.015
K2O	0.03	2.54 ± 0.0		1.71 ± 0 0		2.75 ± 0.0		1.42 ± 0.0		0.60 ± 0.0		2.01 ± 0.0		0.010
P2O5	0.0	0.40 ± 0.0		0.34 ± 0.0		0.29 ± 0.0		0.30 ± 0.0		0.34 ± 0.0		0.40 ± 0.0		0.0
						0.0 ± 0.0		0.0 ± 0.0		0.0 ± 0.0		0.0 ± 0.0		0.0
ppm														
Ba(ppm	34.	1013. ± 9.		807. ± 8.		829. ± 9.		687. ± 8.		250. ± 6.		624. ± 8.		13.
Rb	27.	51. ± 1.		33. ± 1.		66. ± 1.		24. ± 1.		≤Det.		44. ± 1.		4.
Sr	2.	389. ± 2.		1089. ± 3.		424. ± 2.		355. ± 2.		1084. ± 3.		442. ± 2.		3.
Nb	6.	≤Det.		≤Det.		≤Det.		≤Det.		2222. ± 150.		2222. ± 150.		4.
Y	3.	18. ± 1.		19. ± 1.		21. ± 1.		15. ± 1.		17. ± 2.		17. ± 1.		3.
Zr	3.	48. ± 1.		29. ± 0.		53. ± 1.		40. ± 1.		35. ± 0.		62. ± 1.		3.
Cr	13.	114. ± 1.		430. ± 2.		≤Det.		227. ± 2.		137. ± 1		370. ± 2.		1.
Ni	21.	63. ± 2.		143. ± 2.		320. ± 2.		65. ± 2.		77. ± 2.		113. ± 2.		4.
Co	3.	0. ± 0.		0. ± 0.		0. ± 0.		0. ± 0.		0. ± 0.		0. ± 0.		2.
Cu	9.	0. ± 0.		0. ± 0.		0. ± 0.		0. ± 0.		0. ± 0.		0. ± 0.		0.
						0. ± 0.		0. ± 0.		0. ± 0.		0. ± 0.		0.
						0. ± 0.		0. ± 0.		0. ± 0.		0. ± 0.		0.
V	0.	265. ± 1.		278. ± 1.		248. ± 1.		224. ± 1.		394. ± 2.		230. ± 1.		0.

† σ_C is the error in the calibration. The ± error given after each value is is $\sigma_I = \sqrt{(\sigma_N'^2 + \sigma_R'^2)}$, see text for further explanation.

SAMPLE		(275)			(280)			(293)			(16)			(15)			(185)			
Wt. %	σ_C †																			Det.
SIO2(w	3.26	46.85	±	0.0	50.95	±	0.0	51.88	±	0.0	50.39	±	0.0	53.74	±	0.0	48.70	±	0.0	0.201
TIO2	0.03	0.40	±	0.0	0.52	±	0.0	0.51	±	0.0	0.79	±	0.0	0.86	±	0.0	0.46	±	0.0	0.006
AL203	0.79	9.82	±	0.0	15.57	±	0.0	13.79	±	0.0	13.08	±	0.0	15.84	±	0.0	11.28	±	0.0	0.180
FE203	0.42	10.89	±	0.0	11.31	±	0.0	11.42	±	0.0	10.79	±	0.0	8.57	±	0.0	11.16	±	0.0	0.008
								0.0	±	0.0	0.0	±	0.0	0.0	±	0.0	0.0	±	0.0	0.007
MNO	0.80	0.18	±	0.0	0.19	±	0.0	0.19	±	0.0	0.17	±	0.0	0.16	±	0.0	0.19	±	0.0	0.050
MGO	0.42	17.01	±	0.0	9.14	±	0.0	9.23	±	0.0	8.20	±	0.0	6.45	±	0.0	13.69	±	0.0	0.015
CAO	0.27	10.68	±	0.0	7.26	±	0.0	8.92	±	0.0	10.83	±	0.0	7.84	±	0.0	11.71	±	0.0	0.106
NA20	0.12	0.35	±	0.0	1.21	±	0.0	1.38	±	0.0	3.18	±	0.0	2.72	±	0.0	0.21	±	0.0	0.015
K20	0.03	1.65	±	0.0	3.54	±	0.0	2.37	±	0.0	2.21	±	0.0	3.42	±	0.0	2.31	±	0.0	0.010
P205	0.0	0.17	±	0.0	0.31	±	0.0	0.32	±	0.0	0.37	±	0.0	0.40	±	0.0	0.28	±	0.0	0.0
								0.0	±	0.0	0.0	±	0.0	0.0	±	0.0	0.0	±	0.0	0.0
ppm																				
Ba(ppm	34.	1190.	±	10.	1706.	±	12.	912.	±	9.	1234.	±	10.	1484.	±	10.	1172.	±	11.	13.
Rb	27.	20.	±	1.	88.	±	1.	50.	±	1.	32.	±	1.	41.	±	1.	37.	±	1.	4.
Sr	2.	131.	±	2.	375.	±	2.	1324.	±	3.	731.	±	2.	1348.	±	3.	97.	±	2.	3.
Nb	6.	≤Det.			≤Det.			≤Det.			8.	±	1.	8.	±	1.	2222.	±	150.	4.
Y	3.	12.	±	1.	17.	±	1.	18.	±	1.	17.	±	1.	18.	±	1.	12.	±	1.	3.
Zr	3.	30.	±	1.	51.	±	1.	40.	±	0.	45.	±	1.	55.	±	0.	33.	±	2.	3.
Cr	13.	1484.	±	3.	401.	±	2.	409.	±	2.	185.	±	2.	58.	±	1.	931.	±	3.	1.
NI	21.	832.	±	3.	167.	±	2.	148.	±	2.	84.	±	2.	43.	±	1.	214.	±	2.	4.
Co	3.	0.	±	0.	0.	±	0.	0.	±	0.	0.	±	0.	0.	±	0.	0.	±	0.	2.
Cu	9.	0.	±	0.	0.	±	0.	0.	±	0.	0.	±	0.	0.	±	0.	0.	±	0.	0.
								0.	±	0.	0.	±	0.	0.	±	0.	0.	±	0.	0.
								0.	±	0.	0.	±	0.	0.	±	0.	0.	±	0.	0.
V	0.	204.	±	1.	288.	±	1.	253.	±	2.	243.	±	1.	285.	±	1.	230.	±	1.	0.
								0.	±	0.	0.	±	0.	0.	±	0.	0.	±	0.	0.

† σ_C is the error in the calibration. The ± error given after each value is is $\sigma_I = \sqrt{(\sigma_N'^2 + \sigma_R'^2)}$, see text for further explanation.

SAMPLE		(172)			(WS88)			(01)			(332)			(25)			(WS41)			
Wt. %	σ_C †																			Det.
SIO2(w	3.26	54.38	±	0.0	51.85	±	0.0	43.53	±	0.0	45.96	±	0.0	46.16	±	0.0	44.90	±	0.0	0.201
TIO2	0.03	0.72	±	0.0	0.79	±	0.0	0.74	±	0.0	0.88	±	0.0	0.79	±	0.0	0.81	±	0.0	0.006
AL203	0.79	13.79	±	0.0	14.65	±	0.0	13.30	±	0.0	16.08	±	0.0	13.95	±	0.0	16.45	±	0.0	0.180
FE203	0.42	9.37	±	0.0	10.91	±	0.0	11.89	±	0.0	10.66	±	0.0	11.85	±	0.0	10.85	±	0.0	0.008
								0.0	±	0.0	0.0	±	0.0	0.0	±	0.0	0.0	±	0.0	0.007
MNO	0.80	0.17	±	0.0	0.20	±	0.0	0.24	±	0.0	0.13	±	0.0	0.21	±	0.0	0.14	±	0.0	0.050
MGO	0.42	6.34	±	0.0	5.46	±	0.0	16.30	±	0.0	5.48	±	0.0	17.59	±	0.0	5.66	±	0.0	0.015
CAO	0.27	9.18	±	0.0	10.40	±	0.0	12.55	±	0.0	18.25	±	0.0	8.89	±	0.0	19.34	±	0.0	0.106
NA20	0.12	3.81	±	0.0	4.78	±	0.0	0.81	±	0.0	1.69	±	0.0	0.0	±	0.0	1.04	±	0.0	0.015
K20	0.03	2.03	±	0.0	0.58	±	0.0	0.60	±	0.0	0.30	±	0.0	0.33	±	0.0	0.30	±	0.0	0.010
P205	0.0	0.41	±	0.0	0.37	±	0.0	0.23	±	0.0	0.56	±	0.0	0.23	±	0.0	0.50	±	0.0	0.0
								0.0	±	0.0	0.0	±	0.0	0.0	±	0.0	0.0	±	0.0	0.0
ppm																				
Ba(ppm	34.	819.	±	8.	172.	±	5.	266.	±	6.	72.	±	4.	135.	±	5.	91.	±	4.	13.
Rb	27.	28.	±	1.	6.	±	4.	9.	±	2.	≤Det.			≤Det.			≤Det.			4.
Sr	2.	887.	±	3.	772.	±	2.	403.	±	2.	1969.	±	4.	365.	±	2.	1990.	±	4.	3.
Nb	6.	5.	±	1.	10.	±	1.	≤Det.			5.	±	1.	2222.	±	150.	2222.	±	150.	4.
Y	3.	20.	±	1.	20.	±	2.	19.	±	2.	22.	±	2.	19.	±	2.	21.	±	2.	3.
Zr	3.	52.	±	1.	67.	±	1.	61.	±	1.	28.	±	0.	64.	±	1.	25.	±	0.	3.
Cr	13.	85.	±	1.	51.	±	1.	944.	±	3.	65.	±	1.	965.	±	3.	73.	±	1.	1.
NI	21.	36.	±	1.	41.	±	2.	402.	±	3.	39.	±	2.	401.	±	3.	41.	±	2.	4.
Co	3.	0.	±	0.	0.	±	0.	0.	±	0.	0.	±	0.	0.	±	0.	0.	±	0.	2.
Cu	9.	0.	±	0.	0.	±	0.	0.	±	0.	0.	±	0.	0.	±	0.	0.	±	0.	0.
								0.	±	0.	0.	±	0.	0.	±	0.	0.	±	0.	0.
								0.	±	0.	0.	±	0.	0.	±	0.	0.	±	0.	0.
V	0.	238.	±	1.	243.	±	1.	251.	±	1.	317.	±	2.	269.	±	1.	345.	±	2.	0.
								0.	±	0.	0.	±	0.	0.	±	0.	0.	±	0.	0.

† σ_C is the error in the calibration. The ± error given after each value is is $\sigma_I = \sqrt{(\sigma_N^2 + \sigma_R^2)}$, see text for further explanation.

SAMPLE		(407)		(358a)		(WS70)		(300)		(374)		(358b)		
Wt. %	σ_C †													Det.
SIO2(w	3.26	50.46 ± 0.0		53.08 ± 0.0		53.76 ± 0.0		50.03 ± 0.0		52.62 ± 0.0		48.15 ± 0.0		0.201
TIO2	0.03	0.95 ± 0.0		0.84 ± 0.0		0.85 ± 0.0		0.47 ± 0.0		0.55 ± 0.0		0.85 ± 0.0		0.006
AL203	0.79	14.02 ± 0.0		14.58 ± 0.0		15.08 ± 0.0		13.21 ± 0.0		11.89 ± 0.0		14.64 ± 0.0		0.180
FE203	0.42	10.98 ± 0.0		9.28 ± 0.0		10.25 ± 0.0		10.30 ± 0.0		10.73 ± 0.0		12.42 ± 0.0		0.008
						0.0 ± 0.0		0.0 ± 0.0		0.0 ± 0.0		0.0 ± 0.0		0.007
MNO	0.80	0.15 ± 0.0		0.17 ± 0.0		0.18 ± 0.0		0.17 ± 0.0		0.19 ± 0.0		0.22 ± 0.0		0.050
MGO	0.42	8.37 ± 0.0		4.75 ± 0.0		5.20 ± 0.0		13.53 ± 0.0		9.18 ± 0.0		7.74 ± 0.0		0.015
CAO	0.27	10.80 ± 0.0		10.93 ± 0.0		8.04 ± 0.0		8.59 ± 0.0		11.32 ± 0.0		10.91 ± 0.0		0.106
NA20	0.12	2.69 ± 0.0		4.89 ± 0.0		4.94 ± 0.0		0.90 ± 0.0		2.13 ± 0.0		2.98 ± 0.0		0.015
K20	0.03	1.27 ± 0.0		1.35 ± 0.0		1.59 ± 0.0		2.56 ± 0.0		1.05 ± 0.0		1.70 ± 0.0		0.010
P205	0.0	0.30 ± 0.0		0.43 ± 0.0		0.44 ± 0.0		0.24 ± 0.0		0.34 ± 0.0		0.39 ± 0.0		0.0
						0.0 ± 0.0		0.0 ± 0.0		0.0 ± 0.0		0.0 ± 0.0		0.0
ppm														
Ba(ppm	34.	527. ± 7.		469. ± 7.		571. ± 7.		1241. ± 10.		468. ± 7.		702. ± 8.		13.
Rb	27.	20. ± 1.		25. ± 1.		29. ± 1.		72. ± 1.		15. ± 1.		27. ± 1.		4.
Sr	2.	1947. ± 4.		1821. ± 4.		1923. ± 4.		228. ± 2.		838. ± 3.		943. ± 3.		3.
Nb	6.	8. ± 1.		≤Det.		≤Det.		≤Det.		2222. ± 150.		2222. ± 150.		4.
Y	3.	14. ± 1.		16. ± 1.		17. ± 1.		17. ± 1.		15. ± 1.		20. ± 1.		3.
Zr	3.	23. ± 0.		26. ± 0.		24. ± 0.		54. ± 1.		47. ± 1.		48. ± 1.		3.
Cr	13.	111. ± 1.		23. ± 1.		13. ± 0.		838. ± 3.		344. ± 2.		37. ± 1.		1.
Ni	21.	56. ± 2.		21. ± 1.		21. ± 1.		405. ± 2.		102. ± 2.		41. ± 2.		4.
Co	3.	0. ± 0.		0. ± 0.		0. ± 0.		0. ± 0.		0. ± 0.		0. ± 0.		2.
Cu	9.	0. ± 0.		0. ± 0.		0. ± 0.		0. ± 0.		0. ± 0.		0. ± 0.		0.
						0. ± 0.		0. ± 0.		0. ± 0.		0. ± 0.		0.
						0. ± 0.		0. ± 0.		0. ± 0.		0. ± 0.		0.
V	0.	321. ± 2.		232. ± 1.		239. ± 1.		240. ± 1.		229. ± 1.		332. ± 2.		0.
						0. ± 0.		0. ± 0.		0. ± 0.		0. ± 0.		0.

† σ_C is the error in the calibration. The ± error given after each value is is $\sigma_I = \sqrt{(\sigma_N'^2 + \sigma_R'^2)}$, see text for further explanation.

SAMPLE		(409)		(395)		(269)		(368c)		(46)		
Wt. %	σ_C †											Det.
SIO2(w	3.26	52.44 ± 0.0		51.73 ± 0.0		45.92 ± 0.0		48.88 ± 0.0		49.57 ± 0.0		0.201
TIO2	0.03	0.65 ± 0.0		0.81 ± 0.0		0.49 ± 0.0		0.75 ± 0.0		0.78 ± 0.0		0.006
AL2O3	0.79	12.78 ± 0.0		14.01 ± 0.0		10.97 ± 0.0		14.68 ± 0.0		14.97 ± 0.0		0.180
FE2O3	0.42	11.61 ± 0.0		10.47 ± 0.0		15.72 ± 0.0		15.40 ± 0.0		11.25 ± 0.0		0.008
						0.0 ± 0.0		0.0 ± 0.0		0.0 ± 0.0		0.007
MNO	0.60	0.18 ± 0.0		0.19 ± 0.0		0.38 ± 0.0		0.22 ± 0.0		0.18 ± 0.0		0.050
MGO	0.42	8.34 ± 0.0		8.10 ± 0.0		17.09 ± 0.0		7.87 ± 0.0		11.54 ± 0.0		0.015
CAO	0.27	10.34 ± 0.0		9.28 ± 0.0		7.99 ± 0.0		9.04 ± 0.0		9.18 ± 0.0		0.106
NA2O	0.12	1.52 ± 0.0		3.58 ± 0.0		0.03 ± 0.0		0.80 ± 0.0		0.87 ± 0.0		0.015
K2O	0.03	1.81 ± 0.0		1.56 ± 0.0		1.10 ± 0.0		3.98 ± 0.0		1.42 ± 0.0		0.010
P2O5	0.0	0.35 ± 0.0		0.26 ± 0.0		0.31 ± 0.0		0.38 ± 0.0		0.46 ± 0.0		0.0
						0.0 ± 0.0		0.0 ± 0.0		0.0 ± 0.0		0.0
ppm												
Ba(ppm	34.	660. ± 8.		769. ± 8.		430. ± 7.		1365. ± 11.		598. ± 8.		13.
Rb	27.	32. ± 1.		24. ± 1.		26. ± 1.		79. ± 1.		23. ± 1.		4.
Sr	2.	640. ± 3.		603. ± 2.		77. ± 2.		993. ± 3.		2150. ± 4.		3.
Nb	6.	≤Det.		5. ± 1.		≤Det.		≤Det.		5. ± 1.		4.
Y	3.	18. ± 1.		13. ± 1.		14. ± 1.		22. ± 1.		23. ± 1.		3.
Zr	3.	55. ± 1.		47. ± 1.		36. ± 2.		33. ± 0.		25. ± 0.		3.
Cr	13.	270. ± 2.		10. ± 0.		2807. ± 5.		19. ± 0.		11. ± 0.		1.
Ni	21.	80. ± 2.		30. ± 1.		478. ± 3.		34. ± 2.		33. ± 2.		4.
Co	3.	0. ± 0.		0. ± 0.		0. ± 0.		0. ± 0.		0. ± 0.		2.
Cu	9	0. ± 0.		0. ± 0.		0. ± 0.		0. ± 0.		0. ± 0.		0.
						0. ± 0.		0. ± 0.		0. ± 0.		0.
						0. ± 0.		0. ± 0.		0. ± 0.		0.
V	0.	273. ± 1.		282. ± 1.		226. ± 1.		365. ± 2.		335. ± 2.		0.
						0. ± 0.		0. ± 0.		0. ± 0.		

† σ_C is the error in the calibration. The ± error given after each value is is $\sigma_E = \sqrt{(\sigma_N'^2 + \sigma_R'^2)}$, see text explanation.